STRUCTURAL AND FUNCTIONAL CHARACTERIZATION OF THE *Bordetella pertussis* CyaC ACYLTRANSFERASE

NIRAMON THAMWIRIYASATI

A THESIS SUBMITTED IN PARTIAL FULFILLMENT
OF THE REQUIREMENTS FOR
THE DEGREE OF DOCTOR OF PHILOSOPHY
(MOLECULAR GENETICS AND GENETIC ENGINEERING)
FACULTY OF GRADUATE STUDIES
MAHIDOL UNIVERSITY
2010

Thesis
entitled

STRUCTURAL AND FUNCTIONAL CHARACTERIZATION OF THE *Bordetella pertussis* CyaC ACYLTRANSFERASE

……
Miss Niramon Thamwiriyasati
Candidate

……
Assoc. Prof. Chanan Angsuthanasombat, Ph.D.
Major-advisor

……
Prof. Emeritus Prapon Wilairat, Ph.D.
Co-advisor

……
Assoc. Prof. Albert J. Ketterman, Ph.D
Co-advisor

……
Assist. Prof. Gerd Katzenmeier, Ph.D.
Co-advisor

……
Prof. Banchong Mahaisavariya, M.D
Dean
Faculty of Graduate Studies
Mahidol University

……
Assoc. Prof. Apinunt Udomkit, Ph.D.
Program Director
Doctor of Philosophy Program in
Molecular Genetics and Genetic Engineering
Institute of Molecular Biosciences
Mahidol University

Thesis
entitled

STRUCTURAL AND FUNCTIONAL CHARACTERIZATION OF THE *Bordetella pertussis* CyaC ACYLTRANSFERASE

was submitted to the Faculty of Graduate Studies, Mahidol University
for the degree of Doctor of Philosophy
(Molecular Genetics and Genetic Engineering)
on
March 24, 2010

……
Miss Niramon Thamwiriyasati
Candidate

……
Assoc. Prof. Apinunt Udomkit, Ph.D.
Chair

……
Assoc. Prof. Chanan Angsuthanasombat, Ph.D.
Member

……	……
Prof. Emeritus Prapon Wilairat, Ph.D.	Assoc. Prof. James R. Ketudat-Cairns, Ph.D.
Member	Member
……	……
Assist. Prof. Gerd Katzenmeier, Ph.D.	Assist. Prof. Busaba Powthongchin, Ph.D.
Member	Member
……	……
Prof. Banchong Mahaisavariya, M.D.	Prof. Prasert Auewarakul, M.D., Dr. med.
Dean	Director
Faculty of Graduate Studies	Institute of Molecular Biosciences
Mahidol University	Mahidol University

ACKNOWLEDGEMENTS

I would like to express my sincere appreciation to many persons, especially my major advisor, Assoc. Prof. Chanan Angsuthanasombat, for his warm guidance, valuable advice and encouragement during the various stages of this thesis project. I would also like to thank my co-advisors, Prof. Prapon Wilairat, Assoc. Prof. Albert J. Ketterman and Assist. Prof. Gerd Katzenmeier for their constructive comments and discussions for this research project. I would like to give my sincere thanks to Assoc. Prof. Chun-Jung Chen for his great advice in X-ray crystallography and Dr. Panapat Uawithya for his guidance and advice in homology modeling.

My appreciation also is extended to Assist. Prof. Busaba Powthongchin, Dr. Jongrak Kittiworakarn and Dr. Suang Rungpragayphan for their great help in sharing the success of this work and Ms. Anchalee Nirachanon for managing all documents and scholarship budgets during the whole project period.

I would like to thank to all BT and BP members, especially Ms. Somsri Sakdee, Dr. Somphob Leetachewa and all my friends for their great assistance in solving problems in Taiwan and wonderful friendships. Finally, I am grateful to express my deepest appreciation to my parents for their care and encouragement.

I am particularly indebted to the Royal Golden Jubilee Ph.D. program, conducted by the Thailand Research Fund (TRF) that provided me the good opportunity for doing this project.

Niramon Thamwiriyasati

STRUCTURAL AND FUNCTIONAL CHARACTERIZATION OF THE *Bordetella pertussis* CyaC ACYLTRANSFERASE

NIRAMON THAMWIRIYASATI 4737269 MBMG/D

Ph.D. (MOLECULAR GENETICS AND GENETIC ENGINEERING)

THESIS ADVISORY COMMITTEE: CHANAN ANGSUTHANASOMBAT, Ph.D., PRAPON WILAIRAT, Ph.D., ALBERT KETTERMAN, Ph.D., GERD KATZENMEIER, Ph.D.

ABSTRACT

CyaC-acyltransferase mediates activation of adenylate cyclase-hemolysin toxin (CyaA), a virulent factor of human respiratory tract pathogen *Bordetella pertussis*, *via* transfering fatty-acyl group from the acyl-acyl carrier protein (acyl-ACP) onto the protoxin. Here, the recombinant 21-kDa CyaC expressed in *Escherichia coli* mainly as an inclusion body was successfully refolded into monomeric protein and purified to ~90% purity with ~70% yield recovery. The refolded protein was able to *in vitro* activate proCyaA-PF, a protoxin of CyaA with a truncation of adenylate cyclase domain, and to hydrolyze the oxygen-ester linkage of *p*-nitrophenyl derivatives with a preference for acyl chains of 14-16 carbons. The *p*-nitrophenyl derivatives could be utilized by CyaC as an alternative substrate to acyl-ACP for proCyaA-PF activation. Among trial derivatives, *p*-nitrophenyl palmitate (pNPP) activated proCyaA-PF to the highest hemolytic activity, signifying physical palmitoylation of the toxin. A homology-based CyaC structure inferred a conceivable role of a catalytic triad including Ser^{30}, His^{33} and Tyr^{66} in substrate catalysis. Alanine substitutions of these individual residues caused a drastic decrease in catalytic efficiency toward pNPP and abolished acylation of CyaA-PF toxin. Taken together, this led to the possibility that CyaC-acyltransferase has a mechanism similar to that of a serine esterase, in which Ser^{30} is an essential part of a catalytic triad *via* acyl-enzyme intermediate catalysis.

KEY WORDS: *Bordetella pertussis*/ ADENYLATE CYCLASE-HEMOLYSIN TOXIN/ ACYLTRANSFERASE/ PALMITOYLATION

142 pages.

การศึกษาโครงสร้างและหน้าที่การทำงานของเอนไซม์ Acyltransferase (CyaC) จากเชื้อแบคทีเรีย *Bordetella pertussis*

STRUCTURAL AND FUNCTIONAL CHARACTERIZATION OF THE *Bordetella pertussis* CyaC ACYLTRANSFERASE

นิรมล ธรรมวิริยสติ 4737269 MBMG/D

ปร.ด. (อณูพันธุศาสตร์และพันธุวิศวกรรมศาสตร์)

คณะกรรมการควบคุมวิทยานิพนธ์: ชนันท์ อังศุธนสมบัติ Ph.D., ประพนธ์ วิไลรัตน์ Ph.D., ALBERT KETTERMAN, Ph.D., GERD KATZENMEIER, Ph.D.

บทคัดย่อ

CyaC-acyltransferase เป็นเอนไซม์ที่ใช้กระตุ้นความเป็นพิษของโปรตีน Adenylate cyclase-hemolysin (CyaA) ซึ่งเป็นปัจจัยสำคัญชนิดหนึ่งของเชื้อ *Bordetella pertussis* ที่ก่อให้เกิดโรคทางเดินหายใจ โดย CyaC ทำหน้าที่ในการย้ายหมู่ acyl จากโปรตีนที่ขนส่งหมู่ acyl (acyl-acyl carrier protein หรือ acyl-ACP) ไปยังโปรตีน proCyaA ในการศึกษาครั้งนี้ ได้ทำการการผลิต เอนไซม์ CyaC ที่มีขนาด 21 kDa จากการใช้เชื้อ *Escherichia coli* ได้เป็นผลึกโ ปรตีนที่ส่วนใหญ่อยู่ในรูปไม่ละลายน้ำ และประสบความสำเร็จในการจัดเรียงโครงสร้างการม้วนตัวของโปรตีนให้เป็นเอนไซม์ที่ละลายน้ำและทำงานได้ในรูปแบบของโมเลกุลเดี่ยวที่มีความบริสุทธิ์ 90% และได้ผลผลิต 70% จากทั้งหมด CyaC ที่ได้สามารถกระตุ้นการทำงานของโปรตีน proCyaA-PF (โปรตีน CyaA ที่ยังไม่สามารถทำงานได้ (inactive) และขาดส่วนของ adenylate-cyclase domain) ภายในหลอดทดลองและสามารถทำปฏิกิริยาการแยกสลายด้วยน้ำ (hydrolysis) ต่อสารตั้งต้น *p*-nitrophenyl derivatives โดยทำปฏิกิริยาสูงสุดที่กรดไขมันที่มีความยาวของคาร์บอน 14 ถึง 16 ตัว นอกจากนี้พบว่า CyaC ยังสามารถใช้ *p*-nitrophenyl derivatives เป็นตัวให้หมู่ acyl แทนโปรตีน acyl-ACP ได้ และจากการเปรียบเทียบชนิดของสารตั้งต้นต่างๆในการกระตุ้นการทำงานของ proCyaA-PF พบว่า pNPP เป็นตัวให้หมู่ palmitoyl ที่กระตุ้นให้ CyaA-PF มีความเป็นพิษโดยการทำให้เม็ดเลือดแดงแตกสูงที่สุด ซึ่งเน้นให้เห็นถึงความสำคัญของการเติมหมู่ palmitoyl ของสารพิษนี้ จาก การใช้โปรแกรมทำนายโครงสร้างสามมิติ (3D-homology modeling) ของ CyaC ชี้ให้เห็นถึงการทำงานของเอนไซม์ที่ใช้กรดอะมิโนสามตัวทำงานร่วมกัน (catalytic triad) ได้แก่ Ser^{30}, His^{33} และ Tyr^{66} เมื่อแทนที่กรดอะมิโนเหล่านี้ด้วย Alanine มีผลให้โปรตีนกลายพันธุ์ทุกตัวลดประสิทธิภาพการสลาย pNPP ลงอย่างมาก และทำให้ไม่มีการเติมหมู่ palmitoyl ไปยังโปรตีน CyaA-PF เกิดขึ้น จากผลการทดลองทั้งหมดแสดงให้เห็นว่า CyaC น่าจะมีการทำงานบางอย่างที่คล้ายกับเอนไซม์ Serine esterase โดยมีกรดอะมิโน Ser^{30} เป็นตัวสำคัญของ catalytic triad โดยการใช้ acyl-enzyme intermediate เป็นตัวกลางในการทำปฏิกิริยากับสารตั้งต้น

142 หน้า

CONTENTS

CONTENTS (cont.)

CONTENTS (cont.)

CONTENTS (cont.)

CONTENTS (cont.)

LIST OF TABLES

LIST OF FIGURES

LIST OF FIGURES (cont.)

LIST OF FIGURES (cont.)

LIST OF ABBREVIATIONS

% (v/v)	Percent volume by volume
% (w/v)	Percent weight by volume
Å	Angstrom
sec	Second (s)
min	Minute (s)
h	Hour (s)
mm	Millimeter (s)
μm	Micrometer (s)
nm	Nanometer (s)
g	Gram (s)
mg	Milligram (s)
μg	Microgram (s)
ng	Nanogram (s)
ml	Milliliter (s)
μl	Microliter (s)
M	Molar (s)
mM	Millimolar (s)
μM	Micromolar (s)
pmol	Picomole (s)
psi	Pound-force per square inch
°C	Degrees Celsius
bp	Base pair (s)
kb	Kilobase (s)
kDa	Kilodalton (s)
U	Unit (s)

LIST OF ABBREVIATIONS (cont.)

AC	Adenylate cyclase domain
ACT	Adenylate cyclase-hemolysin toxin
ATP	Adenosine triphosphate
Amp	Ampicillin
BSA	Bovine serum albumin
B. pertussis	*Bordetella pertussis*
cAMP	Cyclic adenosine monophosphate
CyaA	Adenylate cyclase-hemolysin toxin
CyaA-PF	Pore-forming domain of adenylate cyclase-hemolysin toxin
CyaC	Acyltransferase
CD	Circular dichroism
CTAB	Cetyl trimethylammonium bromide
DABA	*L*-2,4-diaminobutyric acid acetyltransferase
DNA	Deoxyribonucleic acid
DNase	Deoxyribonuclease
dNTPs	Deoxynucleotide triphosphates (dATP, dGTP, dTTP, dCTP)
DTT	1,4-Dithiothreitol
EDTA	Ethylenediaminetetraacetic acid
E. coli	*Escherichia coli*
et al.	And others
FPLC	Fast performance liquid chromatography
Hly	Hemolysin
IPTG	Isopropyl-β-D-thiogalactopyranoside
L	Liter (s)
LB	Luria-Bertani medium
LC	Liquid chromatography

LIST OF ABBREVIATIONS (cont.)

MS	Mass spectrometry
MALDI-TOF	Matrix assisted laser desorption ionisation time-of-flight
OD	Optical density (-ies)
PAGE	Polyacrylamide gel electrophoresis
PCR	Polymerase chain reaction
PF	Pore-forming fragment
PMSF	Phenylmethylsulphonylfluoride
pNPA	Para-nitrophenyl acetate
pNPC	Para-nitrophenyl caprylate
pNPD	Para-nitrophenyl decanoate
pNPM	Para-nitrophenyl myristate
pNPP	Para-nitrophenyl palmitate
pNPS	Para-nitrophenyl stearate
ProCyaA-PF	Pore-forming domain of inactive adenylate cyclase-hemolysin toxin
RBS	Ribosome binding site
RNA	Ribonucleic acid
RNase	Ribonuclease
RTX	Repeat-in-Toxin
rpm	Revolutions per minute
SDS-PAGE	Sodium dodecyl sulphate-polyacrylamide gel electrophoresis
T_a	Annealing temperature
TAE	Tris acetate EDTA
TLCK	Tosyl-*L*-lysine chloromethyl ketone
Tris	Tris (hydroxymethyl)-aminomethane
UV	Ultraviolet
V	Volt (s)

CHAPTER I
INTRODUCTION

Bordetella pertussis, an important human pathogen causing whooping cough, secretes a 1706-amino acid-long adenylate cyclase-hemolysin toxin (CyaA) which is one of the key virulence factors of this bacterium (1). CyaA is a bifunctional protein which is a unique member of RTX (Repeat-in-Toxin) family composed of N-terminal adenylate cyclase (AC) domain (400 amino acids) and hemolysin or pore-forming (PF) domain (1306 amino acids) (2). The toxin encoded by the *cyaA* gene of the *cyaCABD* gene cluster is firstly expressed as an inactive CyaA protoxins (proCyaA) (3). Later, proCyaA is converted intracellulary to the mature toxin by amide-linked palmitoylation (4) catalyzed by a coexpressed accessory acyltransferase (CyaC) (5). CyaC transfers the acyl group from acyl-acyl carrier protein (acyl-ACP) to proCyaA *via* the ε-amino group of Lys^{983} located within the conserved RTX region of the PF domain (6).

The primary targets of CyaA are myeloid phagocytic cells, such as macrophages, neutrophils and dendritic cells (7). These cells express the CD11b/CD18 ($\alpha_M\beta_2$ integrin) as a toxin receptor that binds CyaA with high affinity (8). Upon binding to the surface of target cells, CyaA delivers its catalytic AC domain across the cytoplasmic membrane into the cell. The AC domain is subsequently activated by cytoplasmic calmodulin (9) and catalyzes uncontrolled conversion of ATP to high levels of cAMP, leading to cell death by apoptosis (10). The CyaA toxin can also exert hemolytic activity against sheep erythrocytes, in addition to the myeloid CD11b-expressing cells (11, 12). This could be due to the capacity of CyaA to form small cation-selective channels in cellular membranes, causing colloid-osmotic cell lysis (11). Both cytotoxic and hemolytic activities have been shown to be exerted only by the active palmitoylated CyaA, but not proCyaA (6). The conjugated palmitoyl group was suggested to increase the membrane affinity of CyaA for efficient attachment to

the target membranes by acting as either a mediator of membrane association or a determinant of specific protein-protein interactions (13, 14).

It has been shown in previous studies that the recombinant CyaA-PF protein (residues 482-1706) co-expressed with CyaC in *E. coli* was found to be *in vivo* palmitoylated at Lys^{983} to become hemolytically active (15), indicating that the activation of CyaA-PF by CyaC is necessary for hemolytic activity. However, the precise mechanism of CyaA acylation by CyaC-acyltransferase has not yet been clearly elucidated. In this study, the recombinant CyaC-acyltransferase was over-expressed in *E. coli* and successfully refolded *in vitro*, and was demonstrated to be able to hydrolyze *p*-nitrophenyl derivatives and activate proCyaA-PF to become hemolytically active. CyaC has been shown to hydrolyze the various acyl chain lengths (C8-C18) of *p*-nitrophenyl derivatives with preferential hydrolysis toward *p*-nitrophenyl myristate (pNPM) and *p*-nitrophenyl palmitate (pNPP), and the modifying palmitoyl group on CyaA toxin exhibits the highest toxicity. In addition, a plausible three-dimensional CyaC structure built by homology-based modeling suggested a conceivable role of catalytic triad (Ser^{30}, His^{33} and Tyr^{66}) in comparison with chymotrypsin. Single-alanine substitutions of the proposed catalytic residues suggest that these residues are essential for acyl-enzyme intermediate reaction. Thus the thesis work reports a novel finding on serine esterase activity of CyaC-acyltransferase against the substrate analogs through a possible mechanism related to the known hydrolytic reaction *via* a catalytic triad.

CHAPTER II
OBJECTIVES

So far, there are no data to indicate how CyaC catalyzes the formation of an internal amide by fatty acylation of CyaA and the critical residues of CyaC are still unknown. Knowledge of the three-dimensional structure is a prerequisite for the rational design of site-directed mutations in a protein and can be of great importance for obtaining detailed functional information. Structural information often greatly enhances understanding of how a protein functions and how it interacts with other molecules. In order to get insight into the role of the *B. pertussis* CyaC-acyltransferase in the acylation reaction, the specific objectives of this study were:

(1) To characterize the acyltransferase activity of CyaC based on the *in vitro* activation system.

(2) To obtain the three-dimensional structure of CyaC protein by homology-based modeling and/or X-ray crystallography.

(3) To study the structure-function relationships of CyaC *via* site-directed mutagenesis.

CHAPTER III
LITERATURE REVIEW

3.1 General Background of *Bordetella pertussis*

3.1.1 Biology and morphology

Bordetella pertussis is a causative agent of whooping cough or pertussis that classified in the genus *Bordetella* within the family *Alcaligenaceae*. This genus comprises eight species, four of which cause infections of the upper respiratory tract in different host organisms (**Table 3.1**) (16-18). *B. pertussis* is a small Gram-negative aerobic coccobacillus that appears singly or inpairs (19). It is an obligate human pathogen with no known animal or environmental reservoir (17-19). The bacteria are nutritionally fastidious and are usually cultivated on rich media supplemented with blood such as Chocolate agar or Bordet Gengou agar, which are originally isolated in 1906 by Bordet and Gengou (20). Even on blood agar, the organism grows slowly and requires 3-6 days to form pinpoint colonies. Hemolytic phenotype was clearly seen by clear zone around the colonies (**Figure 3.1**).

A) **B)** **C)**

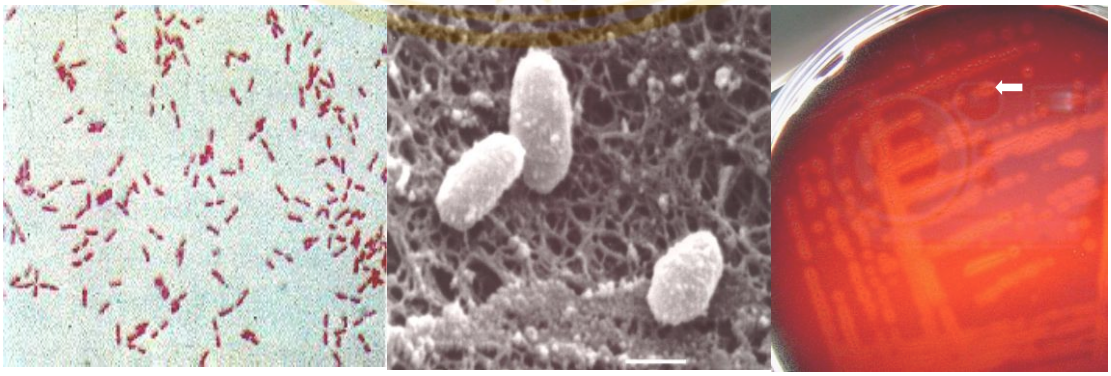

Figure 3.1 Morphology of *Bordetella pertussis* (18-20)
B. pertussis is a Gram-negative bacterium *via* Gram stain, viewed under light microscope (A). Its shape appears single or inpairs under scanning electron microscope (B). Colonies of *B. pertussis* are small glistening mercury-like droplets on Bordet Gengou blood agar. Hemolysis zones around the colonies were indicated by the arrow (C). Figures B and C were displayed by Powthongchin, B (21).

Table 3.1 Host specificities of *Bordetella* species (16-19)

Species	Reservoir	Site of isolation
B. pertussis	human	respiratory tract
B. parapertussis	human, sheep	respiratory tract
B. bronchiseptica	animals, birds	respiratory tract, blood
B. avium	birds, poultry	respiratory tract
B. hinzii	birds, human	respiratory tract, blood
B. holmesii	human	blood
B. trematum	human	ear, skin
B. petrii	-	environment

3.1.2 Pathogenesis

B. pertussis colonizes the ciliated cells of the respiratory epithelium causing severe respiratory disease by the secreted toxins (16-18). There are four important steps relating to *B. pertussis* infection: attachment, evasion of host defenses, local damage, and systemic manifestations. Infection is initiated by the attachment of the *B. pertussis* organisms to the ciliated epithelium of the upper respiratory tract *via* the adhesions, especially filamentous hemagglutinin (FHA) (18). Evasion of host defenses is facilitated by adenylate cyclase-hemolysin toxin (CyaA) and pertussis toxin (PTX) (22). Local tissue damage of the ciliated epithelial cells may be due to tracheal cytotoxin (TCT), dermonecrotic toxin (DNT), and perhaps CyaA (18).

The whooping cough or pertussis disease has three stages. The first stage, colonization or initial catarrhal stage, is marked by an irritating cough and slight fever, lasting 1-2 weeks. The second stage, paroxysmal stage, is characterized by an inspiratory ‘whoop’ as air rushes into the lungs against narrowed glottis, which lasts 1-6 weeks. The last stage, period of convalescence, is marked by decreased paroxysms, persistent cough and secondary bacterial infections (16, 22). Whooping cough is a highly transmissible, in which transmission of disease occurs *via* respiratory droplets expelled by infected individuals. The whooping cough disease remains a major health

problem and results in high morbidity and mortality in many countries. In the United States, 5000-7000 cases are reported every year. The most recent epidemic occurred in 2005 (25,616 reported cases). After the introduction of a vaccine, the number of cases gradually declined, reaching a low in the mid-1970s (22). However, incidence of pertussis has increased steadily since the 1980s and shifts to adolescents which are the major source of transmission to partially immunized or non-immune infants since 1990 (22, 23). Up to date, incidence in 2007 was 3.6/100,000 when 10,454 cases of pertussis were reported by WHO (23).

3.1.3 Virulence factors

Virulence factors of *B. pertussis* are typically divided into two main functional categories: adhesins and toxins (**Figure 3.2**) (17, 24).

3.1.3.1 Adhesins

Adhesin is a bacterial product that enables bacteria to adhere and colonize a host. *B. pertussis* produces a number of adhesins found at the surface of the organism, including filamentous hemagglutinin (FHA), fimbriae, the serum-resistance protein and the attachment factor (24).

FHA is a major adhesin 220-kDa filamentous protein found on the cell surface of *B. pertussis*. FHA binds to galactose residues on a sulfated glycolipid called sulfatide, a common molecule found on the surface of ciliated cells. The bacterium might bind preferentially to phagocyte *via* integrin CR3 site in order to facilitate its own engulfment. In addition to FHA, *B. pertussis* produces fimbriae that the minor subunit Fim D binds to integrin VLA5 and sulfated sugars (17). Fimbriae play a role in infection of the laryngeal mucosa whereas FHA is important for colonization of the entire respiratory tract.

The other adhesins are the autotransporters pertactin (PRN) and the tracheal colonization factor (TCF). Both proteins are also able to bind phagocytic cells *via* their Arg-Gly-Asp (RGD) sequence of binding sites on β_1 integrin. During infection, all these adhesins induce synthesis of antibodies (24).

3.1.3.2 Toxins

Apart from adhesins, *B. pertussis* expresses a variety of substances with toxic activity in the class of exotoxins and endotoxins (24, 25).

Pertussis toxin (PTX) is a two-component, A+B bacterial exotoxin. The A subunit (S1) is an ADP-ribosyl transferase. The B component, composed of five polypeptide subunits (S2-S5), binds to specific carbohydrates on cell surfaces. Following binding of the B component to host cells, the A subunit is inserted through the membrane and gains ADP-ribosylation to the membrane-bound regulatory protein G_i. The G_i protein is inactivated and cannot perform its normal function to inhibit the eukaryotic adenylate cyclase. As a result, intracellular cyclic AMP level increases leading to disruption of cellular functions of phagocytes and decrease of phagocytic activities as its consequences (24, 25).

Adenylate cyclase - hemolysin toxin (CyaA, ACT or AC) is a secreted bifunctional protein harboring a calmodulin-dependent adenylate cyclase activity and a hemolytic activity. This toxin binds to integrin CR3 of macrophages, enters the cell and induces apoptosis of the cell. PTX and CyaA toxins induce synthesis of antibodies during the infection (25).

Dermonecrotic toxin (DNT) is a 102-kDa heat-stable protein. DNT inhibits the elevation of alkaline phosphatase activity and stimulate DNA and protein synthesis without cell division, leading to polynucleation (17). It causes inflammation and local necrosis adjacent to sites where *B. pertussis* is located (24).

Tracheal cytotoxin (TCT) is a low molecular weight glycopeptide, which is a fragment of peptidoglycan secreted by the bacteria. It destroys tracheal ciliated cells by inducing the synthesis of interleukin-1 and nitric oxide causing ciliostasis and inhibiting the regeneration of the respiratory tract epithelium. Tracheal cytotoxin (TCT) is a low molecular weight glycopeptide, which is a fragment of peptidoglycan secreted by the bacteria. It destroys tracheal ciliated cells by inducing the synthesis of interleukin-1 and nitric oxide causing ciliostasis and inhibiting the regeneration of the respiratory tract epithelium (24, 25).

In addition to these well-characterized adhesins and toxins, *B. pertussis* expresses a series of other factors, which may also be involved in its pathogenicity as revealed by the genome sequence (2).

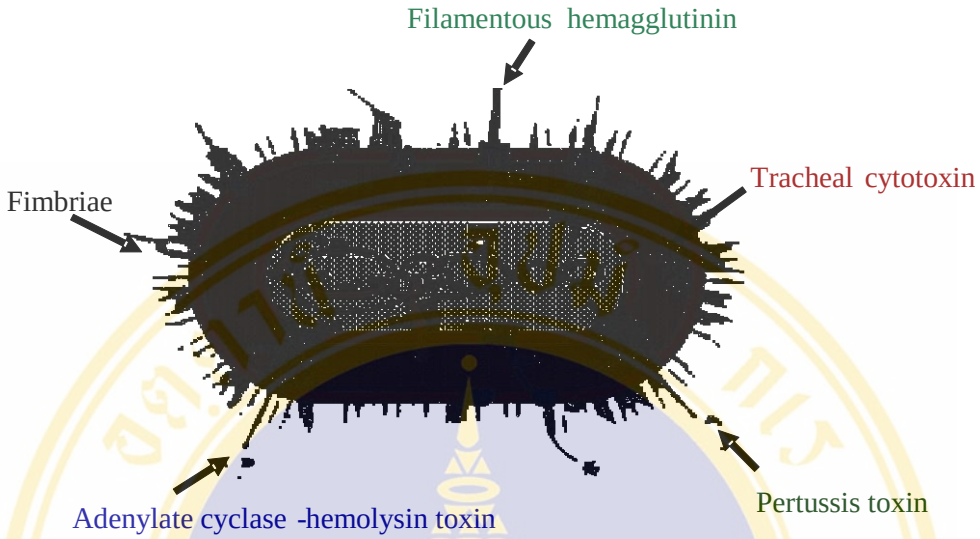

Figure 3.2 Virulence factors of *B. pertussis* (17)

B. pertussis produces a number of virulence factors, which include the pertussis toxin, adenylate cyclase-hemolysin toxin, filamentous hemagglutinin, fimbriae and trachel cytotoxin.

3.2 Adenylate Cyclase-Hemolysin Toxin

All of the *Bordetella* species that infect mammals secrete a bifunctional calmodulin-dependent toxin, adenylate cyclase-hemolysin (CyaA). CyaA is classified into a member of the RTX (Repeat-in-Toxin) family of bacterial pore-forming toxins due to its tandem repeated nonapeptides, Gly-Gly-X-Gly-X-Asp-X-U-X (X = any amino acid, U = a large hydrophobic amino acid such as Phe, Leu, Ile, etc.), which is supposed to be the calcium-binding sites (**Table 3.2**) (26). Unlike other RTX toxins, CyaA is a unique member of RTX family containing an enzymatic activity. CyaA toxin is an important invasive toxin secreted by *B. pertussis*, as mutants lacking this toxin are virtually avirulent in an animal infection model (27). In the murine respiratory model, CyaA was shown to play an important role during the early phase of lung colonization by the bacteria (27, 28). It is also a good protective antigen (immunodominant epitope) against *B. pertussis* infection in mice, as shown by Guiso and co-workers (29).

Table 3.2 Members of the RTX family (26)

Toxin	Bacterium	Cell-type specificity	Species specificity	Size (kDa)
HlyA	*Escherichia coli*	Erythrocytes and epithelial and other cells	Human, murine, bovine and others	110
EhxA	*E. coli*	Erythrocytes and leukocytes	Bovine	107
MmxA	*Morganella morganii*	Erythrocytes and epithelial and other cells	Human, murine, bovine and others	110
ApxIA	*Actinobacillus pleuropneumoniae*	Erythrocytes and epithelial and other cells	Human, murine, bovine and others	105
ApxIIA	*A. pneumoniae*	Leukocytes	Porcine	103
ApxIIIA	*A. pneumoniae*	Leukocytes	Porcine	120
LtxA	*A. actinomycetemcomitans*	Leukocytes	Human	114
LktA	*Pasteurella haemolytica*	Leukocytes	Bovine	105
CyaA	*Bordetella pertussis*	Broad	Broad	200

3.2.1 *cya* Operon

The synthesis, maturation and secretion of CyaA depend on the *cya* gene cluster, which comprises five genes: *cyaA, B, C, D* and *E* (**Figure 3.3A**). The structural gene, *cyaA*, encoding the proCyaA toxin, is controlled by a single promoter P_{cyaA}. Another promoter ($P_{cyaB,D,E}$) located between *cyaA* and *cyaB* controls the expression of CyaB (ATP binding cassette, ABC), CyaD (membrane fusion protein, MFP) and CyaE (outer membrane protein, omp) (25). All these gene products play a role in the export of CyaA toxin to the extracellular medium by type I secretory system (30). The *cyaC* gene is separated from the polycistron by a 260-bp intergenic region and is transcribed in the opposite orientation under control of the P_{cyaC}. The enzyme acyltransferase, the product of *cyaC* gene, converts the inactive precursor of the CyaA toxin to its active form by amide-linked palmitoylation (31).

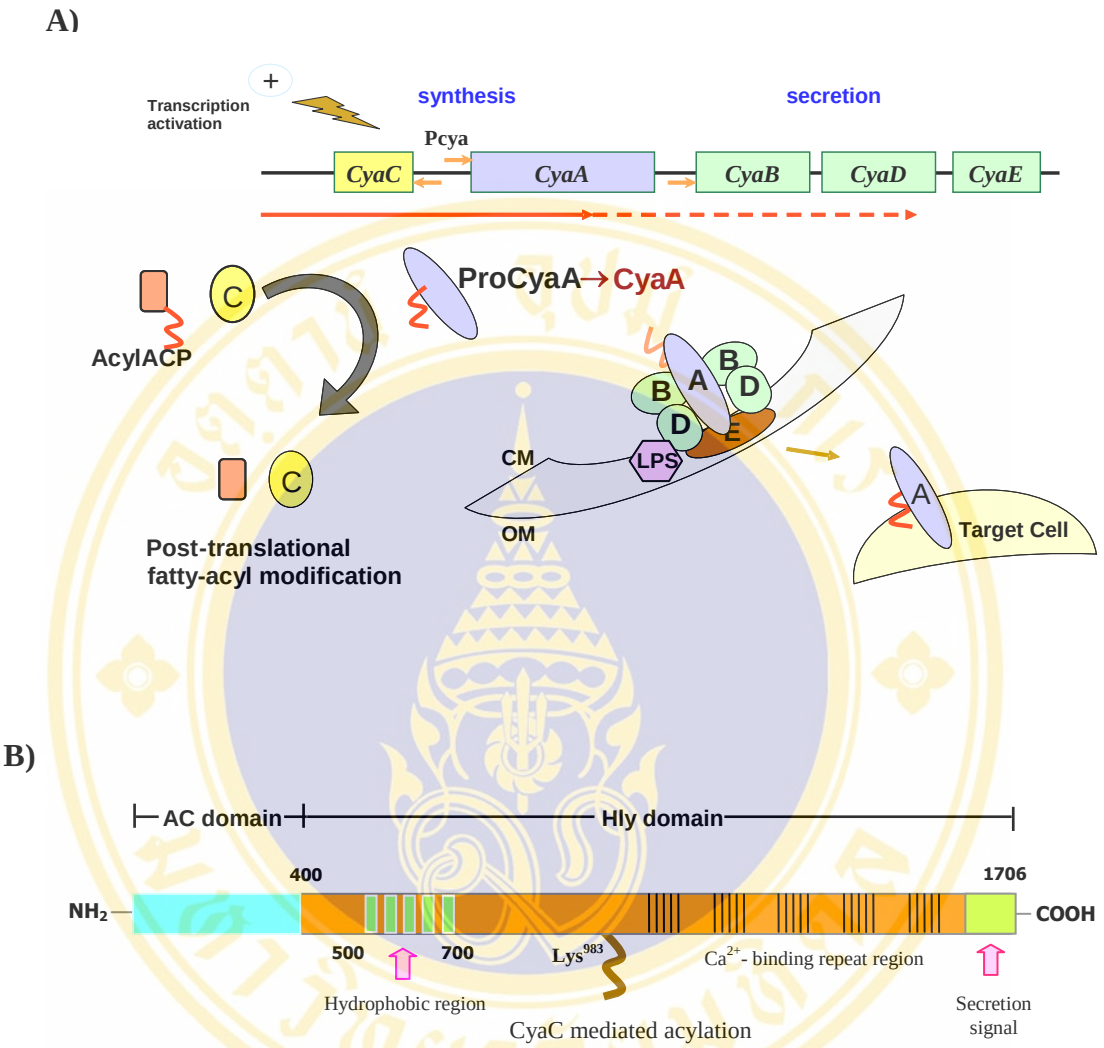

Figure 3.3 The *cya* operon and structural organization of CyaA (Adapted from Ladant, D. *et al* (25) and Stanley, P. *et al*. (14))

(A) The *cya* operon is composed of five genes: *cyaA*, *B*, *C*, *D* and *E*. CyaA, the structural gene encoding the toxin is under the control of a single promoter (P_{cyaA}). Another promoter between *cyaA* and *cyaB* ($P_{cyaB,D,E}$) controls the expression of *cyaB*, *D* and *E* whose products are essential for the secretion of CyaA. The gene *cyaC*, encoding acyltransferase enzyme, is transcribed in the opposite direction to that of the other genes in the *cya* operon. The *cyaA* gene encodes proCyaA toxin which is converted intracellulary to the active CyaA toxin by amide-linked palmitoylation. The activation reaction is catalyzed by CyaC using acyl-ACP as the donor of fatty acids.

(B) Structural organization of CyaA toxin. The adenylate cyclase domain encompasses the 400 N-terminal residues. The hemolytic domain encompasses the remaining C-terminal residues, containing the hydrophobic region, palmitoylation site of Lys^{983} (mediated by CyaC) and calcium binding repeat consensus sequence GGXGXDXUX (RTX region).

3.2.2 Structure of CyaA

CyaA is a 1,706-amino acid residue bifunctional protein (~177 kDa) synthesized as a single polypeptide chain. It is composed of two functional domains, an N-terminal adenylate cyclase (AC) and a C-terminal hemolytic moiety (Hly) or pore-forming (PF) domain (**Figure 3.3B**). A catalytic AC domain (residues 1-400) is responsible for conversion of ATP to cyclic AMP (cAMP). The 1,306-residue PF domain endows with hemolytic activity and mediates binding and delivery of the catalytic domain into eukaryotic cells (11, 25).

The PF domain comprises of four subregions: (i) a hydrophobic region (residues 500-700) is believed to be involved in insertion of the toxin into the target cell membrane; (ii) an acylation region (residues 800-1,000) where post-translational activation of the protoxin is accomplished; (iii) a glycine-aspartic acid repeat region (residues 1,000-1,600) which contains ~35-40 nonapeptide repeats of a consensus sequence (GGXGXDXUX), characteristic of the RTX toxins; and (iv) a 106-residue non-processed C-terminal secretion signal (2). The nonapeptide repeats are arranged in a tandem fashion and may fold into a characteristic parallel β-roll motif that constitutes a novel type of calcium-binding structure, as revealed by the three-dimensional structure of the *Pseudomonas aeruginosa* alkaline protease (32). These repeats are responsible for low-affinity calcium binding (33).

3.2.3 Post-translational modification of CyaA

Activation of all RTX-A toxin to the mature toxin involves a post-translational fatty-acyl modification at conserved lysine residues by RTX-C acyltransferase (**Table 3.3**). The mechanism of RTX-toxin acylation has been characterized in substantial detail for *E. coli* α-hemolysin (HlyA) as it is acylated at both Lys^{564} (KI) and Lys^{690} (KII) by acyl-ACP-dependent HlyC-acyltransferase (14). Similar to *E. coli* HlyA, the recombinant CyaA toxin produced in *E. coli* has also been shown to have two-site acylation at Lys^{860} and Lys^{983} (13) while the *B. pertussis* native toxin has been shown to be acylated only at Lys^{983} (4). Only acylation of Lys^{983} corresponding to Lys^{690} of *E. coli* was shown to be crucial for CyaA activity (6) and is necessary for CyaA to lyse sheep erythrocytes, J774 macrophages and Jurkat T cells

(35). LktA is also acylated at Lys^{554}, which corresponds to Lys^{564} of HlyA. The modification of other RTX protoxins has not been investigated, but the C gene sequences of the RTX determinants are highly conserved and it is assumed that all toxins are modified by a similar mechanism. Modification of the protoxin is essential for cytotoxic activity and may create a conformational change in the RTX-A protein that is necessary for interaction of the toxin with the target cell membrane (26, 33).

Table 3.3 The conserved KI and KII positions of RTX toxin (14)

Toxin	Activity	Position of:	
		KI	KII
CyaA	Adenylate cyclase/hemolysin	K860	K983[a]
HlyA	Hemolysin	K564 [a]	K690[a]
EhxA	Enterohemorrhagic hemolysin	K550	K675
ApxIA	Hemolysin	K560	K686
ApxIIA	Hemolysin	K557	N687
ApxIIIA	Leukotoxin	K571	K702
AaltA	Leukotoxin	K562	K687
AshA	Hemolysin	K557	N687
LktA	Leukotoxin	K554	N684
PllktA	Leukotoxin	K550	S680

[a] Identified as acylated residue in *vivo*-expressed toxin.

3.2.4 Calcium requirement for CyaA activity

CyaA is a calcium-binding protein that undergoes conformational changes upon binding of calcium (32, 33). The calcium binding properties of CyaA have been analyzed into two classes of different affinities (33). Binding of calcium to a small number of high affinity binding sites might be necessary for the hemolytic activity of the toxin. In addition, binding of calcium to RTX repeat motifs with low affinity sites that induces major structural rearrangements of CyaA may be involved in delivery of the AC catalytic domain into target cells (13, 33).

3.2.5 Interaction of CyaA with target cell membrane

CyaA binds specifically to target cells through the surface glycoprotein $\alpha_M\beta_2$ integrin (known as CD11b/CD18 or CR3) (8), which is expressed on myeloid phagocytic cells, such as macrophages, neutrophils, and dendritic cells. The main receptor-interacting domain of CyaA is located within the glycine and aspartate-rich region (32). Calcium binding and post-translational acylation of CyaA were both shown to be required for a tight and productive interaction of CyaA with cells expressing the CD11b/CD18 receptor (8, 34). The conjugated palmitoyl group was suggested to increase the membrane affinity of CyaA for efficient attachment to the target membranes by acting as either a mediator of membrane association or a determinant of specific protein-protein interactions (14). However, this toxin is also toxic to other cell types (*e.g.* sheep erythrocytes) which lack the CD11b/CD18 receptor, suggesting different cell-invasive mechanisms (3, 35) (**Figure 3.4**).

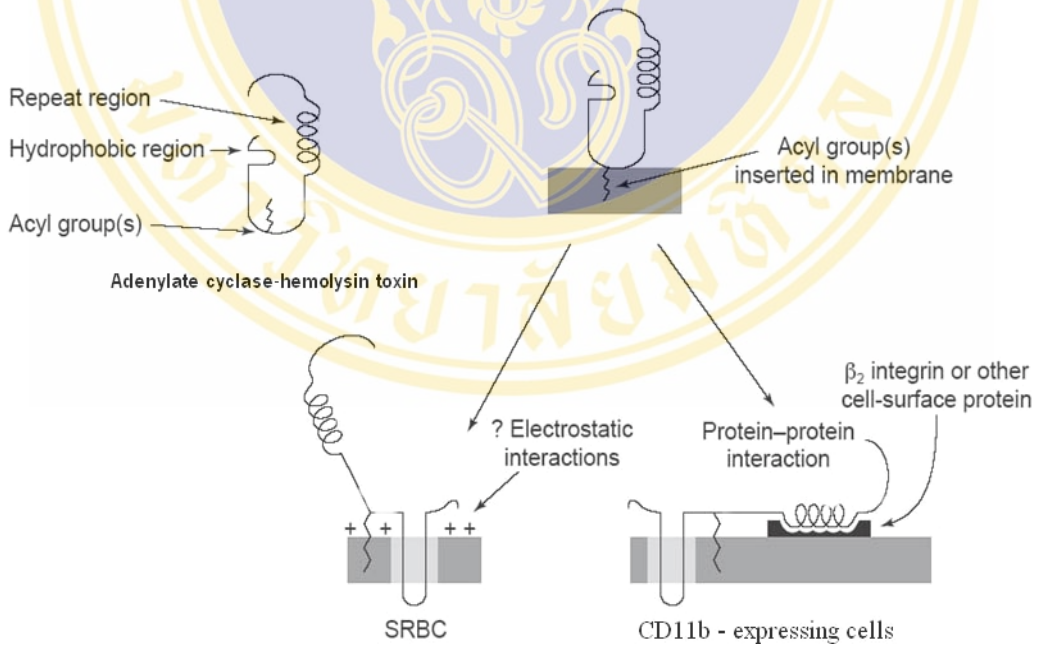

Figure 3.4 Interaction of the different target cells by acylation sites (3)

Acyl group in the active CyaA toxin could be inserted in to the membrane upon interaction with the different target cells, including sheep red blood cells (SRBC) and CD11b - expressing cells.

3.2.6 Mechanism of action of CyaA

Mechanism of the CyaA toxicity is a complex process. The exact toxicity is still unclear. However, the action of CyaA toxin into the eukaryotic cells normally occurs *via* two main steps, intoxication and hemolysis (36, 37). Upon binding to the receptor on immune effector cells, the activated CyaA delivers its catalytic AC domain to the interior of the cytoplasmic membrane. After membrane translocation, the AC enzyme is activated by binding to the intracellular calmodulin and subsequently catalyzes the uncontrolled conversion of ATP to cAMP. Thereafter, the production of unusually high levels of cAMP inhibits normal functions of phagocytes, leading to cell apoptosis (37). This process referred to as "intoxication" or "toxin/cell invasive" activity (37). In a parallel process, the toxin also hemolyzes sheep erythrocytes *via* oligomerization mechanism presumed to include pore formation and osmotic lysis (36, 38). Intoxication and hemolysis were appeared at strikingly different toxin concentrations and different time scales, suggesting the distinct mechanism (39). Moreover, an increase in potassium efflux has been observed from sheep erythrocytes and Jurkat cells (a human T-cell leukemia line), which begins within minutes of toxin addition (39).

Similar to other hemolysins, the CyaA toxin has been shown to produce transmembrane ion conductance in artificial lipid bilayers (40). Single channel properties of a pore formed by the CyaA toxin were found to be cation-selective and considerably smaller than that of *E. coli* hemolysin (HlyA, a RTX-toxin prototype). Osmotic protection assays on sheep erythrocytes and planar lipid bilayers showed that CyaA formed a moderately water permeable pore with a diameter of 0.6-0.8 nm, which is significantly smaller than the 2-3 nm pore estimated for HlyA toxin (39, 40). Therefore, CyaA is considered as a weak hemolysin when compared to HlyA (39). The CyaA toxin-mediated pore formation in planar lipid bilayers and in lysis of erythrocytes indicated oligomerization of CyaA toxin (39-41). It has been reported that intoxication and hemolytic activities were accomplished by different membrane-inserted CyaA conformers, one acting as an AC-delivering monomer and the other as an uncharacterized pore-forming oligomer (36).

3.3 CyaC, a novel acyltransferase

The ability to transfer an acyl group to an internal lysine residue of a target protein distinguishes CyaC from all other bacterial acyltransferases, indicating the various constitutive acyltransferases. The deduced amino acid sequence of the *cyaC* gene has no significant homology to that of any known acyltransferases such as the lipid A acyltransferases (42), the *Rhizobium* Nod factor acyltransferases NodL and NodA (43), or the well characterized acyltransferases, such as glycerol-3-phosphate acyltransferases (44) or eukaryotic *N*-myristoyltransferases (45). CyaC may therefore be an acyltransferase that is structurally and functionally distinct from all other acyltransferases. Bacterial and eukaryote acyltransferases generally accept either acyl coenzyme A (acyl-CoA) or acyl-ACP as an acyl donor, but ACP is a strict requirement for CyaC-directed pro-CyaA acylation (acyl-CoA cannot be used). So far, there is no evidence to indicate the role of CyaC action, which would define as a catalyst enzyme, because CyaC and CyaA proteins produced together *in vivo* from the same operon. Toxin formation has generally been assayed by cell binding, cell invasive and hemolytic activity as an indirect assay (5). Definition of the function of CyaC and the mechanism reaction, which involves the internal acylation, are necessary to dispel these ambiguities.

3.4 Mechanism of protein acylation

Protein acylation (lipidation) is involved in the maturation of many proteins in both prokaryotic and eukaryotic cells, including viral oncogene products, but it is achieved by various mechanisms, which differ according to the fatty acid transferred, the amino acid modified, and the fatty acyl donor (46). Myristic and palmitic acids are the most common fatty acids cross-linked to protein. Proteins sorted to the bacterial outer membrane or eukaryotic plasma membrane undergoes processing in which an acyl group is attached to the N-terminal amino acid; enzymes with acyltransferase, lipase, or esterase activity use catalytic mechanisms involving ester-linked acyl groups attached to serine and cysteine residues. Numerous instances of protein internal-fatty acylation, generally *via* thiol esterification (*S*-acylation) of cysteine residues, have

been reported (*e.g.*, Ras, trimeric G-proteins and FabB) (14). As can be seen in **Figure 3.5**, the internal acylation of proCyaA through amide linkage (*N*-acylation) does not equate to any of these but instead appears to be limited to its related toxins and perhaps a handful of eukaryotic proteins.

The mechanism of protein acylation is usually studied in the term of palmitoylation exclusively to describe *S*-acylation. *S*-acylation is unique in that it is the only reversible lipid modification (47). It has been proposed that acyltransferases might act as enzymes that recognize specific sequences on proteins and transfer lipids to the target cysteine. This reaction is thought to occur through a thioester intermediate, which is similar to known acyltransferases in lipid metabolism (**Figure 3.6B**). However, research on protein palmitoylation has been plagued by an inherent property of the target proteins: under appropriate conditions, they can be autopalmitoylated in the absence of an apparent enzyme (48). Autoacylation of purified proteins occurs at the same specific sites as in the presumably enzyme mediated reaction *in vivo*, albeit at a slower rate (**Figure 3.6A**). This has led to the speculation that protein palmitoylation is not necessarily enzyme mediated (49). Therefore, palmitoylation can occur spontaneously. Under appropriate conditions, the activation energy that is required for transferring palmitate from Pal-CoA to a peptide is only one-fifth of the energy that is required for enzyme-catalyzed acyl-transfer reactions (**Figure 3.6C**) (49). Therefore, palmitoylation can occur spontaneously. The crucial aspect of this transfer reaction is the formation of a reduced deprotonated cysteine (a thiolate) as the target for palmitate (48). The thiolate anion can then act as a nucleophile on the thioester bond in Pal-CoA to catalyze the generation of the palmitoylated protein.

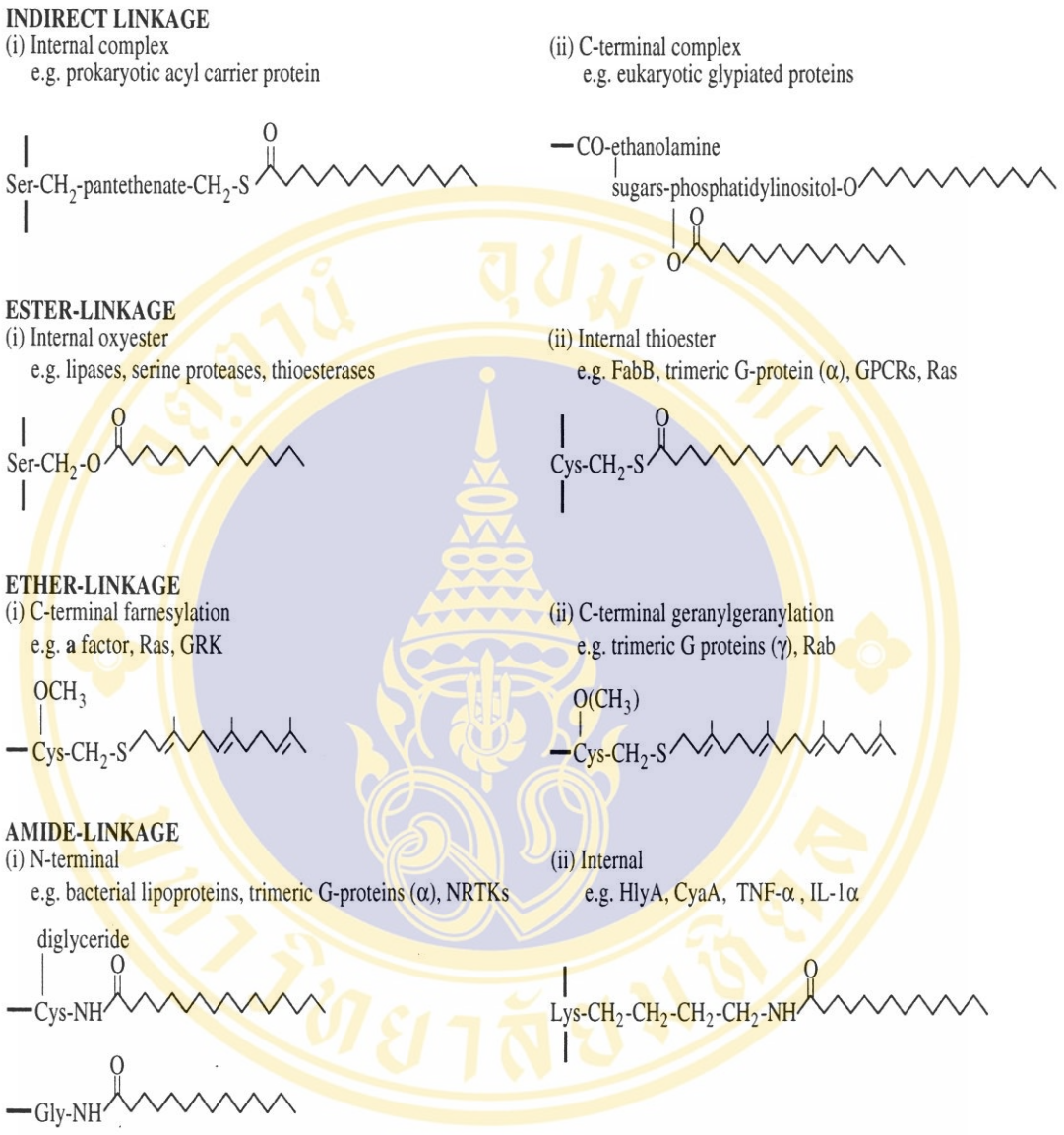

Figure 3.5 Major classes of lipidated proteins in prokaryotes and eukaryotes (14)

The structure of the lipid and their attachment to the protein peptide backbone are shown, except for the complex indirect linkages of pantetheinylated and glypiated proteins. For heterotrimeric G-proteins, the particular modified subunit is indicated in parentheses. The placement of the methyl group of geranylated proteins in parentheses indicates that carboxymethylation is not universal.

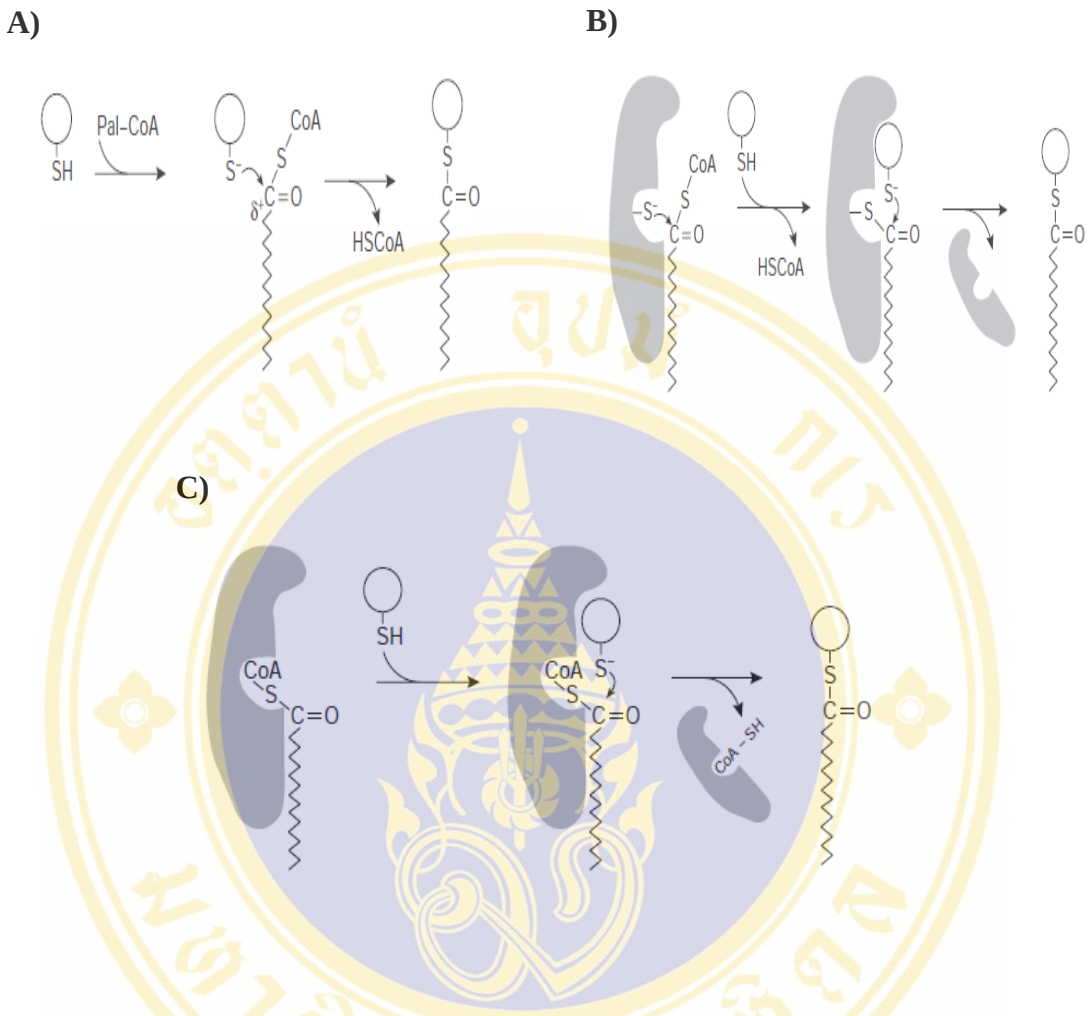

Figure 3.6 Potential mechanisms of palmitoylation (50)

(A) Basic mechanism. The reduced sulphydryl group on the target protein is deprotonated to form a thiolate. The thioester bond between the protein and palmitate is formed as a consequence of a nucleophilic attack of the thiolate on the α-carbon of palmitoyl-CoA (Pal-CoA).

(B) Formation of a thioester intermediate. The palmitoyltransferase forms a thioester intermediate with palmitate, then binds to a target protein and catalyses the transfer of palmitate. For simplicity, the targeting of the substrate protein to the membrane is not shown.

(C) Transfer protein-assisted palmitoylation. The Pal transfer protein binds to CoA or Pal-CoA through a binding pocket and presents Pal-CoA to a target protein, which might then bind to the transfer protein. Nucleophilic attack of the thiolate of the target protein on the α-carbon of bound Pal-CoA allows the formation of a thioester bond. After this reaction, the CoA might remain bound to the transfer protein.

CHAPTER IV
MATERIALS AND METHODS

4.1 Materials

4.1.1 Chemicals and reagents

Ampicillin	Sigma
Chloramphenicol	Sigma
Cetyl trimethyl ammonium bromide (CTAB)	Sigma
RNaseA	Sigma
Isopropyl-β-D-thiogalactopyranoside (IPTG)	Sigma
1, 4-Dithiothreitol (DTT)	Sigma
Coomassie brilliant blue R-250	Sigma
Phenylmethylsulphonylfluoride (PMSF)	Sigma
p-Nitrophenyl acetate (pNPA)	Sigma
p-Nitrophenyl caprylate (pNPC)	Sigma
p-Nitrophenyl decanoate (pNPD)	Sigma
p-Nitrophenyl myristate (pNPM)	Sigma
p-Nitrophenyl palmitate (pNPP)	Sigma
p-Nitrophenyl stearate (pNPS)	Sigma
Urea	Sigma
Deoxyribonucleotide triphosphates (dNTPs)	Promega
Anti-RTX monoclonal antibody-9D4	Listlabs
Standard DNA markers	Gibco BRL, New England Biolabs
SDS-PAGE molecular mass standards	Bio-RAD
Bradford protein assay reagent	Bio-RAD

All other unlisted chemicals and reagents were analytical grade purchased from various suppliers.

4.1.2 Enzymes and accessory buffers

Pfu DNA polymerase (cloned)	Promega
T_4 DNA Ligase	Promega
α-Chymotrypsin (TLCK treated, type VII from bovine pancreas)	Sigma
Restriction endonucleases	New England Biolabs/Promega

All restriction endonuclease enzymes and their buffers were commercially provided by specified companies.

4.1.3 Recombinant plasmids

The recombinant plasmids, pCyaAC-PF encoding CyaA-PF with CyaC, pCyaA-PF (without CyaC) or pCyaC (**Figure 4.1**) containing the T7 promoter, which have been cloned from the *B. pertussis* DMST15659 Thai isolate (15) were used as a DNA template for site-directed mutagenesis and protein expression.

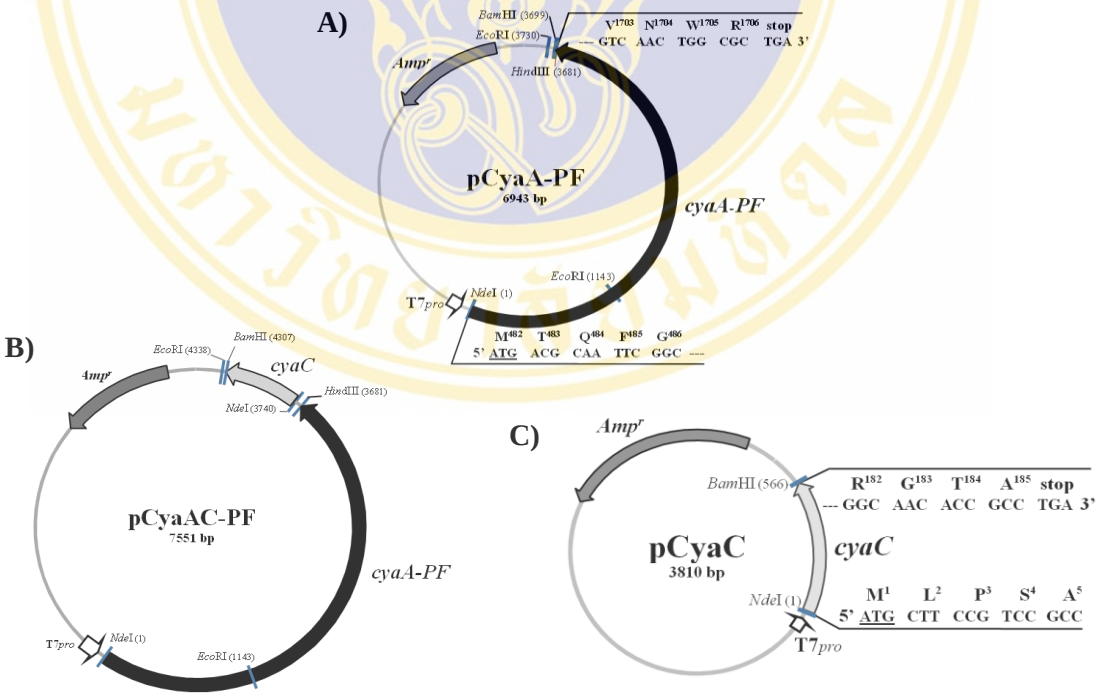

Figure 4.1 Physical map of the recombinant plasmids (15)

The figure shows the recombinant plasmids containing (A) truncated-CyaA without CyaC (pCyaA-PF, proCyaA-PF), (B) truncated-CyaA with CyaC (pCyAC-PF, CyaA-PF) and (C) acyltransferase (pCyaC, CyaC) under the control of T7 promoter. The origin of replication, multicloning sites and ampicillin resistance (*Ap*) gene are shown.

4.1.4 Bacterial strains

E. coli, strain JM109 [*endA1*, *recA1*, *gyrA96*, *thi*, *hsdR17*(r_k^-, m_k^+), *relA1*, *supE44*, Δ*(lac-pro AB)*, (F' *traD36 proAB lacI*^{q}Δ(lacZ)M15)] was purchased from Promega.

E. coli, strain BL21(DE3)pLysS [F^-, *ompT*, *hsdS*$_B$(r_B^-, m_B^-), *dcm*, *gal*, λ(DE3), pLysS, Cm^r] was purchased from Promega.

E. coli strain JM109 was used for general DNA manipulation whereas *E. coli* strain BL21(DE3)pLysS was used for expression of the recombinant plasmids.

4.1.5 Synthetic oligonucleotide primers

All mutagenic oligonucleotide primers were purchased from Sigma PROLIGO, Singapore. The sequences of these oligonucleotides are shown in **Table 4.1**. Single letter codes for amino acid were placed above their corresponding nucleotide sequences. Introduced restriction endonuclease recognition sites are underlined. The bold letters indicate mutated nucleotides or amino acid residues.

Table 4.1 Complementary oligonucleotide primers designed to substitute a coded residue in CyaC with alanine

Primer[a]	Sequence	Restriction site
	M N **A** P M H R D W P	
S30A_f	5' -GATGAACGCTCCCATGCATCGCGACTGGCCGGT- 3'	
S30A_r	3' -GACCGACACCTACTTGCGAGGGTACGTAGCGCTG- 5'	*NruI*[b]
	P M **A** R D W	
H33A_f	5' -CCCATGGCCCGCGACTGG- 3'	
H33A_r	3' -TGAGAGGGTACCGGGCGC- 5'	*NcoI*[b]
	V A **A** C S W	
Y66A_f	5'-GTTGCAGCATGCAGCTGGGC- 3'	
Y66A_r	3'- ACGGCCAACGTCGTACGTCG- 5'	*PstI*[c]

[a] f and r represent forward and reverse primers, respectively.
[b] Recognition sites introduced for restriction enzyme analysis are underlined. Bold letters indicate mutated nucleotide residues.
[c] Deleted recognition sites.

4.1.6 Luria-Bertani (LB) medium

One liter of LB broth contains 10 g peptone, 5 g yeast extract and 10 g NaCl. LB agar was prepared by adding 15 g bacto-agar in one litre of LB broth. The medium was sterilized by autoclaving at 121°C, 15 psi for 15 min. For selective medium, ampicillin and chloramphenicol were aseptically added to 100 µg/ml and 34 µg/ml final concentrations, respectively at 45-50°C.

4.1.7 Sheep erythrocytes

Sheep erythrocytes drawn in Alsever's solution were purchased from National Laboratory Animal Center, Mahidol University.

4.1.8 Miscellaneous

15 and 50 ml centrifuge tubes (polypropylene)	CORNING®
96 well-flat bottom plates	Maxi®sorb, NUNC
QIAquick® gel extraction kit	Macherey-Nagel
Mini-PROTEAN II system	Bio-RAD
Geldoc® system	Bio-RAD
GeneAmp® PCR System 2400 thermal cycler	Perkin-Elmer
Mega™BACE 500 DNA sequencing system	Amersham Bioscience
Spectra MAX 250 ELISA plate reader	Molecular Device
UV 1601 spectrophotometer	Shimadzu
Trans-blot SD	Bio-Rad
Bruker Reflex IV MALDI-TOF-MS	Bruker
Finnigan LTQ Linear Ion Trap Mass Spectrometer	Thermo Electron

4.2 Methods

4.2.1 Plasmid extraction (51)

A single colony of *E. coli* was inoculated into 3 ml LB medium containing 100 µg/ml ampicillin (for *E. coli* JM109) or 100 µg/ml ampicillin and 34 µg/ml chloramphenicol [for *E. coli* BL21(DE3)pLysS] then grown at 37°C with 200 rpm shaking overnight. Bacterial cell pellet was harvested in 1.5 ml microfuge tube by centrifugation at 5,000×*g* for 1 min. The pellet was resuspended in 200 µl of STET buffer (8% sucrose, 0.1% Triton X-100, 50 mM EDTA and 50 mM Tris, pH 8.0) and 5 µl of lysozyme solution (10 mg/ml). The mixture was incubated at room temperature of 5-10 min then boiled for 45 sec and centrifuged at 10,000×*g* for 15 min. The pellet was removed with sterile toothpick and plasmid DNA and low molecular weight RNA were recovered from the supernatant by addition of 5% CTAB into supernatant fraction to give 1/10 (v/v) of CTAB. The solution was mixed by vortexing and centrifuged at 10,000×*g* for 5 min. The pellet was resuspended in 300 µl of 1.2 M NaCl and 3 µl of RNaseA by vigorously vortexing and incubated at 37°C for 30 min. Proteins and plasmid DNA were separated by adding an equal volume of chloroform, mixed and centrifuged at 10,000×*g* for 5 min. The aqueous phase was transferred to a new microcentrifuge tube. Plasmid DNA was precipitated by adding two volumes of absolute ethanol and kept at -20°C for 30 min. The mixture was centrifuged at 10,000×*g* for 15 min at 25°C to pellet the DNA and then the pellet was washed with 70% ethanol, air dried and dissolved in 20 µl of sterile distilled water.

4.2.2 Purification of DNA from agarose gel

Purification of DNA was performed by QIAquick® gel extraction kit according to the manufacturer's protocol. The excised gel was transferred into 1.5 ml microcentrifuge tube. Three volume of QG buffer was added to 1 ml volume of gel (100 mg ~ 100 µl) and the mixture was then incubated at 50°C for 10 min with vortexing the tube every 2-3 min. After the gel was completely dissolved, one gel volume of isopropanol was added to the sample and mixed. The sample was applied to the QIAquick column, centrifuged at 16,500×*g* for 1 min, followed by discarding the

flow-through. For washing, 0.75 ml of PE buffer was added and the column was centrifuged at 16,500×*g* for 1 min. The flow-through was discarded and the column was centrifuged at 16,500×*g* for additional 1 min to completely remove the residual ethanol from PE buffer. The column was placed into a new microcentrifuge tube and 30 µl of EB (10 mM Tris-HCl, pH 8.5) or sterile MilliQ water was added to the center of QIAmembrane to elute the bound DNA. The column was incubated at room temperature for 1 min and centrifuged at 16,500×*g* for 1 min.

4.2.3 Agarose gel electrophoresis of DNA (51)

An appropriate amount of agarose powder was dissolved in 1×TAE buffer (40 mM Tris-HCl, 40 mM acetic acid, 2.5 mM EDTA, pH 8.0) under boiling temperature to ensure the homogeneity of the gel solution. When the gel mixture was cooled down to about 60°C, the mixture was poured into the mold and allowed to cool and solidify at 25°C. DNA sample was mixed with gel-loading dye [15% (w/v) ficoll 400, 0.1% bromophenol blue, 5 mM EDTA] at ratio 1:5 and loaded into a well of the gel submerged in TAE buffer. After electrophoresis was completed, the gel was stained in 2 µg/ml ethidium bromide solution for 5 min and destained in water for 10 min. The DNA patterns were visualized under UV light by the Geldoc® system. The amount of DNA was estimated by comparing the stained DNA bands with the standard DNA markers (λDNA digested with *Hin*dIII or *Bst*EII) of known amounts under UV light. The total DNA in solution was measured using 260 nm-absorbance (A_{260}). One optical density of DNA at 260 nm is about 50 µg/ml of double stranded DNA.

4.2.4 Restriction endonuclease digestion of plasmid DNA (51)

Plasmid DNA was analyzed by restriction endonuclease digestion. The digestion reaction was performed in 20 µl of mixture containing 200-300 ng of plasmid DNA, 1× restriction endonuclease buffer, 5-10 U of restriction endonuclease and double distilled water to a final volume of 20 µl. The reaction was carried out at the recommended temperature and time. The final DNA digestion patterns were analyzed by agarose gel electrophoresis.

4.2.5 Preparation of competent cells by $CaCl_2$ method (51)

An overnight culture of a single colony of *E. coli* in 3 ml LB broth was inoculated into new LB broth at 1:100 dilution and incubated at 37°C until OD_{600} was between 0.3-0.4. The cell culture was chilled on ice for 15 min before 10 ml of culture was transferred into pre-chilled 15-ml tube. The cells were pelleted by centrifugation at 3,000×*g*, 4°C for 10 min. The pellet was resuspended in 5 ml of ice-cold 0.1 M $CaCl_2$, placed on ice for 20 min and then centrifuged at 3,000×*g*, 4°C for 10 min. The cells pellet was resuspended in 1 ml of ice-cold 0.1 M $CaCl_2$ and left on ice for 1 h. Glycerol was added to the cell suspension to 20% (v/v) final concentration. The cell suspension was kept at -80°C. The efficiency of the competent cell was determined by transforming 10 ng of pET-17b into 200 µl of the competent cell suspension.

An aliquot of 200 µl of *E. coli* JM109 or *E. coli* BL21(DE3)pLysS competent cells was mixed with 50 ng *Dpn*I-digested PCR product or 1 ng DNA plasmid and immediately placed on ice for 30 min. The mixture was incubated at 42°C for 90 sec and immediately placed on ice for 5 min. After adding 800 µl of LB-broth, the transformed cells were incubated at 37°C for 1 h with shaking. An aliquot of the culture (200 µl) was spread on LB-agar plate containing 100 µg/ml ampicillin (for *E. coli* JM109) or 100 µg/ml ampicillin and 34 µg/ml chloramphenicol [for *E. coli* BL21(DE3)pLysS] and then incubated at 37°C overnight. The recombinant clones were verified by restriction analysis (*see* **Method 4.2.4**).

4.2.6 Protein expression

E. coli BL21(DE3)pLysS harbouring each expression plasmid was inoculated in 3 ml LB broth with 100 µg/ml ampicillin and 34 µg/ml chloramphenicol and incubated at 37°C with shaking at 200 rpm overnight. 1% inoculation of overnight culture was inoculated into a new flask of LB broth containing 100 µg/ml ampicillin and 34 µg/ml chloramphenicol and incubated with agitation at 30°C to OD_{600} of 0.5-0.6. Toxin expression was induced with isopropyl-β-D-thiogalactopyranoside (IPTG) at a final concentration of 0.1 mM for another 6 h. The culture was harvested by centrifugation at 5,000×*g* for 10 min. 1 OD_{600} (10^8 cells) of the *E. coli* cell culture was

collected to analyze protein profiles on sodium dodecyl sulphate-polyacrylamide gel electrophoresis (SDS-PAGE).

4.2.7 Sodium dodecyl sulphate-polyacrylamide gel electrophoresis (SDS-PAGE) (51)

Protein sample was prepared by mixing the sample with 4× loading buffer (60 mM Tris-HCl pH 7.5, 2% SDS, 10% glycerol, 0.025% bromophenol blue, 100 mM DTT) in 3:1 (v/v) ratio and boiled at 100°C for 5 min. The heated sample was vigorously mixed using vortex and centrifuged at 10,000×*g* for 10 min to precipitate any insoluble materials. Supernatant equivalent to 0.1 OD_{600} of the cell culture was loaded into each well in the casted polyacrylamide gel for SDS-PAGE analysis.

SDS-PAGE was performed using the Bio-Rad Mini-Protean II system. SDS-PAGE gel system is composed of separating and stacking gels. The separating gel consisted of 3% cross-linker (bis-acrylamide), 10% or 12% acrylamide, 0.375 M Tris-HCl (pH 8.8) and 0.1% SDS. The stacking gel contains 3% cross-linker, 5% gel, 0.125 M Tris-HCl (pH 6.8) and 0.1% SDS. The gel was run in Tris-glycine buffer (25 mM Tris, 192 mM glycine, 0.1% SDS) (51). Broad range protein marker (Bio-RAD) was used as a molecular mass standard. Electrophoresis was performed with constant voltage of 100 V/gel at 25°C. After electrophoresis, the protein bands on the gel were visualized by 1 h-soaking in staining solution containing 50% ethanol, 10% glacial acetic acid and 0.1% Coomassie brilliant blue R-250 in water. The gel was then soaked in destaining solution (10% ethanol and 10% glacial acetic acid) overnight or until the background was clear.

4.2.8 Protein concentration assay (52)

Protein concentrations were determined with the Bio-RAD protein assay reagent, based on the method described by Bradford (52). The calibration curve was constructed with bovine serum albumin (BSA) as a protein standard. BSA standards were prepared by making dilution ranging from 1, 2, 3, 4 and 5 µg/50 µl of BSA in distilled water. Each standard protein and sample solution were mixed with 200 µl of dye reagent (Bradford reagent) in a 96-well flat bottom microtiter plate (Maxi®sorb,

NUNC). The solution was mixed and incubated at 25°C for 10 min. The absorbance of samples and standards were measured at 595 nm with a SpectraMAX 250 ELISA plate reader (Molecular Device). The protein concentrations of samples were calculated from the standard curve.

4.2.9 Preparations of soluble and refolded CyaC proteins

For preparation of soluble CyaC, the supernatant was subsequently centrifuged at 18,000×*g*, 4°C for 20 min. The initial purification of the 21-kDa soluble CyaC protein was accomplished by using a cation-exchange FPLC system (8-ml Mono S column; GE Healthcare). The column was equilibrated with buffer A (25 mM HEPES, pH 7.0) containing 1 mM 1,4-dithiothreitol (DTT). Chromatographic separations were achieved with an increasing step gradient of buffer B (1M NaCl in buffer A, 1 mM DTT) [20%B (5 column volumes), 20-30%B (2.5 column volumes) and 30-100%B (2.5 column volumes)]. Elution fractions across 700 mM NaCl-peak were pooled and subjected to further purification by hydrophobic interaction chromatography (5-ml HiTrap™ Phenyl HP column, GE Healthcare). The column was equilibrated with buffer A containing 2 M NaCl. Elution was achieved via stepwise decreased concentrations of NaCl (from 2 to 0 M) in buffer A. Subsequently, the eluted fraction of 2 M NaCl was loaded onto a size-exclusion FPLC system (25-ml Superdex™75 10/300 GL column) equilibrated with buffer A at flow rate of 0.4 ml/min. Eluted peak fractions containing the 21-kDa protein were pooled and concentrated by ultrafiltration at 4°C in a 50-ml Centriprep column (10-kDa cutoff, Amicon). Purified CyaC protein was analyzed for its purity by SDS-PAGE (12% gel).

For preparation of refolded CyaC, insoluble inclusions were washed with 80 mM K_2HPO_4 (pH 6.5), 0.8 M NaCl, 0.1% Triton X-100 at 4°C, followed by twice washing with cold distilled water. CyaC inclusions (1-5 mg/ml) were solubilized in 20 mM Tris-HCl (pH 8.0), supplemented with 8 M urea at room temperature for 1 h. After centrifugation at 18,000×*g*, 4°C for 20 min, the urea-unfolded CyaC protein was initially refolded in a Superdex™75 column equilibrated with refolding buffer (20 mM Tris-HCl (pH 8.0), 2 M urea, 150 mM NaCl) at a flow rate of 0.4 ml/min. Urea in the eluted fraction containing refolded monomeric CyaC was removed by stepwise

dialysis against 300 volumes of 20 mM Tris-HCl (pH 8.0) and 150 mM NaCl with decreasing urea concentrations of 1 and 0.5 M at 4°C for 4 h at each step, and finally dialyzed twice against the same buffer without urea. The refolded CyaC protein obtained after centrifugation as above was analyzed by SDS-PAGE (12% gel). The identities of the purified soluble or refolded 21-kDa CyaC proteins were then verified by mass spectrometric analysis (*see* **Method 4.2.11**).

4.2.10 Purification of proCyaA-PF

Initial purification of the 126-kDa CyaA-PF protein was accomplished on an anion-exchange FPLC system (5-ml Hitrap Q HP column, GE Healthcare). The column was equilibrated with buffer A (20 mM Tris-HCl (pH 8.0), 5 mM $CaCl_2$). Chromatographic separations were achieved with a stepwise gradient of buffer B (1 M NaCl in buffer A) at the flow rate of 1 ml/min [45%B (5 column volumes), 55%B (5 column volumes) and 100%B (5 column volumes)]. Elution fractions across 550 mM NaCl-peak were pooled and further purified by size-exclusion FPLC system (25-ml Superdex 200 column, GE Healthcare) equilibrated with buffer A at a flow rate of 0.4 ml/min. Eluted peak fractions containing the 126-kDa protein were pooled and concentrated by ultrafiltration at 4°C using 50-ml Centriprep column (100-kDa cutoff, Amicon). The purity of CyaA protein was analyzed by SDS-PAGE (12% gel).

4.2.11 Mass spectrometric analysis

The expected protein separated by SDS-PAGE (12% gel) was eluted out from the excised gel by soaking with 0.1 M NH_4HCO_3 solution and the eluted protein was subsequently digested with trypsin at a substrate:enzyme ratio of 10:1. Trypsin-generated peptide fragments were separated on a 0.18×100 mm C18 column (Thermo Electron, USA). Two approaches, matrix-assisted laser desorption ionisation time of flight mass spectrometry (Bruker Reflex IV MALDI-TOF-MS) and liquid chromatography-tandem mass spectrometry (Finnigan LTQ Linear Ion Trap Mass Spectrometer, Thermo Electron), were employed to analyze the purified trypsin-generated peptide fragments as performed by the Genome Institute, BIOTEC, Thailand.

4.2.12 Western blot analysis (51)

The gels containing protein samples separated on 10% SDS-PAGE were equilibrated in the transfer buffer (39 mM glycine, 48 mM Tris-HCl (pH 9.2), 0.0375% SDS, 10% methanol) for 10 min. One piece of nitrocellulose membrane and 8 pieces of filter paper per one gel were cut to the same size as the gel. The membrane and filter papers were equilibrated in the transfer buffer for 10 min. Protein samples were electrophoretically transferred from the gel to a nitrocellulose membrane using a semidry blot apparatus (Trans-blot SD, Bio-Rad). A sandwich placed on the graphite electrode was made with the 4 pieces of filter paper, the nitrocellulose membrane, the SDS-PAGE gel and then another 4 pieces of filter paper. The electroblotting was carried out at constant current of 3×mA per cm^2 of gel for 1 h. Then, the nitrocellulose was washed in 1× PBS buffer (120 mM NaCl, 16 mM Na_2HPO_4, 4 mM KH_2PO_4, pH 7.4). To pre-block the non-specific binding of antiserum, the membrane was immersed in Blotto solution (5% skim milk in 1× PBS buffer) at 25°C for 2 h with rocking. To detect the CyaA-PF toxin, the primary antibody, mouse anti-RTX toxin monoclonal antibody-9D4 which is specific to the RTX epitope of CyaA (Listlabs, USA) was added into the same blocking solution at the 1:4,000 dilution and incubated with rocking at 25°C for 2 h. To detect the CyaC band, the primary mouse anti-CyaC polyclonal antibody (kindly provided by Rungpragayphan S., Silpakorn University, Thailand) was used as the primary antibody at 1:700 dilution. The membrane was washed 3 times with 1× PBS-0.1% Tween-20 (PBS-T) for 10 min each. After that, the membrane was incubated with the secondary antibody (alkaline phosphatase conjugated anti-mouse IgG) in 1× PBS-5% skim milk at a 1:20,000 dilution at 25°C for 2 h. The membrane was then washed once with PBS-T and 3 times with 1× PBS for 10 min each. The membrane was incubated in carbonate buffer (100 mM $NaHCO_3$, 1 mM $MgCl_2$, pH 9.8) containing the developer solution [5-bromo-4-chloro-3-indolyl phosphate/nitroblue tetrazolium (BCIP/NBT)] until blue-black bands were seen. After the color reaction was completed, the membrane was rinsed with distilled water and kept dry in dark place.

4.2.13 *In vitro* activation of proCyaA-PF by CyaC

Toxin activation *in vitro* mediated by CyaC was performed by mixing 10 µg of purified CyaC monomer with *E. coli* cell lysate (~1 mg total proteins) containing ~10 µg proCyaA-PF (~1% of the total cell proteins evaluated by densitometry) and cytosolic acylating factors (fatty acids and acyl-ACP). The mixture was adjusted to 1-ml with hemolysis buffer (25 mM HEPES (pH 7.4), 150 mM NaCl and 3 mM $CaCl_2$) and reacted at 37°C for 30 min.

To use *p*-nitrophenyl derivatives as the source of acyl donors, the *in vitro* CyaA-PF activation reaction was set up by mixing 10 µg purified proCyaA-PF and 15 µg purified CyaC with various concentration of *p*-nitrophenyl derivatives. The activation reaction was pre-incubated in 1 ml of Tris-buffered saline (TBS) buffer (20 mM Tris-HCl (pH 7.4), 150 mM NaCl and 5 mM $CaCl_2$) at 37°C for 5 min. The activation mixture was subsequently tested for hemolytic activity of the acylated CyaA-PF protein.

4.2.14 Hemolytic activity assay (53)

Sheep whole blood was centrifuged at 1,500×*g*, 4°C for 10 min to pellet the red blood cells. Packed sheep erythrocytes were washed 2 times and resuspended in TBS buffer. Then, 10-µl resuspended sheep erythrocytes (10^9 cells) were added to 1-ml activation mixture. The assay mixture was incubated at 37°C for 6 h and then centrifuged at 10,000×*g* for 2 min to remove unlysed cells. Hemoglobin released in the supernatant was measured at OD_{540}. Spontaneous hemolysis of the negative control sample was determined by incubating cells in buffer alone. The OD_{540} value corresponding to complete hemolysis was obtained by lysing the erythrocytes with 0.1% Triton-X 100, and used as a positive control. Percentage of hemolysis was calculated by {[OD_{540} sample−OD_{540} negative control]/[OD_{540} of 100% hemolysis −OD_{540} negative control]}×100. The results were the mean of at least three independent experiments performed in duplicate for each reaction.

4.2.15 Enzymatic assay

To determine whether CyaC could exert esterase activity, pNPA and pNPP were used as chromogenic substrates for the assay of ester-bond hydrolysis. Esterolytic reaction was determined from the formation of *p*-nitrophenol (pNP) product (**Figure 4.2**) by measuring OD_{400} (ε = 11.6 $mM^{-1}cm^{-1}$) (54) with a SoftMax Pro spectrophotometer (0.7-cm light-path). The assay was conducted on a 96-well flat bottom microtiter plate (Maxi®sorb, NUNC).

Specific activity was calculated by using purified CyaC (4.5 µg) added to 300 µl of 50 mM Tris-HCl (pH 7.4) containing 1 mM pNPA (1% (v/v) final acetonitrile concentration) or 100 µM pNPP (5% (v/v) final isopropanol concentration). The reaction was performed simultaneously with a CyaC-free blank as a control. The rate of reactions (ΔA_{400nm}/min) at the maximum linear rate for both the test and blank were converted to specific activity according to the following formula.

$$\textbf{Specific activity (µmol/min/mg)} = \frac{(\Delta A_{400nm}\text{ /min Test} - \Delta A_{400nm}\text{ /min Blank})\ (1000)}{(11.6)\ (\text{mg enzyme/ml RM})}$$

1000 = Conversion to micromoles
11.6 = Millimolar extinction coefficient ($mM^{-1}cm^{-1}$)
RM = Reaction Mixture

The amount of enzyme liberating 1 µmol of pNP per min under the conditions used was defined as one enzyme unit (U). Specific activity (µmol/min/mg protein or U/mg protein) of ester bond hydrolysis was used to determine the activity of each protein sample in comparison with α-chymotrypsin (TLCK treated, type VII from bovine pancreas, Sigma). Enzymatic activity was assayed in duplicate for three independent experiments.

4.2.16 *In vitro* kinetic studies

Reaction velocities were performed using a constant concentration of enzyme at 15 µg/ml (730 nM) in 50 mM Tris-HCl (pH 7.4) at 25°C. Steady-state kinetics were recorded by varying the concentrations of *p*-nitrophenyl derivative substrates from 10 µM – 500 µM in the presence of 5% (v/v) isopropanol. Kinetic parameters (K_m and V_{max}) were determined from non linear fitting of untransformed data to a Henri-Michaelis-Menten equation (eq.) by GraphPad Prism 5 (GraphPad software, San Diego, CA, U.S.A.):

$$v_o = V_{max}[S] / (K_m + [S]) \qquad \text{(eq.)}$$

where v_o is the observed initial velocity, V_{max} is the maximal velocity, [S] is the substrate concentration, and K_m is the Michaelis constant. The catalytic constant (k_{cat}) and the catalytic efficiency (k_{cat}/K_m) were calculated by using the active enzyme concentration.

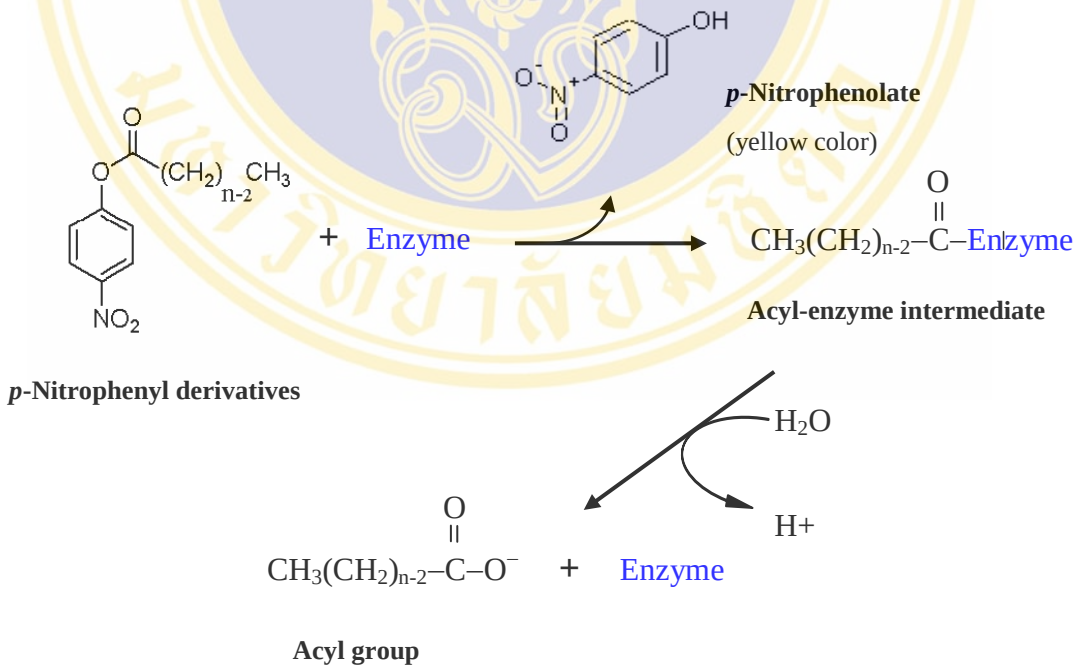

Figure 4.2 Enzymatic activity assays *via* hydrolysis of *p*-nitrophenyl ester bond

These observations have been interpreted in terms of a two-stage reaction sequence in which the enzyme (1) reacts with the *p*-nitrophenyl derivatives to release *p*-nitrophenolate ion forming a covalent acyl-enzyme intermediate that (2) is hydrolyzed to release acyl group.

4.2.17 Ligand binding assay

The ligand binding assay of CyaC was measured by intrinsic fluorescence emission techniques. Binding of palmitate to CyaC was measure by fluorescence quenching at 345 nm upon excitation at 293 nm. Fluorescence spectra were recorded with a fluorescence spectrophotometer (Hitachi F-4500; Taiwan). For the titration experiment, 25 μM CyaC was instantly incubated with various proportions of substrate (0-500 μM) at pH 8.0, 25°C. The change in fluorescence intensity was assumed to depend on the amount of protein-ligand complex, which allowed the calculation of *a*, the fraction of unoccupied ligand binding site on the protein: $a = (F-F_{sat})/(F_0- F_{sat})$. Here, *F* is the fluorescence intensity at a certain titration ratio, F_{sat} is the corrected fluorescence intensity of CyaC solution with its sites saturated, and F_0 is the initial corrected fluorescence intensity. These data were then used to construct a plot of $P_T a$ versus $R_T a/(1-a)$ according to the equation: $P_T a = (1/n)[R_T a/(1-a)] – K_d^{app}/n$, where P_T is the total protein concentration, n is the number of binding sites per molecule, R_T is the total substrate concentration, and K_d^{app} is the apparent dissociation constant.

4.2.18 Circular dichroism (CD) analysis

CD measurements of the 21-kDa FPLC-purified CyaC protein were performed on a Jasco J-715 CD spectropolarimeter in far UV region (190-280 nm) at 25°C using a rectangular quartz cuvette (0.2-mm optical path-length). Samples were prepared in 20 mM Tris-HCl (pH 8.0) with protein concentrations of 0.4 mg/ml. CD spectra were recorded at a scanning rate of 20 nm/min with a 2-nm spectral bandwidth and 2-ms response times. After background subtraction, CD signals (mdeg) averaged from five measurements were converted into mean residue ellipticity ($deg \cdot cm^2 \cdot dmole^{-1}$) by the following formula: $\Delta\varepsilon = (\theta) \times 10^6/(c \times d \times mdeg_{CSA290})$; where θ is the measured ellipticity (millidegrees), c is the sample concentration (M), $mdeg_{CSA290}$ is milidegrees of standard CSA at 290 nm (≅ 42.34), d is the optical path length of the sample cell (cm). Secondary structure contents were estimated from the spectra using CDPro software (55).

4.2.19 Homology-based modeling

Multiple sequence alignments of eight homologous RTX-C proteins were aligned with that of CyaC and known structure of *L*-2,4-diaminobutyric acid acetyltransferase (DABA) (PDB code 3d3s) from *Bordetella parapertussis* by using the ClustalX program (56). Manual adjustment of the alignment, based on inter-sequence checks, was performed to generate the final sequence alignment. A three-dimensional (3D) model of CyaC was generated based on the DABA structure with the WHATIF program (57). Side-chain orientations were replaced by more favorable rotamers based on local backbone conformations that were provided in database. Insertion regions in the model relative to DABA template was accomplished by extracting from a short fragment database using the loop-search algorithm (DGINS) in the WHATIF program (57). The entire CyaC structure was initially subjected to energy minimization using GROMOS96 simulation software (58). Packing environments, bond lengths and bond angles were analyzed with the CHECK option in the WHATIF program (57). Stereochemical parameters of the modeled structure were analyzed with the PROCHECK program (59).

4.2.20 Protein crystallization

CyaC protein was initially screened for crystals using the Phoenix crystallization robot (Art Robbins Instruments, NSRRC, Taiwan) and commercially available sparse-matrix screens from Qiagen (Valencia, California, USA) and Hampton Research (Aliso Viejo, California, USA): 10-kit box (96×10 = 960 conditions) including Grid Screens (PEG, ammonium sulfate, DMP and NaCl), Crystal Screen I & II, Wizard I & II, Crystal Screen Lite, Index I & II, Memfac & Natrix, PEG/Ion, SaltRx I & II, Classics Suite and JCSG core I & II.

Robot automatic screening was done by mixing 0.5 μl of the purified protein (~8 mg/ml) with an equal volume of the reservoir solution for 96 well sitting drop plates. The mixture drop was then equilibrated against 100 μl of the reservoir solution at 20°C.

In order to optimize crystal growth conditions, the modified conditions was setup by vapor-diffusion method in hanging drops containing the purified protein (5-10 mg/ml). Hanging drop crystallizations were carried out in 48 well tissue culture plates. A small (2 μl) sample droplet of protein containing buffer (1 μl) and precipitating agent (1 μl) is suspended from a glass microscope coverslip in a well containing a reservoir solution (100 μl) at 20°C.

4.2.21 Crystallographic data collection and processing

Protein crystals were soaked in a cryo-protectant solution containing 20% glycerol before being mounted in a cryo-loop (0.1 mm) and then flash-cooled in liquid nitrogen to 110 K. X-ray diffraction data were collected at beam line BL13B at the National Synchrotron Radiation Research Center (Hsinchu, Taiwan). All diffraction data were processed and scaled with the *HKL2000* package including the *DENZO* and *SCALEPACK* programs, respectively (60). Molecular replacement and refinement procedures were performed using *CNS v1.2* (61).

4.2.22 Site-directed mutagenesis

The method used in this project was based on Stratagene's QuickChange™ Site-directed mutagenesis kit (**Figure 4.3**). The pCyaC or pCyaAC recombinant plasmid containing the *cyaC* genes, which has been cloned into pET-17b vector, was used as a template. The method made use of *Pfu* DNA polymerase, which replicated both strands of DNA plasmid with high fidelity without displacing the mutant oligonucleotide primers. A GeneAmp® PCR System 2400 (Perkin Elmer) was used to perform polymerase chain reactions (PCR) for all samples.

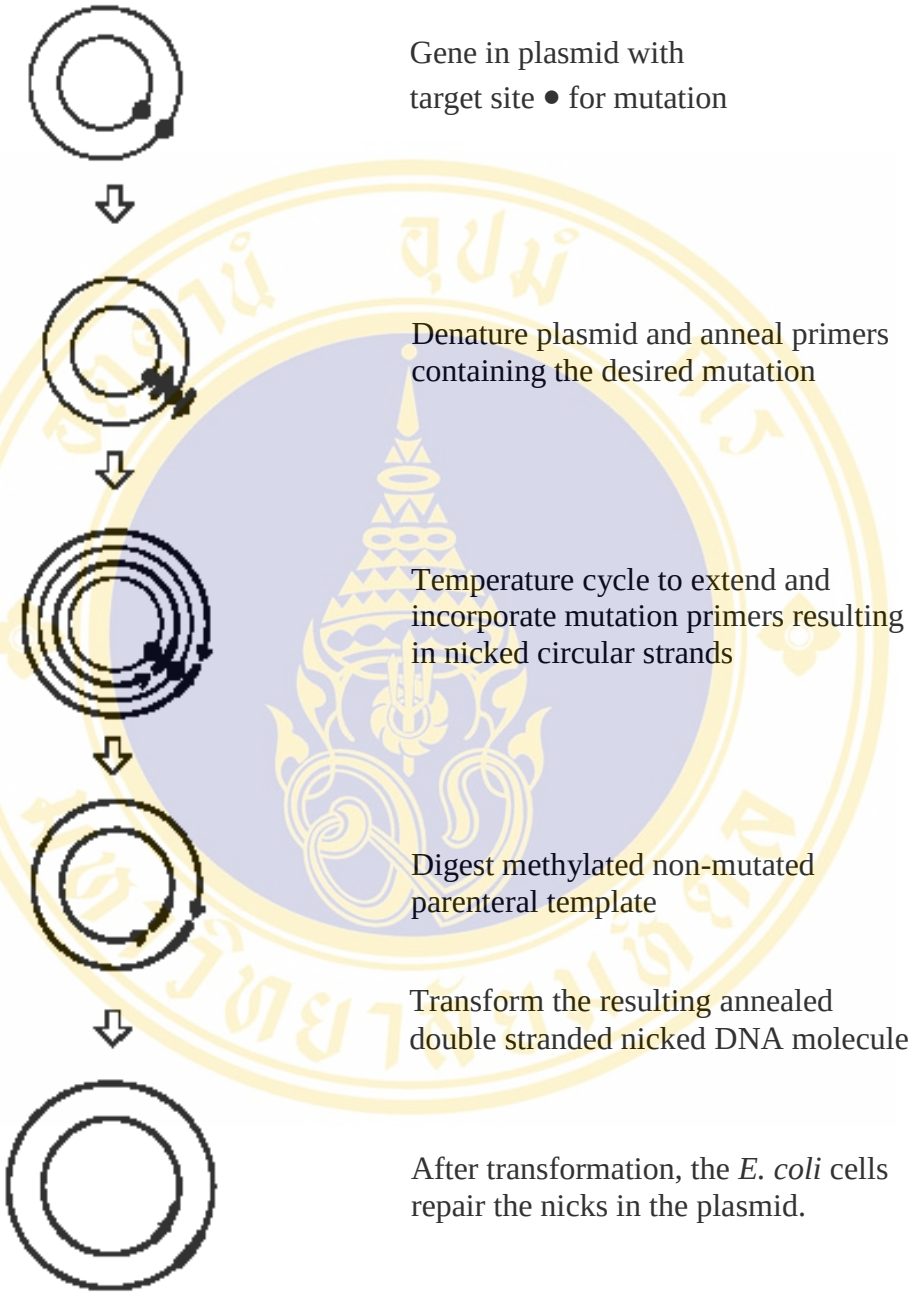

Figure 4.3 Overview of QuickChange site-directed mutagenesis method

The figure shows site-directed mutagenesis method redrawn from Stratagene's QuickChange instruction manual.

4.2.22 PCR conditions

An automated GeneAmp PCR System 2400 thermal cycler (Perkin-Elmer, CA, USA) was used to perform PCR for all samples as conditions shown in **Table 4.1**.

The 50 µl PCR reaction mixture was composed of

DNA template	100	ng
dNTPs	50	µM each
Forward primer	10	pmol
Reverse primer	10	pmol
5x *Phusion* HF buffer	10	µl
DMSO	1.5	µl
Phusion DNA polymerase	0.5	µl (1 U)
Sterile distilled water making total volume to	50	µl

The reaction mixture was carried out with the following conditions as shown in **Tables 4.2 and 4.3**. After the amplification reaction was finished, the PCR products were examined by 0.8% agarose gel electrophoresis.

4.2.24 Digestion of mutated PCR products

Each amplified reaction was added with 1 µl of *Dpn*I restriction endonuclease and incubated at 37°C for 2 h. The *Dpn*I digested the parental DNA template and left only mutated nicked plasmid. *Dpn*I restriction endonuclease is specific for methylated and hemimethylated DNA (5′-G^{me}A↓TC-3′). DNA isolated from almost all *E. coli* strains is *dam* methylated and it would be therefore susceptible to *Dpn*I digestion. The *Dpn*I-digested PCR products were analyzed by 0.8% agarose gel electrophoresis before being transformed into *E. coli* competent cells.

Table 4.2 Temperature cycling parameters for site-directed mutagenesis

Segment	**Temperature** (°C)	**Time** (min:sec)	**Cycles**
1	98	0:30	1
2	98	0:10	25
	T_a*	0:30	
	72	2:30	
3	72	7:00	1

* The annealing temperatures (T_a) are shown in Table 4.3.

Table 4.3 Annealing temperature (T_a) for each mutant

pCyaC mutants	**Annealing temperature** (°C)	**pCyaAC-PF mutants**	**Annealing temperature** (°C)
S30A	60	S30A	62
H33A	50	H33A	53
Y66A	60	Y66A	60

4.2.25 Transformation of mutant plasmid DNA into competent cells

The 50 ng *Dpn*I-digested PCR product was mixed with 200 µl of *E. coli* JM109 competent cells. The mixture was immediately chilled on ice for 30 min, following by incubation at 42°C for 90 sec, and then immediately placed on ice for 5 min. An 800 µl aliquot of LB broth was added into the transformed cells, gently mixed and incubated at 37°C for 1 h. Transformed cells were collected by centrifugation at 2,000×*g* for 2 min. Medium was decanted and the cell pellet was gently resuspended in 200 µl of LB broth. The transformed cells were spread gently over the surface of the LB agar plate containing 100 µg/ml ampicillin by a sterile glass rod. The agar plate was incubated at 37°C for 16 h until *E. coli* colonies were clearly seen on the agar plate.

4.2.26 Screening for mutant plasmids

Restriction endonuclease analysis was used to screen for each mutant plasmid based on a recognition site which is silently introduced into each pair of mutagenic oligonucleotide primers. The 20 µl digestion reaction was composed of 1 µg of DNA sample, 1× restriction enzyme digestion buffer, and approximately 5 U of restriction endonuclease and sterile distilled water to make up to the 20 µl total volume. The digestion reaction was incubated at 37°C for 2 h with appropriate enzymes. The recommended restriction enzyme digestion buffers were supplied by the enzyme manufacturers. To visualize the restriction patterns, electrophoresis of the digested DNA was carried out in a horizontal 0.8% agarose gel in TBE buffer at 100 V for 1 h. The agarose gel was stained with ethidium bromide (2 mg/ml) for 5 min and destained with large volume of water. DNA patterns were visualized under UV light and digitalized by Geldoc® system from Bio-RAD.

4.2.27 DNA sequencing analysis of the mutant plasmids

To confirm the resulting mutation, a BigDye™Terminator Cycle Sequencing Kit (Perkin-Elmer, USA) was used to prepare samples for sequence analysis based on fluorescent-labeled terminator cycle sequencing. Each CyaC mutant was expressed, purified and characterized according to the method described above for the wild type.

CHAPTER V
RESULT I:
EXPRESSION, PURIFICATION AND FUNCTIONAL CHARACTERIZATION OF CyaC-ACYLTRANSFERASE

Several studies have clearly shown that the 170-kDa CyaA protoxin (proCyaA) essentially requires CyaC-acyltransferase as an accessory protein for toxin activation *via* post-translational acylation to become an active toxin (5, 6). Recently, it has been shown that only the 126-kDa CyaA-pore forming (PF) domain (without the AC domain) co-expressed with CyaC in *E. coli* was able to be *in vivo* palmitoylated at Lys^{983} to become hemolytically active (15). In the present study, the functional and structural details of the CyaC-acyltransferase using the CyaA-PF fragment as a target of toxin acylation were further investigated *in vitro*.

5.1 Expression of the CyaC, proCyaA-PF and CyaA-PF proteins

CyaC, proCyaA-PF and CyaA-PF were expressed in *E. coli* strain BL21(DE3)pLysS harboring recombinant plasmid either pCyaC, pCyaA-PF or pCyaAC-PF, respectively, utilizing the T7 promoter. The expression was achieved after 6 h-induction with 0.1 mM IPTG at 30°C.

The 21-kDa CyaC protein (theoretical pI/MW: 9.25/20,510.31) was produced as inclusions (~100 mg/liter of culture) together with small amount of the soluble form (≤5 mg/liter of culture) (**Figure 5.1A**). It is noteworthy that the soluble fraction could not be increased by reducing cultivation temperature (to 25°C or 18°C) that is dissimilar to what has been observed for other proteins (62).

The 126-kDa proCyaA-PF protein (theoretical pI/MW: 4.34/126,188 was expressed almost exclusively as soluble protein (~10 mg/liter of culture) (**Figure 5.1B**,

lane 1). In addition, the recombinant clone containing pCyaAC-PF was able to express both the 126-kDa CyaA-PF and 21-kDa CyaC proteins as soluble proteins (**Figure 5.1B,** lane 2). This clone represents the CyaA-PF toxin activated by CyaC *in vivo*. It should be noted that either the 126-kDa recombinant CyaA-PF protein expressed in the absence or presence of CyaC-acyltransferase was found almost exclusively in the soluble fraction (**Figure 5.1B**, lanes 1 and 2).

5.2 Purification of the soluble CyaC protein

Despite of its low expression, the soluble CyaC portion was able to activate proCyaA-PF *in vitro* as shown by toxin activity against sheep erythrocytes (**Figure 5.2**). Therefore, the soluble CyaC protein was presumed to adopt a native-folded form.

The soluble CyaC was purified using three-consecutive chromatographic techniques. The protein was predominantly eluted from cation-exchanger at concentration of 700 mM NaCl (**Figure 5.3**), subsequently eluted from HIC with 2 M NaCl (**Figure 5.4**) and finally eluted from gel filtration (GF) column as a single peak with molecular weight corresponding to 21-kDa. The purified soluble CyaC existed as a monomer, achieved ~90% purity with and ~20% yield recovery (~1 mg/liter of culture), as analyzed by SDS-PAGE (**Figure 5.5**). This optimized purification allowed to obtain sufficient amounts of the purified soluble CyaC protein for subsequent investigations of its properties.

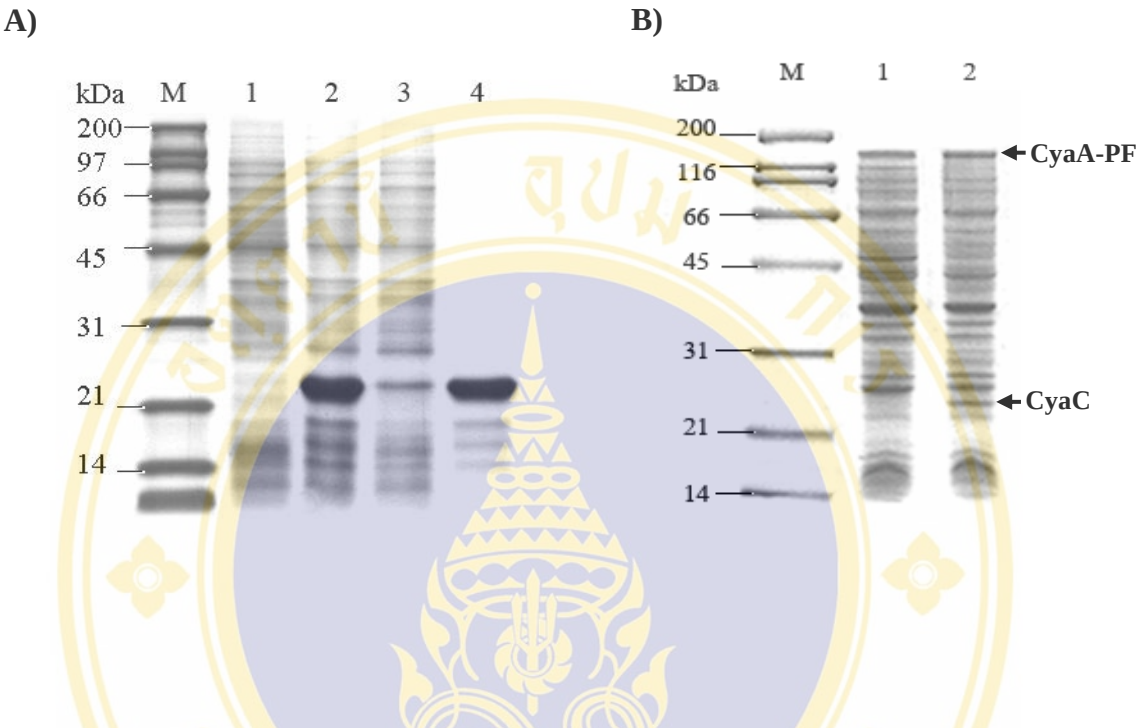

Figure 5.1 SDS-PAGE (Coomassie blue-stained 12% gel) of cell lysate from *E. coli* containing the 21-kDa CyaC, 126-kDa proCyaA-PF and 126-kDa CyaA-PF proteins

(A) Soluble and insoluble fractions of CyaC. Lanes 1 and 2 are whole cell lysates harboring pET-17b and pCyaC, respectively. Lanes 3 and 4 are supernatant and pellet fractions, respectively, obtained after centrifugation of the lysate from lane 2.

(B) Soluble fractions of proCyaA-PF and CyaA-PF. Lanes 1 and 2 are soluble fractions of lysate harboring pCyaA-PF and pCyaAC-PF, respectively. M represents molecular mass standards.

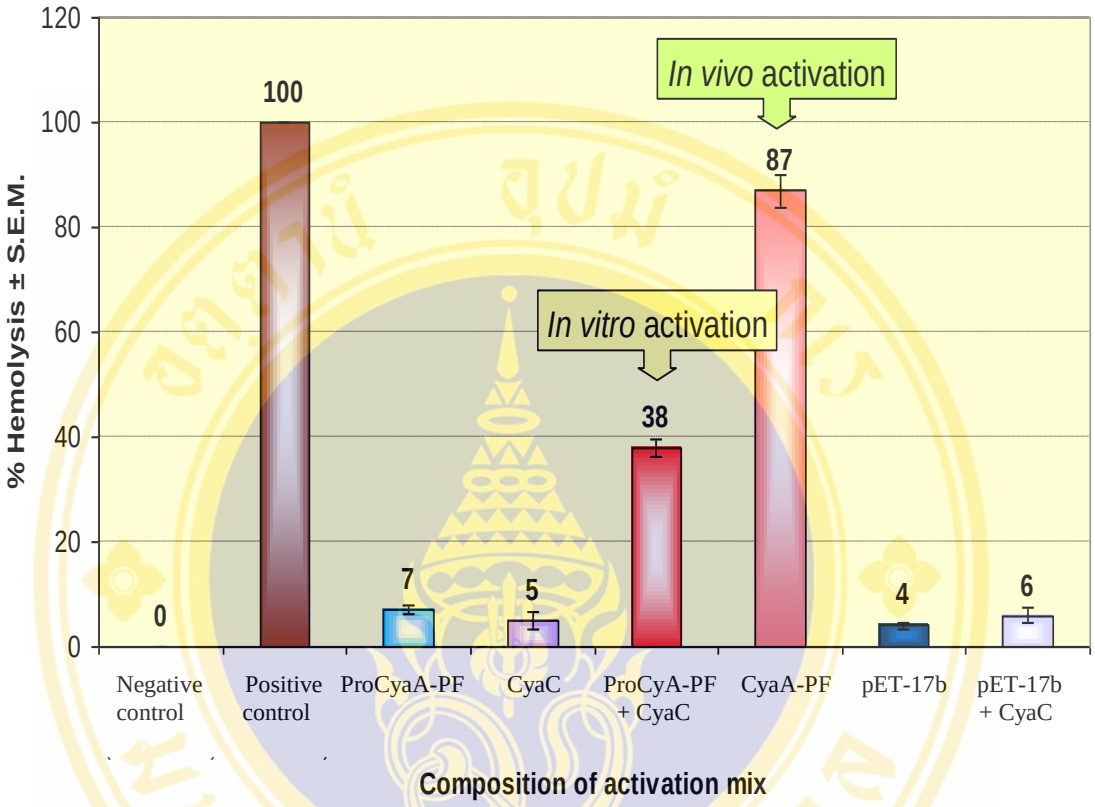

Figure 5.2 Hemolytic activities of soluble CyaC fraction activated CyaA-PF toxin

Compositions of activation mix were incubated with sheep red blood cells (10^9 cells/ml) in hemolysis buffer at 37°C for 6 h. ProCyaA-PF, CyaC and CyaA-PF represent the soluble fraction of crude lysate proteins. Error bars indicated standard errors of the mean from three independent experiments.

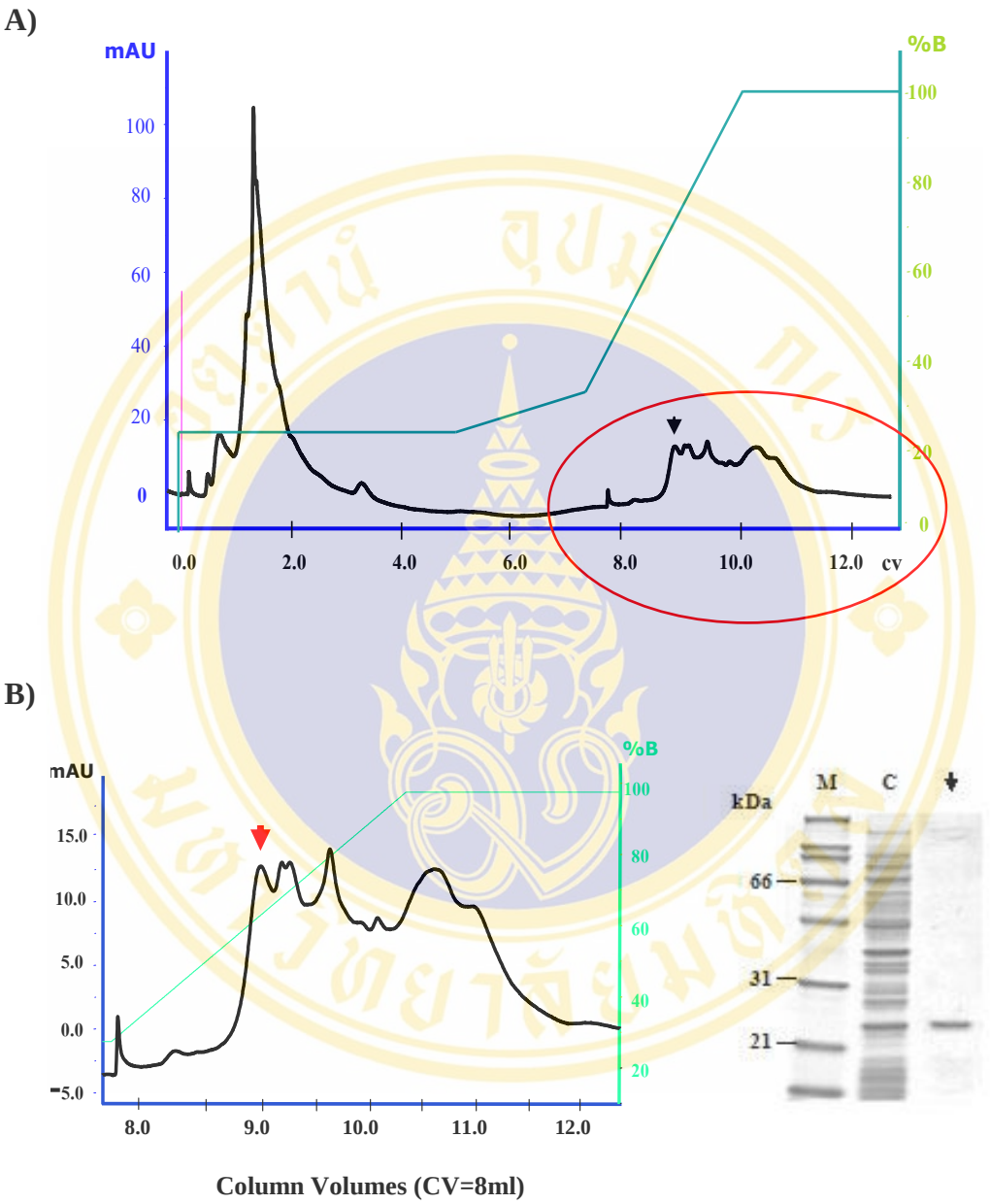

Figure 5.3 Cation-exchange FPLC chromatogram of the purified soluble CyaC protein

(A) Chromatographic elution profile from the cation exchange FPLC system (8-ml Mono S column) with an increased step gradient of buffer B (1M NaCl) in 25 mM HEPES (pH 7.0) [20% B (5 CV), 20-30% B (2.5 CV), 30-100% B (2.5 CV) and 100% B (2.5 CV)].

(B) Magnified scale of the encircled area in (A) of the chromatographic elution profiles of CyaC fractions. The indicated peak is the CyaC fractions eluted across 700 mM NaCl. Inset, 12% SDS gel of the eluted CyaC fraction.

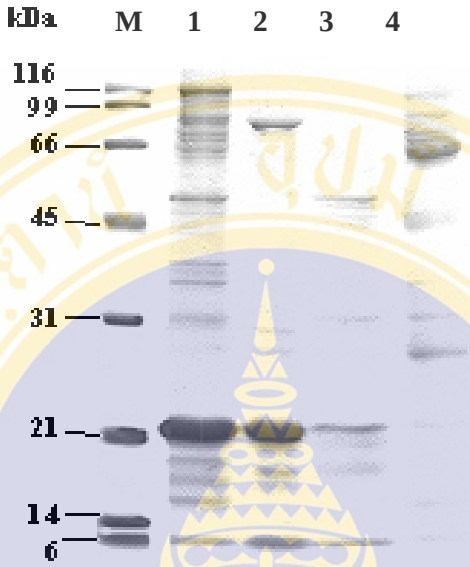

Figure 5.4 Purification of eluted CyaC fraction by HIC

Elution was achieved *via* step gradient of decreasing concentrations (NaCl 2 to 0 M), in 25 mM HEPES, pH 7.0. Lane 1 is the pool factions (8.8-9.0 CV) from cation exchange chromatography. Lanes 2, 3 and 4 are the eluted fraction from the HIC column at NaCl concentrations of 2 M, 1 M and 0.75 M, respectively.

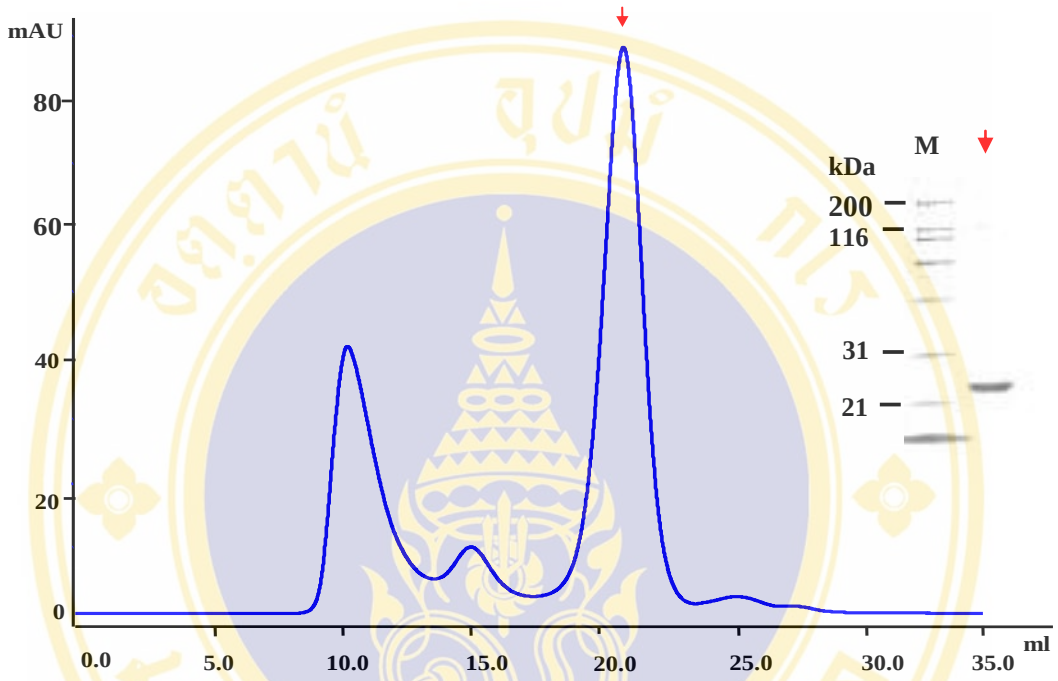

Figure 5.5 Size-exclusion chromatogram of eluted CyaC fractions from partially purified protein from HIC

The chromatographic elution profile from Superdex^{TM}75 column shows absorbance at 280 nm (mAU) and elution volume (ml). Inset, 12% SDS-gel of the selected peak fraction (arrow) containing the 21-kDa purified CyaC monomer. M represents molecular mass standards.

5.3 Purification of the refolded CyaC protein

Attempts were also made to prepare a large quantity of enzymatically active CyaC from the high-yield expressed in inclusions for further crystallization and X-ray crystallographic studies. CyaC inclusion (1-5 mg/ml) was completely dissolved in 8 M urea, at 37°C for 1 h (**Figure 5.6**, lane 1). A fast removal of urea in the refolding step using reciprocal dialysis or a high dilution (10-100 folds) of the unfolded CyaC solution resulted in aggregation of ≥80% of total protein. NaCl was added into refolding solution and successfully suppressed the aggregation.

Herein, one-step reduction of urea to an intermediate concentration (2 M) of the unfolded CyaC solution supplemented with 150 mM NaCl was found to recover a high proportion of refolded monomers (**Figure 5.7**) as observed by size-exclusion chromatography. Thus, this cardinal step allowed to finally obtain the urea-free refolded CyaC protein with ~90% purity and ~70% yield recovery (~70 mg/liter of culture) as analyzed by SDS-PAGE (**Figure 5.8**).

5.4 Identification of the CyaC protein by using LC-MS-MS

The 21-kDa purified protein of both soluble and insoluble fractions were verified to be CyaC-acyltransferase as they contained trypsin-generated peptide sequence that perfectly matched the corresponding CyaC sequence (residues Asp^{35}-Arg^{58}), DWPVHLLARNTLAPIQLGQYILLR, analyzed by LC/MS/MS.

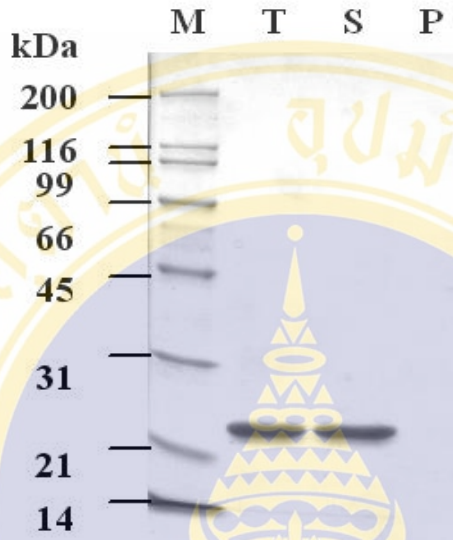

Figure 5.6 Coomassie-stained SDS-PAGE (12% gel) analysis of the urea extracts from insoluble material containing the 21 kDa CyaC protein

Urea extracts were prepared in 50 mM Tris-HCl (pH 8.0), 8 M urea. T, S, P and M represent total protein, soluble protein fraction, insoluble protein fraction and molecular mass standards, respectively.

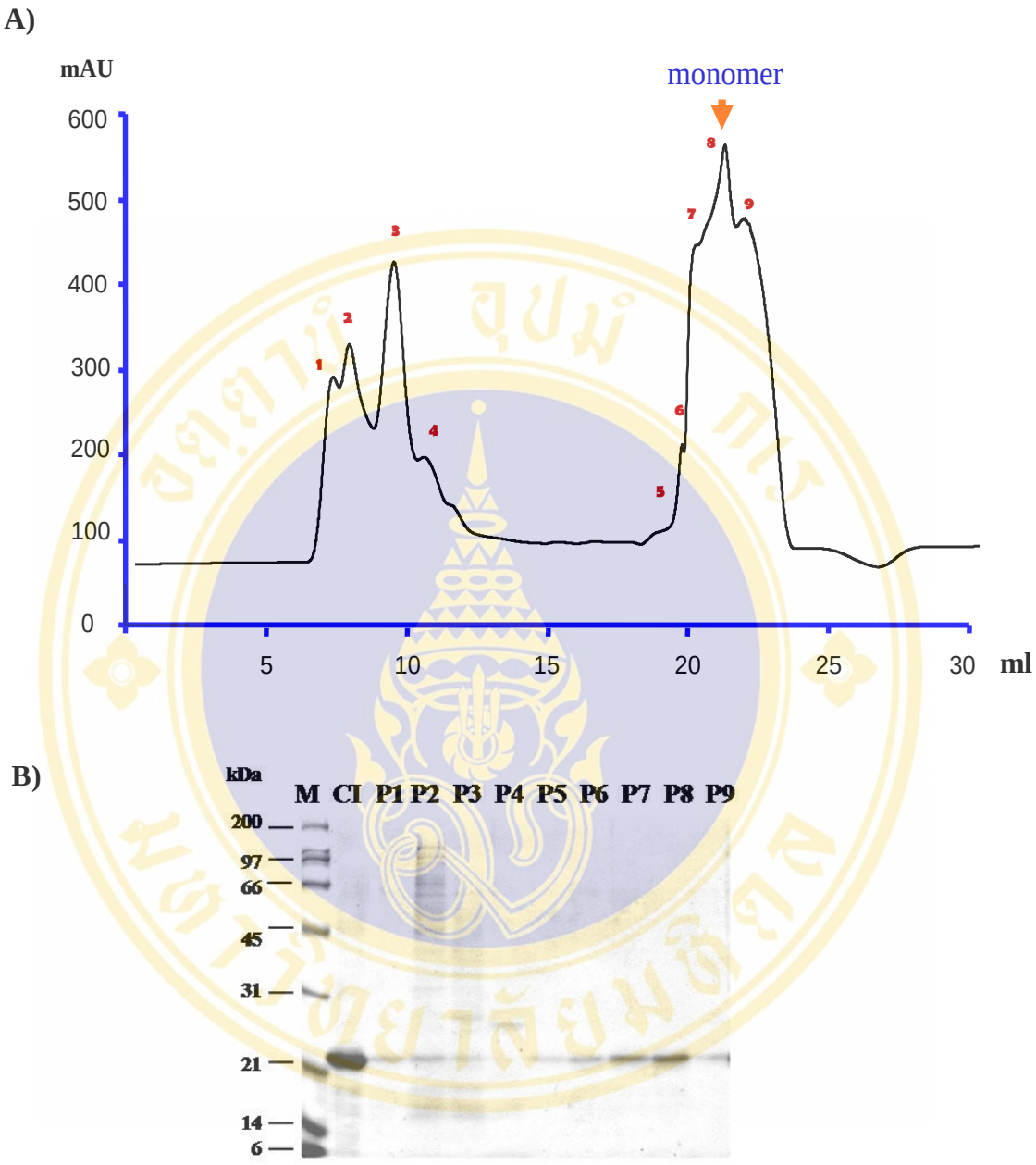

Figure 5.7 Chromatographic elution profile of CyaC refolding in Superdex^{TM}75 column equilibrated with refolding buffer

(A) Chromatographic elution profile from Superdex^{TM}75 shows absorbance at 280 nm (AU) and elution volume (ml). The solubilized CyaC proteins were partially refolded and eluted from a Superdex^{TM}75 column equilibrated with refolding buffer (20 mM Tris-HCl (pH 8.0), 2 M urea and 150 mM NaCl). Elution fractions of corresponding peaks are indicated with numbers.

(B) A 12% SDS-gel of the selected peak fractions (P1-P9), which were collected every 1 ml. M represents molecular mass standards.

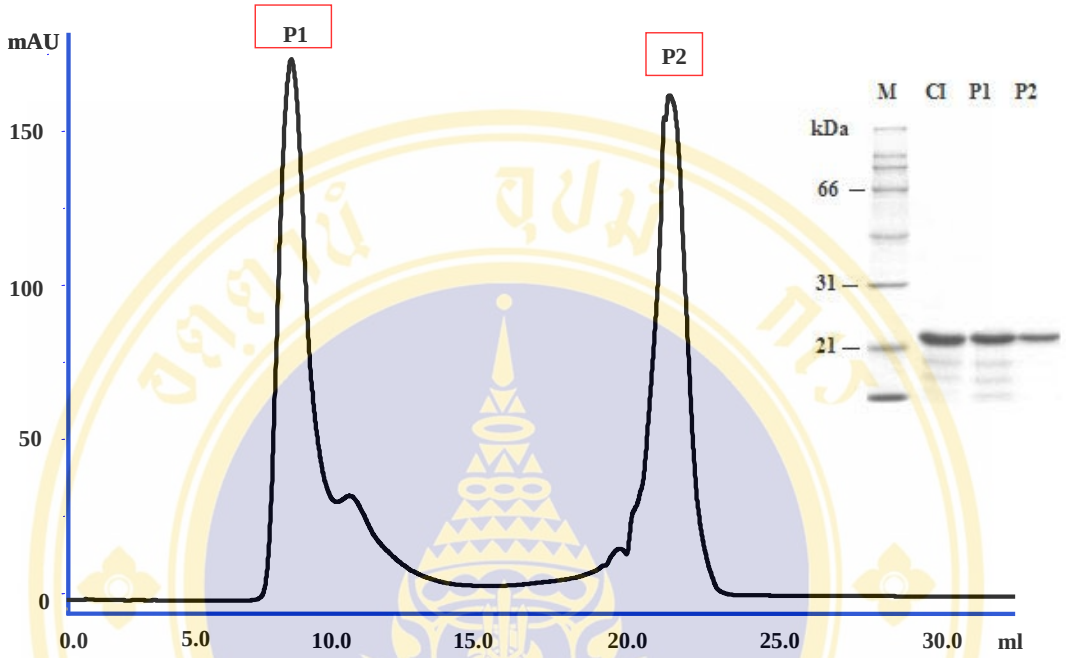

Figure 5.8 Chromatographic elution profile of the pure-refolded CyaC after removal of residual urea from the Superdex^{TM}75 size-exclusion column

Chromatographic elution profile from Superdex^{TM}75, shows absorbance at 280 nm (mAU) and elution volume (ml). CI is the refolded protein after urea step-wise dialysis. P1 and P2 are the final refolded CyaC which separated by gel-filtration Superdex^{TM}75 column equilibrated with 20 mM Tris-HCl (pH 8.0) buffer and 150 mM NaCl into oligomer and monomer, respectively. M represents molecular mass standards.

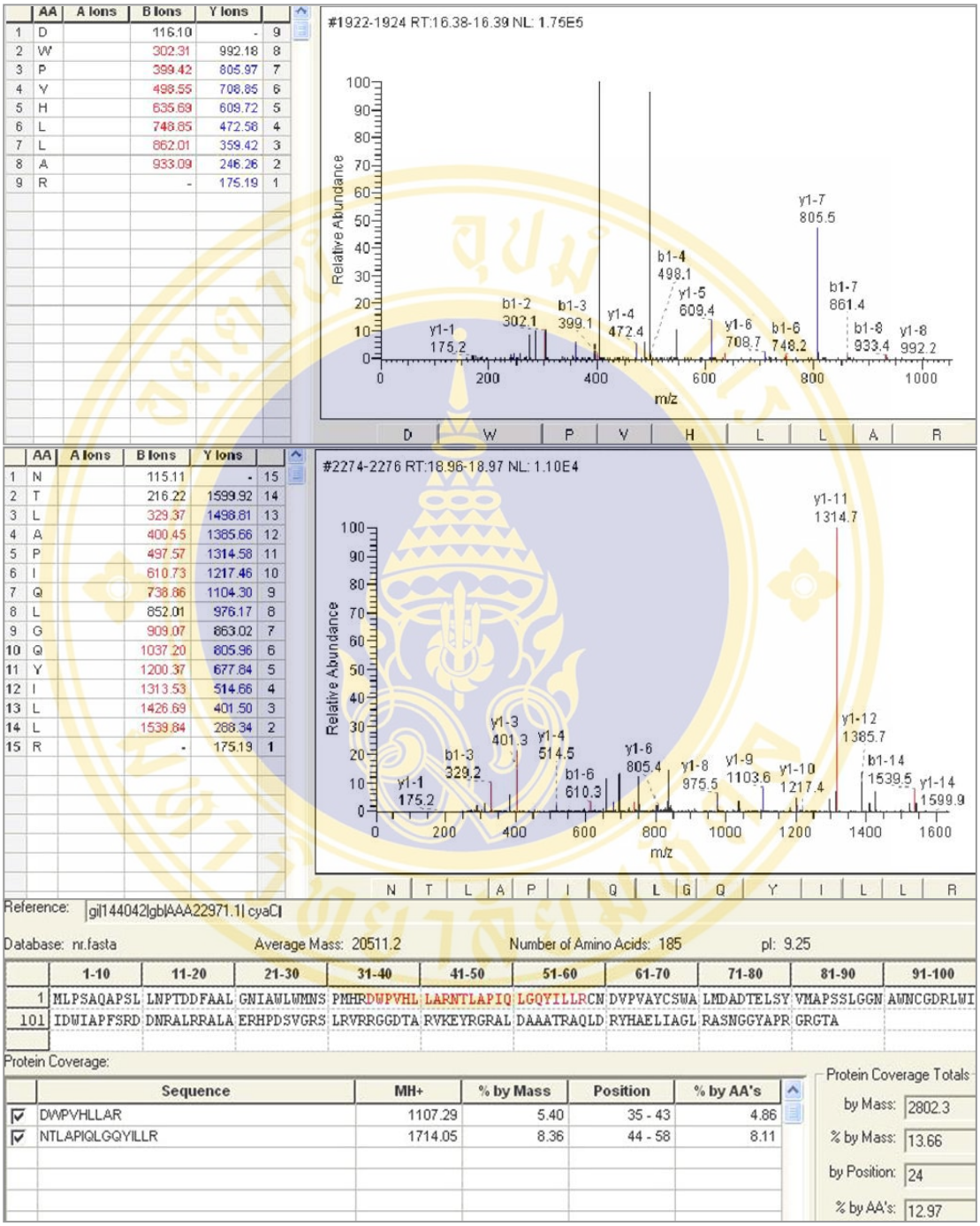

Figure 5.9 LC-MS-MS spectra of the trypsinized peptides of the 21-kDa purified protein

The spectra confirm the amino acid sequences DWPVHLLAR and NTLAPIQLGQYILLR, which perfectly matched the Asp^{35}-Arg^{58} of CyaC, (shown in red), in the database. The *m/z* values of fragment ions (b_i and y_i) were shown.

5.5 Purification of proCyaA-PF proteins

The supernatant of soluble proCyaA fraction was initially subjected to anion-exchange FPLC. Chromatographic separations were achieved with a stepwise gradient of 45% B (4 CV), 55% B (4 CV) and 100% B (4 CV) that is 1 M NaCl, 20 mM Tris-HCl (pH 8.0), 5 mM $CaCl_2$. The peak fractions containing a major protein band of 126 kDa were eluted at a concentration of 550 mM NaCl (55% B) (**Figure 5.10A**). Elution fractions across the 550 mM NaCl-peak from anion exchanger were further purified by gel filtration chromatography. The elution profile from the FPLC revealed that the 126-kDa proCyaA-PF protein was eluted as a single peak (**Figure 5.10B**). The purified soluble proCyaA-PF protein was successfully obtained with ~90% purity and ~30% yield recovery (~3 mg/liter of culture) as analyzed by SDS-PAGE (Figure 5.10). These optimized purification conditions allowed to obtain sufficient amounts of the purified proCyaA-PF protein to be obtained for subsequent investigations of its properties.

5.6 Western blot analysis of proCyaA-PF and CyaC proteins

Western blot analysis was performed to verify the purified proteins. As expected, the purified proCyaA-PF and CyaC were bound to anti-RTX specific monoclonal antibody-9D4 (**Figure 5.11A**), and rabbit anti-CyaC polyclonal antibodies (**Figure 5.11B**), respectively.

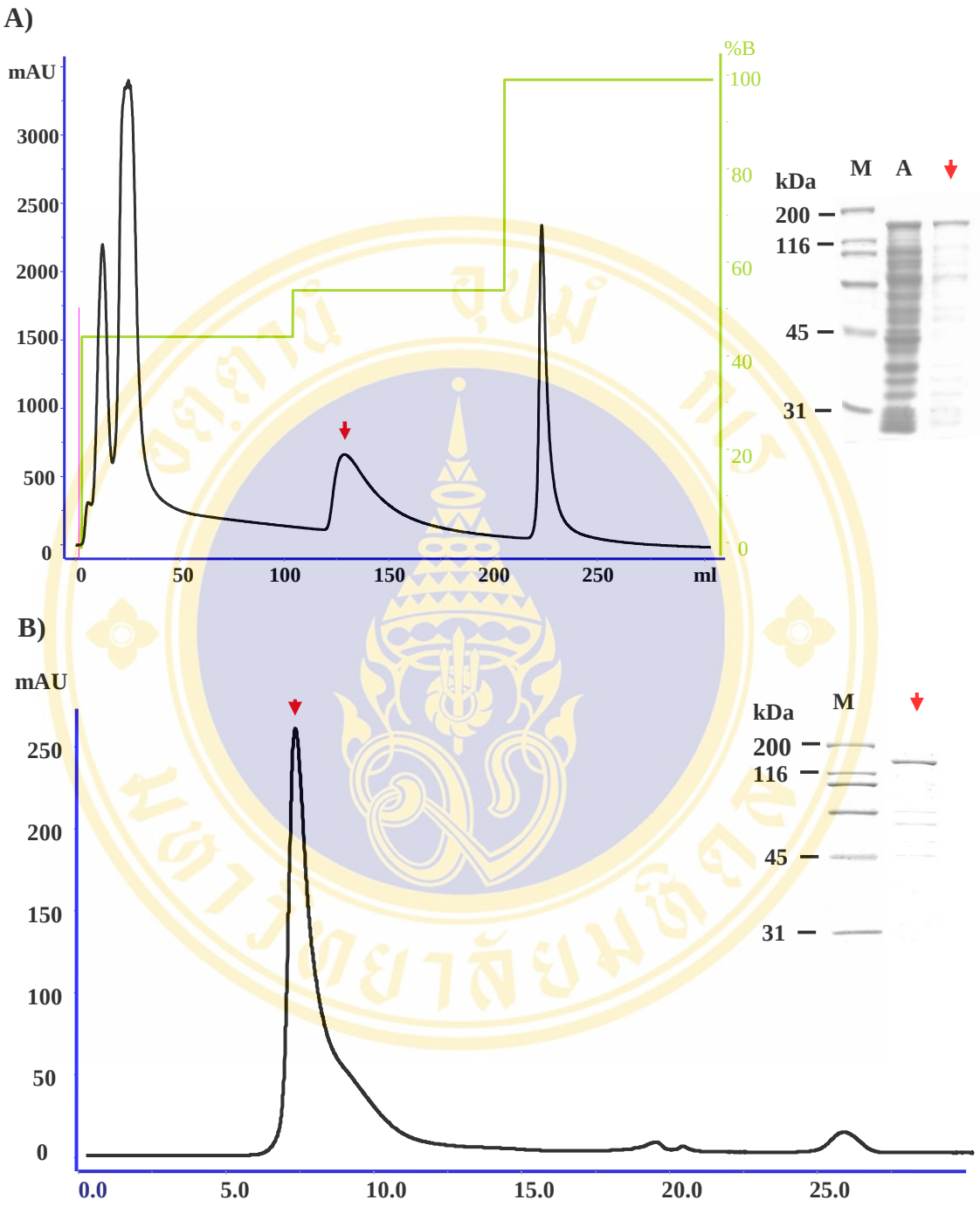

Figure 5.10. Protein purification chromatograms and SDS-PAGE analysis of the proCyaA-PF protein

(A) Chromatographic elution profile from the anion exchange FPLC system (5-ml HiTrapQ column) showing absorbance at 280 nm (mAU), a stepwise gradient of 1 M NaCl (B) [45% B (4 CV), 55% B (4 CV), 100% B (4 CV)] and elution volume (ml).

(B) Elution profiles from Superdex 200 size-exclusion column, showing absorbance at 280 nm (mAU) and elution volume (ml). Inset, SDS-PAGE analysis (Coomassie brilliant blue-stained 12% gel) of the selected peak fraction (arrow) containing the purified CyaA. M represents molecular mass standards.

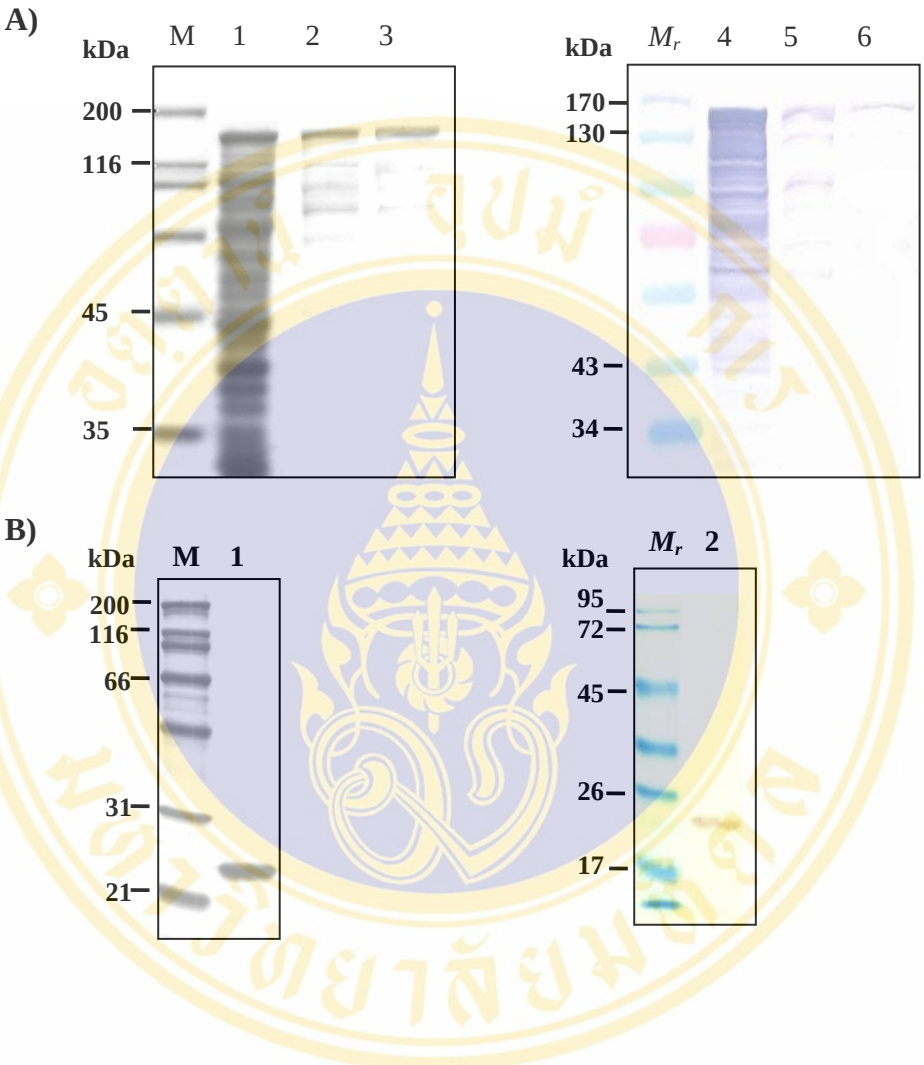

Figure 5.11 Western blot analysis of proCyaA-PF and CyaC proteins

(A) Western blot analysis of proCyaA-PF probed with the anti-RTX monoclonal antibody-9D4 specific to the RTX epitope of CyaA. Lane 1 is the lysate containing proCyaA-PF protein. Lanes 2 and 3 are the purified CyaA-PF protein from anion exchange and gel filtration chromatographies, respectively. Lanes 4, 5 and 6 represent their western blot analysis probed with the anti-RTX monoclonal antibody correspond to lanes 1, 2 and 3, respectively.

(B) Western blot analysis of CyaC probed with rabbit anti-CyaC polyclonal antibody. Lanes 1 and 2 are the purified CyaC protein after refolding and its western blot analysis probed with the rabbit anti-CyaC polyclonal antibody, respectively. M represents molecular mass standards. M_r represents prestained protein ladder.

5.7 Functional characterization of CyaC-acyltransferase

5.7.1 CyaA-PF activation and assessment for hemolysis

Here, proCyaA-PF fragment was used as an acyl acceptor for testing the activating activity of the cloned CyaC protein. The successful activation would result in hemolytically active CyaA-PF that could be detected by hemolytic assay.

When the purified CyaC protein was mixed with the cell lysate containing proCyaA-PF *in vitro*, the mixture showed high hemolytic activity against sheep erythrocytes (~30%), while either the mixture of proCyaA-PF-free lysate with purified soluble CyaC, or the lysate containing proCyaA-PF alone exhibited very weak hemolytic activity (≤5%) (**Table 5.1**).

5.7.2 Hydrolysis of synthetic substrates

It has been shown that some acyl (or acetyl) transferases, e.g. homoserine acyltransferase (63) and arylamine N-acetyltransferase (64), also catalyze a related reaction *in vitro*-namely the hydrolysis of oxygen-ester bond of a non physiological substrate (*i.e.* pNPA). Herein, a spectrophotometric assay was developed for chromogenic detection of esterase activity using two indolyl substrates, which are pNPA and pNPP containing acetyl and palmitoyl (C16:0) units, respectively. Chymotrypsin as its best-known feature of enzyme-catalyzed ester hydrolysis (65) was used as a control in the reaction.

Table 5.2 shows that specific activities of the purified CyaC protein in catalyzing pNPA and pNPP hydrolysis were ~48 U/mg and ~289 U/mg, respectively. Specific activity of the purified CyaC in catalyzing pNPP was much higher than that of pNPA (~6 folds). On the other hand, specific activity of chymotrypsin in catalyzing pNPA was much higher than that of its pNPP hydrolysis (~4 folds).

Table 5.1 *In vitro* activation of CyaA-PF *via* hemolytic activity assays

Reaction mixture[a]	**Hemolytic activity**[b] (% hemolysis ± SEM)
Lysate containing proCyaA-PF + soluble CyaC	31.4 ± 4.6
Lysate containing proCyaA-PF + refolded CyaC	29.4 ± 2.9
ProCyaA-PF-free lysate + soluble CyaC	2.8 ± 0.3
Lysate containing proCyaA-PF	5.0 ± 1.4
Lysate containing CyaA-PF	88.1 ± 6.8

[a] *In vitro* activation reactions were set up by mixing *E. coli* lysate containing ~10 µg proCyaA-PF with 10 µg purified CyaC. Reactions were incubated in HH buffer at 37°C for 30 min.

[b] Samples were incubated with sheep erythrocytes (10^9 cells/ml) in HH buffer at 37°C for 5 h. Percentage of hemolysis was calculated as described in Materials and Methods. The values were averaged from three independent experiments performed in duplicates. SEM represents standard errors of the mean.

Table 5.2 Specific activity of CyaC for hydrolysis of pNPA and pNPP

Substrate	Specific activity[a] (U/mg protein ± SEM)	
	pNPA	**pNPP**
Chymotrypsin	68.5 ± 1.9	16.2 ± 2.0
Refolded CyaC	46.6 ± 1.5	289.4 ± 1.2
Soluble CyaC	49.0 ± 3.2	ND
BSA	3.0 ± 0.7	4.2 ± 1.1

[a] Specific activity of enzyme was obtained using 1 mM pNPA or 100 μM pNPP as the substrate concentration. One unit of enzyme activity is defined as the amount of enzyme liberating 1 μmol of *p*-nitrophenol per min at 25°C. ND is not determined. SEM represents standard errors of the mean.

CHAPTER VI
RESULT II:
KINETIC AND CATALYTIC MECHANISM OF CyaC-ACYLTRANSFERASE

6.1 CyaA-PF activation by using *E. coli* lysate or pNPP

CyaC when supplemented with cytosolic acylating factors of *E. coli* lysate could activate proCyaA-PF toxin. In this activation process, CyaC may cleave acyl group from acyl-ACP, an acyl donor, and transfer the acyl group to CyaA, like the activation of HlyA by HlyC (66, 67). As CyaC was found to be able to cleave acyl group from pNPP, a synthetic substrate of pNP derivatives, it was postulated that the cleaved acyl group could possibly be transferred onto proCyaA-PF resulting activated proCyaA-PF.

From the results shown in **Table 6.1**, *in vitro* activation using the purified proCyaA-PF and CyaC proteins containing pNPP showed ~91% hemolysis, comparing to ~84% hemolytic activity of *in vitro* activation of CyaA-PF by CyaC using lysate of *E. coli*. The negative controls, either the reaction mixture containing proCyaA-PF and CyaC, the reaction mixture containing CyaC and pNPP, reaction mixture containing proCyaA-PF and pNPP or merely *E. coli* lysate, were lower than 5% hemolytic activity. Thus, it showed that pNPP analogue effectively mimicked the acyl-ACP as the acyl donor for CyaA acylation process.

Table 6.1 Hemolytic activities of the *in vitro* acylated CyaA-PF toxin against sheep erythrocytes using purified protein

Reaction mixture[a]	**Hemolytic activity**[b] (% Hemolysis ± SEM)
ProCyaA-PF + CyaC + pNPP	90.5 ± 5.1
ProCyaA-PF + CyaC + *E. coli* lysate	83.5 ± 10.0
ProCyaA-PF + CyaC	1.6 ± 1.0
CyaC + pNPP	4.1 ± 1.0
ProCyaA-PF + pNPP	3.7 ± 1.4
E. coli lysate	3.1 ± 0.8

[a] *In vitro* activation reactions were set up by mixing 10 µg purified proCyaA-PF and 15 µg purified CyaC (10:1 molar ratio) with either 500 µM pNPP or 1 mg *E. coli* cell extract. Reactions were incubated in TBS buffer at 37°C for 10 min.

[b] Samples were incubated with sheep erythrocytes (10^9 cells/ml) in TBS buffer at 37°C for 6 h. Percentage of hemolysis was calculated as described in Materials and Methods. The values were averaged from three independent experiments performed in duplicates. SEM represents standard errors of the mean.

6.2 Acylation analysis by LC-MS-MS

The acylation of CyaA-PF utilizing pNPP as the donor substrate was confirmed by LC-MS-MS of the *in vitro* activated CyaA-PF. As shown in **Figure 6.1**, the mass of tryptic peptide fragment encompassing residues 972 to 984 (E^{972}GVA TQTTAYGK$_{C16:0}$$R^{984}$) indicated the C16:0 acylation at Lys^{983}, comparing to mass of the non-acylated peptide fragment from CyaA-PF toxin expressed in the absence of CyaC and that of the *in vivo* acylated peptide fragment from CyaA-PF toxin co-expressed with CyaC. The result revealed the CyaA-PF was palmitoylated at Lys^{983} upon *in vitro* activation by CyaC with utilizing pNPP as the donor substrate.

6.3 Kinetic analysis of substrate specificity toward pNP-derivatives

The kinetic parameters for hydrolysis of *p*-nitrophenyl derivatives containing different acyl groups (C8-C18) were determined. Steady-state kinetics were studied at the various substrate concentrations of pNP derivatives in 50 mM Tris-HCl, pH 7.4. The reaction was monitored at 400 nm, ε = 11.6 $mM^{-1}cm^{-1}$. Typical plots of substrate saturation curves were obtained in the presence of different substrate concentrations (10 - 500 μM). Catalytic efficiencies, k_{cat}/K_m, were used to compare the substrate preference.

Their kinetic parameters were used as a reference for comparing those of the other substrates shown in **Table 6.2**. The kinetic parameters of *p*-nitrophenyl derivatives showed the catalytic efficiencies of k_{cat}/K_m fluctuated among the various acyl-donors, except for the stearate group. *p*-Nitrophenyl-myristate (pNPM) and *p*-nitrophenyl palmitate (pNPP) were found to be the most effective substrate. The shortest chain length of saturated acyl group (*i.e.* pNPA) had the lowest K_m value, close to 0.1 mM (**Table 6.2**). There was not much difference for the catalytic efficiency between myritoyl- and palmitoyl groups. The K_m value, however, for pNPP was lower than that of the corresponding saturated homologue pNPM.

A)

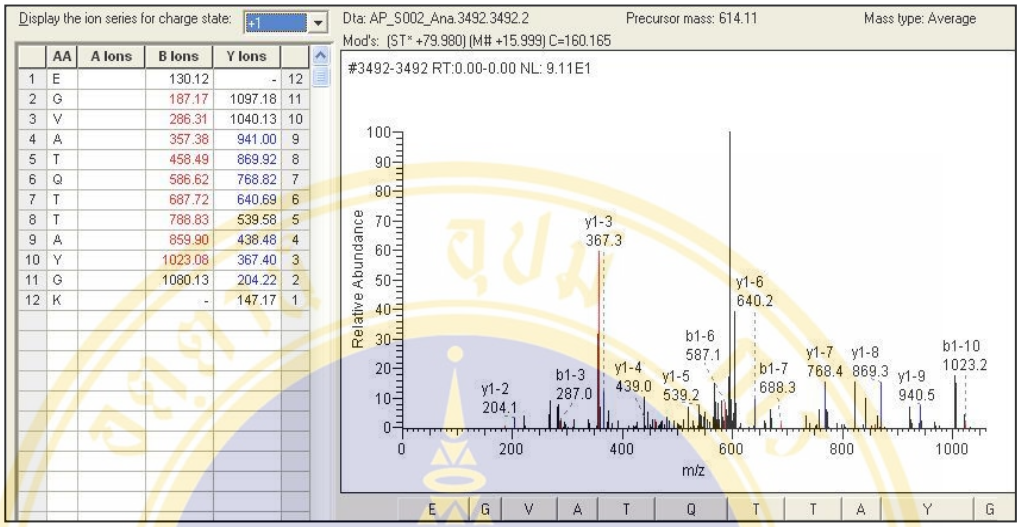

B)

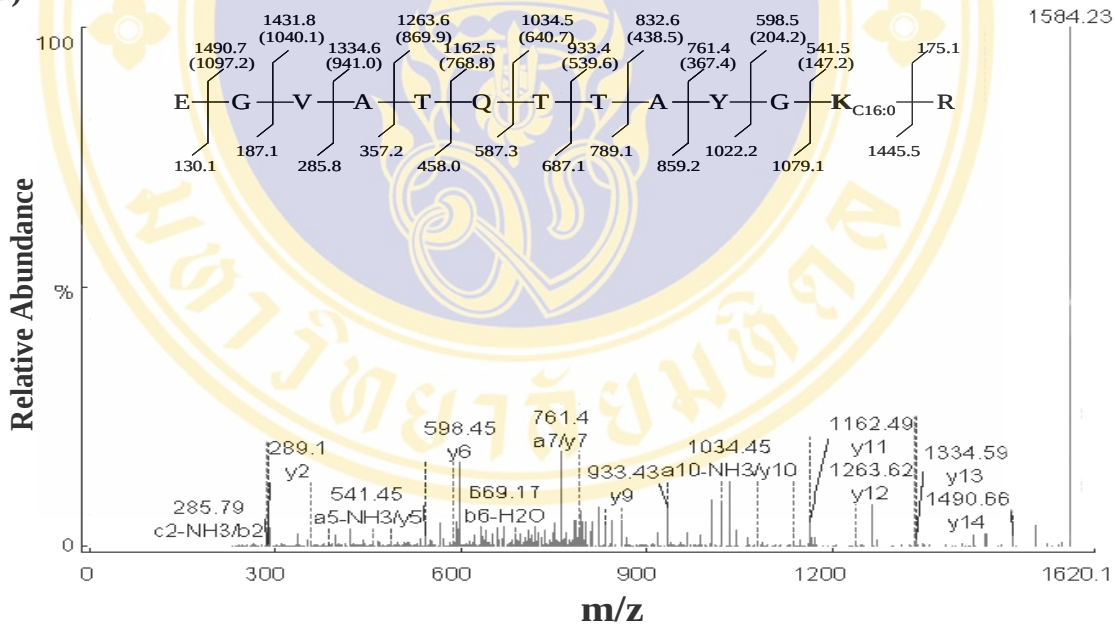

Figure 6.1 Representative LC/MS/MS spectra of non-acylated and acylated peptide fragments

(A) Representative LC-MS-MS spectrum of non-acylated peptide, Glu^{972} to Lys^{983}, digested from the proCyaA-PF protein.

(B) Representative LC-MS-MS spectrum of acylated peptide, Glu^{972} to Arg^{984}, digested from the CyaA-PF protein activated by CyaC *in vitro* demonstrate that palmitoylation occurred on Lys^{983}. The inset shows the m/z values of fragment ions (b_i and y_i) of the acylated peptide. The m/z values in the parentheses refer to that of the non-acylated peptide.

Table 6.2 Kinetic parameters of different acyl chain group of pNP in the acyl hydrolase reaction[a]

Substrate	Acyl chain length	K_m[b] (mM)	V_{max}[c] (μmol.min^{-1}.mg^{-1})	k_{cat} (s^{-1})	k_{cat} / K_m ($s^{-1}mM^{-1}$)
pNPA	2	0.11 ± 0.01	50.07 ± 0.67	17.52 ± 0.23	166.06 ± 10.56
pNPC	8	0.64 ± 0.02	454.50 ± 9.04	159.10 ± 3.26	250.38 ± 4.85
pNPD	10	0.38 ± 0.01	327.57 ± 4.87	114.67 ± 1.69	300.52 ± 2.60
pNPM	14	0.55 ± 0.05	2399.00 ± 95.69	839.17 ± 32.85	1544.95 ± 85.54
pNPP	16	0.34 ± 0.01	1473.67 ± 26.41	515.70 ± 9.20	1530.73 ± 10.12
pNPS	18	1.43 ± 0.09	858.17 ± 34.70	300.37 ± 12.18	210.90 ± 5.33

[a] Kinetic parameters are values for the particular conditions given at the fixed concentration of the CyaC enzyme (15 μg/ml or 730 nM).

[b] K_m is not a binding constant that measures the strength of binding between the enzyme and substrate. Its value includes the affinity of substrate for enzyme, but also the rate at which the substrate bound to the enzyme is converted to product.

[c] V_{max} is the unit of μmol/min/mg protein.

6.4 Hemolytic abilities of CyaA-PF *via* the various acyl-chain length activation

Previous work on CyaC activation of proCyaA-PF showed that *E. coli* lysate containing acyl-ACP was a cofactor in the activation reaction (*see* **Table 5.1**). Similarly, pNPP was also found to act as a cofactor in the activation of proCyaA-PF by CyaC (*see* **Table 6.1**). The effect on toxin activity of altering the fatty acid used by *p*-nitrophenyl-derivatives to acylate the proCyaA-PF in the presence of the CyaC protein was investigated. This was accomplished by using different fatty acids with commercially available of *p*-nitrophenyl derivatives [pNPC (C8), pNPD (C10), pMPM (C14), pNPP (C16) and pNPS (C18)].

The data showed that pNPP substrate conjugated with palmitic acid was the most effective acyl-donor for the *in vitro* activation of proCyaA-PF by CyaC, whereas other fatty acids were less effective for their activity **(Figure 6.2**). The activation with pNPM that produced myristoyl-CyaA-PF product caused roughly half of the lysis compared to the activation with pNPP. Notably, an assay which contained free palmitic acid, pNPA or pNPP alone did not show toxin activity (< 5% hemolysis) (data not shown).

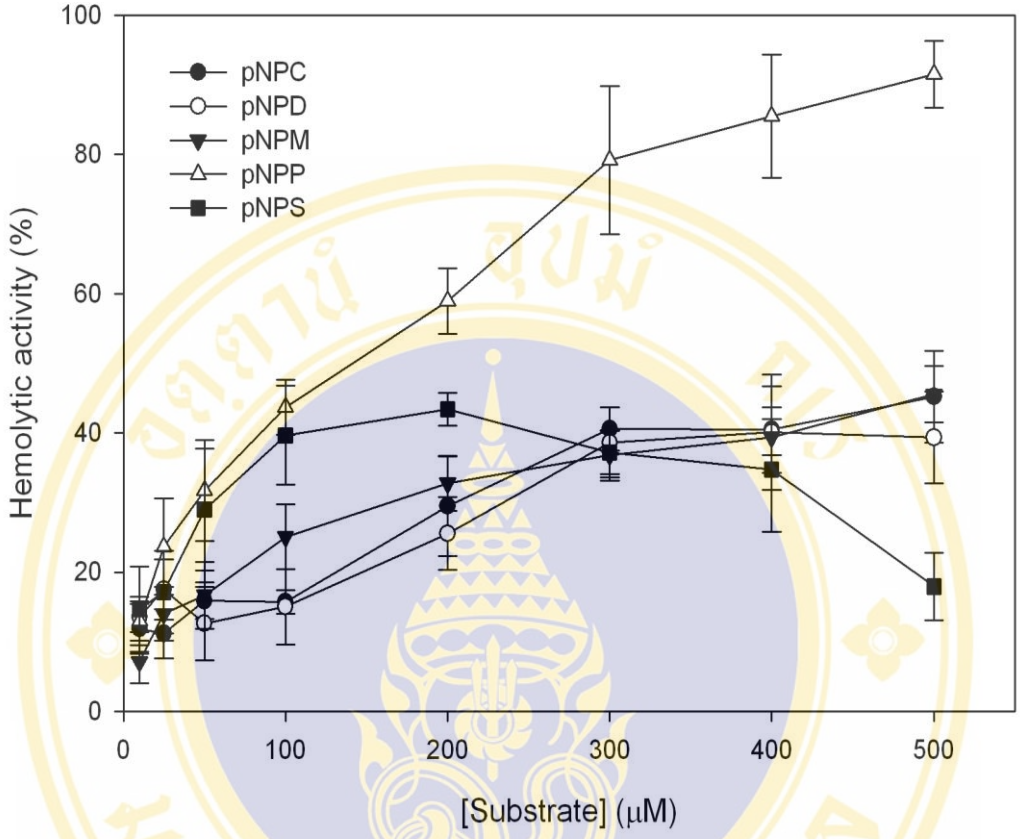

Figure 6.2 Hemolytic abilities of CyaA-PF activated by pNP-derivatives with various acyl-chain lengths

In vitro activation was accomplished by mixing 10 μg purified proCyaA-PF, 15 μg purified CyaC with various concentrations (10-500 μM) of *p*-nitrophenyl derivatives (pNPC (C8), pNPD (C10), pMPM (C14), pNPP (C16) and pNPS (C18). The same amount of proCyaA-PF toxin without activation gave <5% hemolysis. Data are reported as the mean of three independent experiments ± standard errors of the mean.

6.5 Binding affinity of CyaC to palmitate

Most of the intrinsic fluorescence emissions of a folded protein are due to excitation of tryptophan residues, with some emissions due to tyrosine and phenylalanine. Tryptophan fluorescence is strongly influenced by the proximity of other residues (*i.e.*, nearby *protonated* groups such as Asp or Glu can cause quenching of Trp fluorescence). Also, energy transfer between tryptophan and the other fluorescent amino acids is possible, which would affect the analysis, especially in cases where the Förster acidic approach is taken. Therefore, tryptophan fluorescence can be a very sensitive measurement of the conformational state of individual tryptophan residues and may be used as a diagnostic of the conformational state of a protein. The use of intrinsic fluorescence for the study of protein conformation is in practice limited to cases with few tryptophan residues, since each experiences a different local environment, which gives rise to different emission spectra.

Using the fluorescence titration experiments, using Trp fluorescence previously established by Wang *et al*. (43), the binding of long chain fatty acids to CyaC induces changes in Trp fluorescence (λ_{exc} 293 nm). The maximal binding of palmitate was reached to be 10:1 (**Figure 6.3A**). Values yielded for the number of binding sites per molecule and apparent dissociation constant (K_d^{app}) from the slope are listed in **Figure 6.3B**. The binding affinity of palmitate to CyaC was about 3.6 μM (K_d^{app} = 3.59 ± 0.05 μM).

A)

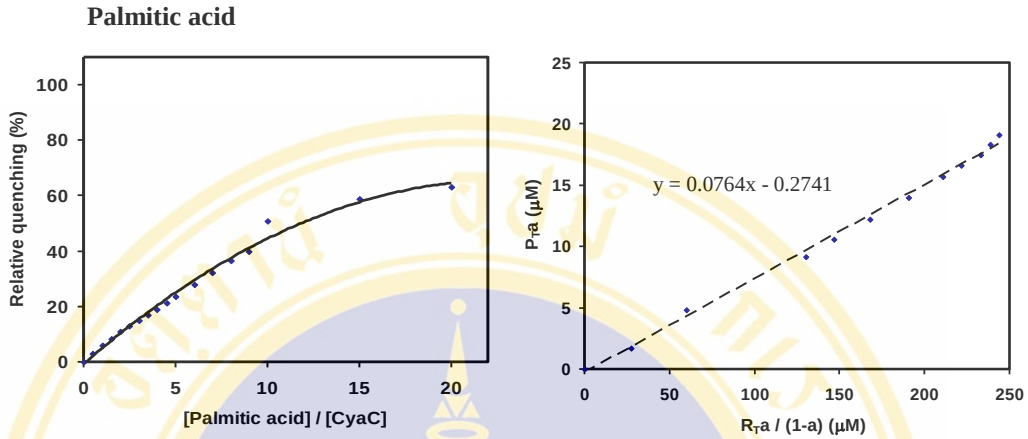

B)

Substrate	**Binding ratio ± SD** (substrate/CyaC)	K_d^{app} **± SD** (10^{-6} M)
Palmitate with CyaC	13.09 ± 0.19	3.59 ± 0.05

[a] n = The number of binding site, K_d = Dissociation constant. Calculation from the equation on linear graph: y = (1/n)x - k/n.

Figure 6.3 Binding ratio of CyaC with palmitate

(A) Titration experiment for binding of CyaC to palmitate measured at 345 nm with excitation at 293 nm (pH 8.0). Binding was determined by the quenching of intrinsic fluorescence of CyaC. The maximal binding ratio (saturation curve) of CyaC to palmitate is 10:1. Right panels: P_T = total protein concentration, R_T = total substrate concentration, a = fraction of unoccupied substrate sites on this protein. Each point represents the mean of duplicate determinations with an average of standard deviation (SD) less than 5-8% of the mean.

(B) Apparent dissociation constants and substrate/CyaC binding ratio.

6.6 Steady-state kinetic data catalyzed by chymotrypsin and CyaC

To gain more insight into the mechanism of enzyme-catalyzed substrate specificity, the kinetic parameters for chymotrypsin and CyaC hydrolysis of pNPA and pNPP substrates were analyzed. Steady-state kinetics were studied for chymotrypsin and CyaC enzymes at various concentrations of pNPA and pNPP in 50 mM Tris-HCl, pH 7.4 (*see* Appendix C). Typical plots of substrate saturation curves obtained in the presence of different concentrations of pNPA (1-1000 μM) and pNPP (10-500 μM) were shown in **Figure 6.4** for chymotrypsin and **Figure 6.5** for CyaC. The results showed an increase in reaction rate with substrate concentration. The stability of the enzyme is affected by many factors, such as temperature, pH and the organic solvent. It was found that enzymes were very stable under the present experimental condition. The stability of each enzyme (in buffer, 25°C) was checked in 5% isopropanol solvent and was found that the activity was found to be retained.

The kinetic parameters for the hydrolysis of pNPA and pNPP catalyzed by chymotrypsin and CyaC are also compared in **Table 6.4**. The K_m value of chymotrypsin was very low for pNPA (0.004 mM), but increased 20-fold for hydrolysis of pNPP substrate (0.081 mM). The catalytic constants (k_{cat}) were estimated from the V_{max} values using a molecular mass of 29-kDa for chymotrypsin and 21-kDa for CyaC. The value of the turnover number for CyaC toward pNPP is 500 times greater than that for chymotrypsin. In contrast to chymotrypsin, the catalytic efficiency of CyaC on pNPP is much higher than that on pNPA.

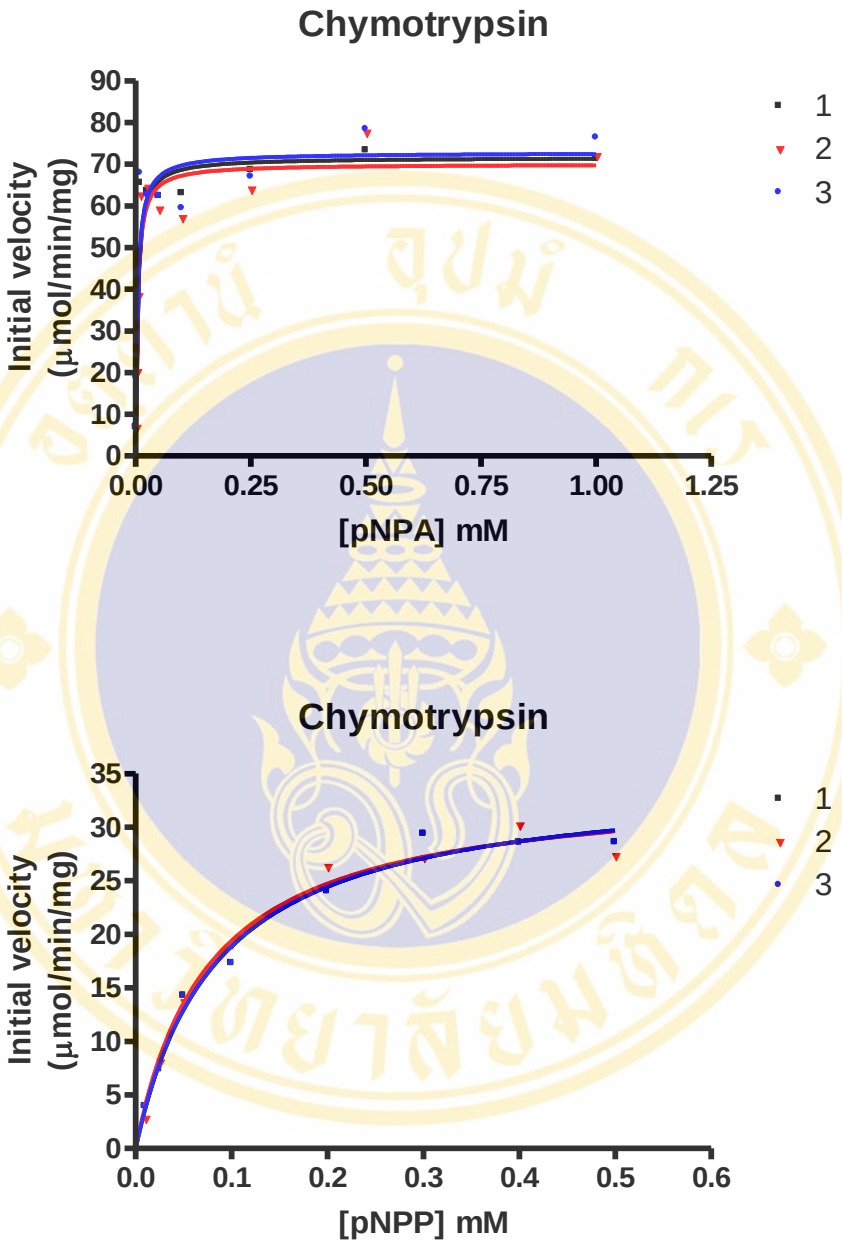

Figure 6.4 Chymotrypsin catalyzed substrate hydrolysis rates at different substrate concentrations

The graph shows the reaction velocities of chymotrypsin for hydrolysis of pNPA and pNPP at concentrations in the range of 1-1000 µM. Assay was performed at 25ºC in 50 mM Tris-HCL, pH 7.4. Kinetic parameters were determined from nonlinear fitting of untransformed data to the Michaelis-Menten equation. Data are reported as the means of duplicate in three independents (lines 1, 2 and 3).

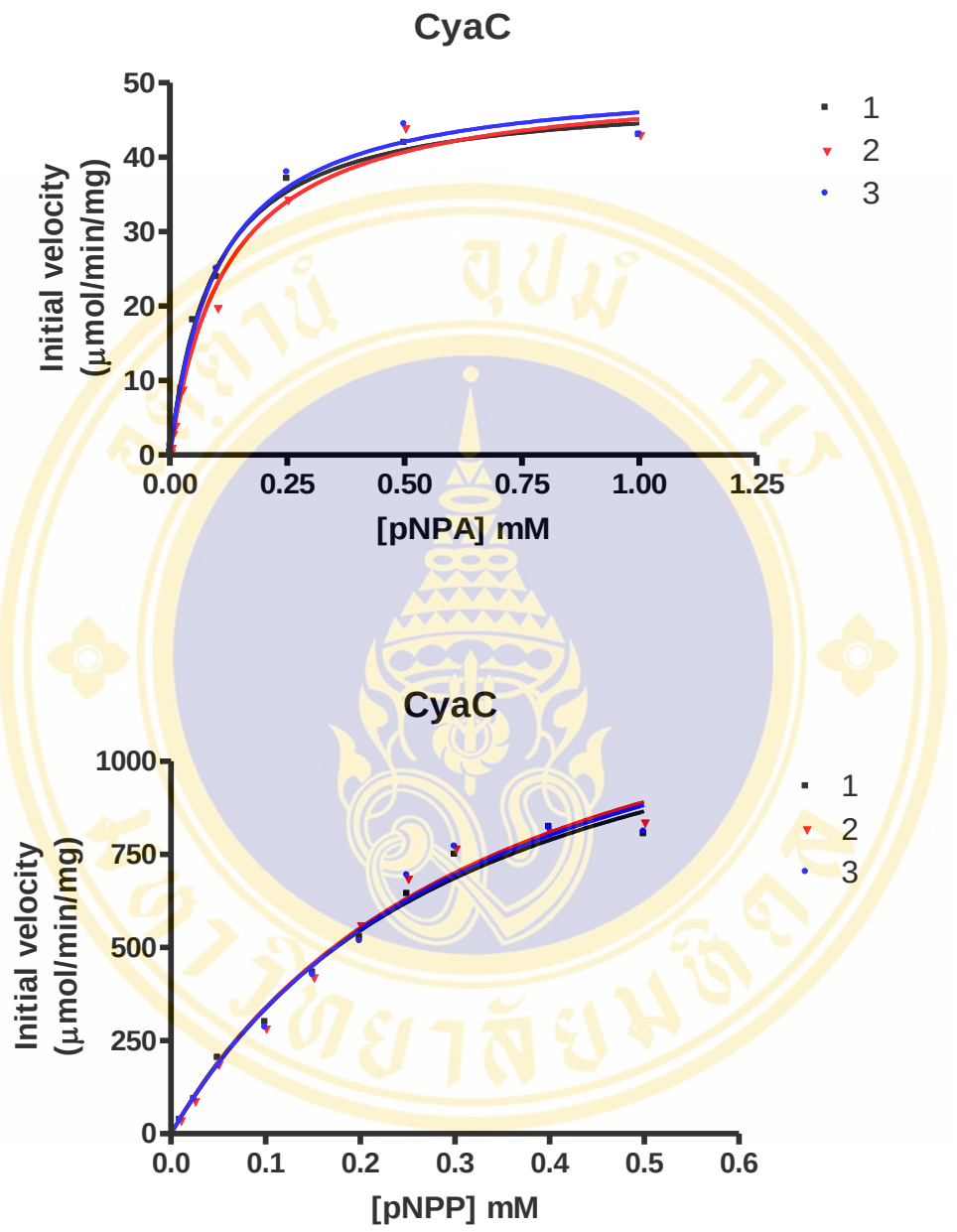

Figure 6.5 CyaC catalyzed substrate hydrolysis rates at different substrate concentrations

The graph shows the reaction velocities of CyaC for hydrolysis of pNPA and pNPP at concentrations in the range of 1-1000 µM. Assay was performed at 25ºC in 50 mM Tris-HCl, pH 7.4. Kinetic parameters were determined from nonlinear fitting of untransformed data to the Michaelis-Menten equation. Data are reported as the means of duplicate in three independent experiments (lines 1, 2 and 3).

Table 6.3 Kinetic parameters for chymotrypsin and CyaC hydrolysis of pNPA and pNPP [a]

Kinetic parameters	pNPA		pNPP	
	Chymotrypsin	CyaC	Chymotrypsin	CyaC
K_m (mM)	0.004 ± 0.001	0.106 ± 0.014	0.081 ± 0.005	0.337 ± 0.014
V_{max} (μmol.min^{-1}.mg^{-1})	71.46 ± 1.36	50.07 ± 1.15	34.49 ± 0.33	1473.67 ± 45.74
k_{cat} (s^{-1})	29.77 ± 0.57	17.52 ± 0.40	14.37 ± 0. 14	515.70 ± 15.93
k_{cat}/K_m (s^{-1}mM^{-1})	6950	166	177	1531

[a] V_{max} is the unit of μmol/min/mg protein. K_m is not a binding constant that measures the strength of binding between the enzyme and substrate. Its value includes the affinity of substrate for enzyme, but also the rate at which the substrate bound to the enzyme is converted to product.

CHAPTER VII
RESULT III:
STRUCTURE DETERMINATION OF CyaC PROTEIN

7.1. Structure determination of CyaC protein *via* X-ray crystallography

7.1.1 Crystallization of the refolded CyaC protein

The purified refolded CyaC proteins (8 mg/ml) as screen for crystallization against 960 conditions of precipitated solutions (*see* **Method 4.2.20**). It was found that almost all drops (>80%) yielded precipitated protein (**Figure 7.1**), indicating the instability of CyaC protein in solution and its lack of crystallization. However, it was also found in the condition of 30% w/v polyethylene glycol (PEG) 8000 + 0.2 M ammonium sulfate that the drop appeared to contain the nucleated protein (microcrystals) which is typical for the crystal appearing at an initial stage of crystal growth (**Figure 7.2**).

As shown in phase diagram of crystallization thermodynamics (**Figure 7.3A**), the condition should be shifted to promote the crystal formation by variation of protein or salt concentrations and pH (68). Various conditions used to lower the solubility of the molecule are shown in **Figures 7.3B and C**. Under the second trial conditions, no crystal of CyaC protein was obtained.

A) B)

Figure 7.1 Crystal screen results against the reservoir solutions of 960 conditions

(A) Clear drops were observed about < 20% and (B) precipitated drops were appeared >80% among the total conditions

A) B)

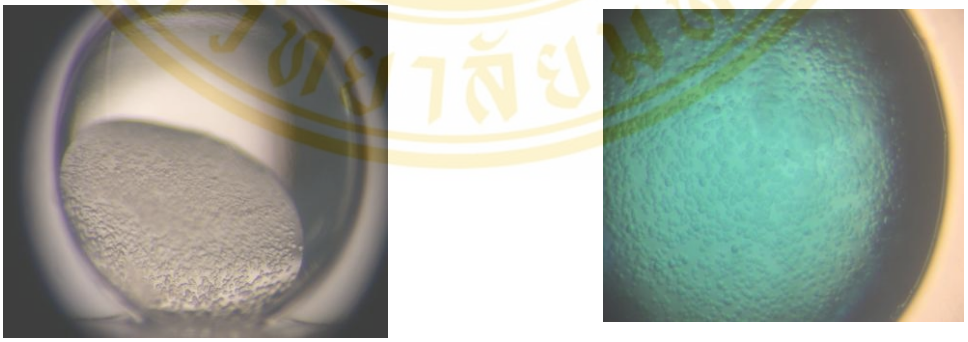

Figure 7.2 Nucleated crystals (seed) of refolded CyaC protein from the condition of 30% w/v PEG 8000 and 0.2 M ammonium sulfate

Nucleation (small crystal) could be seen in the crystallization drop (A) and IZIT dye testing display the blue color of the protein crystal (B).

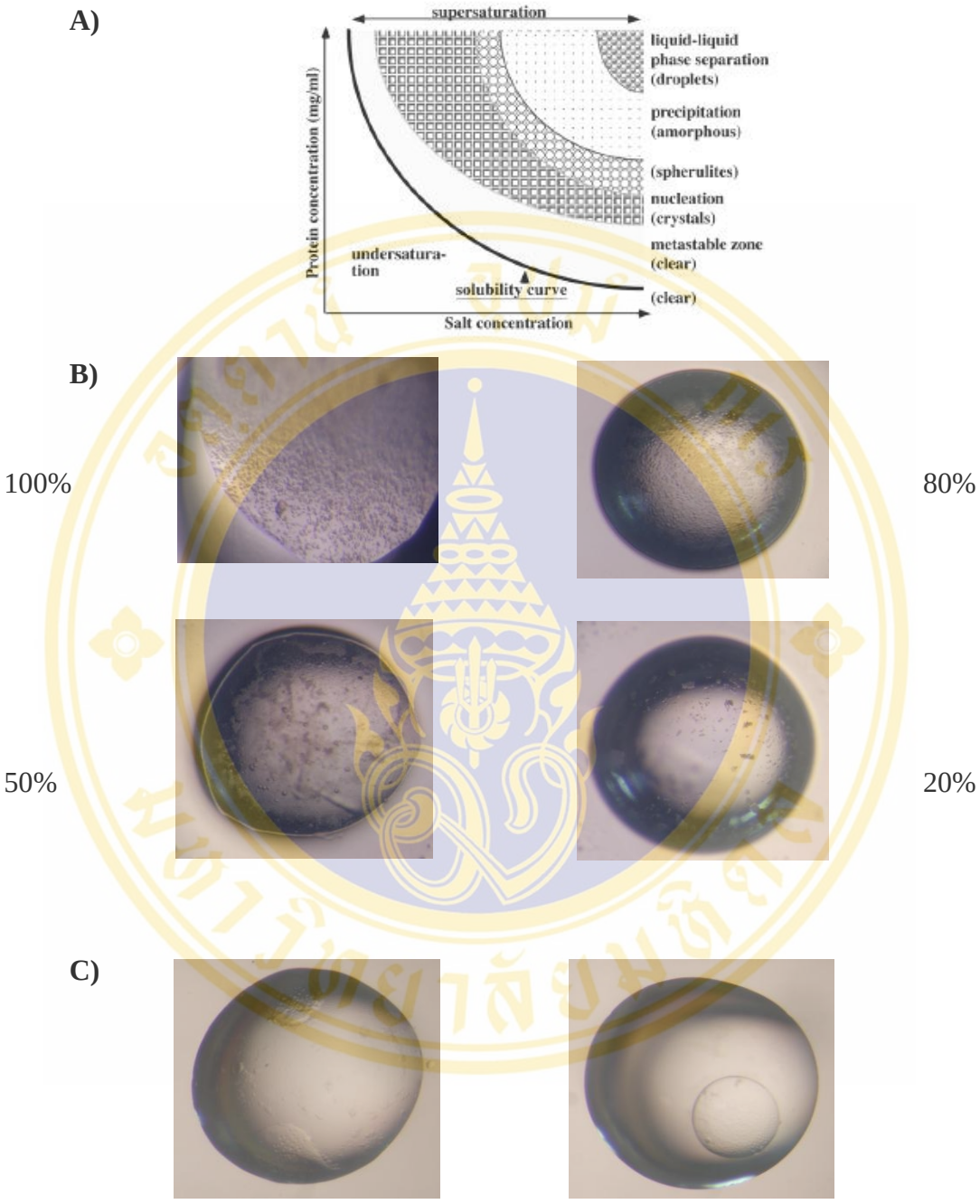

Figure 7.3 The possible crystal growth from the condition of 30% w/v PEG 8000 + 0.2 M ammonium sulfate

(A) Phase diagram of crystallization thermodynamics. In the nucleation zone, the protein begins to nucleate and form crystals, as opposed to amorphous precipitates. Below saturation, no crystals or precipitates are observed (68).
(B) Nucleation (small crystal) could be seen in the crystallization drop and the effect of reduction of the concentration of PEG and ammonium sulfate. The percentages of dilution are indicated beside the photographs.
(C) Phase separation could be seen in the crystallization drop when the pH was adjusted to 4.0 with 0.1 mM acetate buffer.

7.1.2 Crystallization of the soluble CyaC protein

For screening crystallization of the soluble CyaC proteins, most drops (>80%) were clear at the concentration of 1 mg/ml. Increasing the concentration to 5 mg/ml caused aggregation of protein. To achieve the concentration of 5 mg/ml without aggregation, 20% glycerol were added to the protein solution and used for screening crystallization.

Crystallization of CyaC was performed with three kits, Classics Suite, JCSG core I and JCSG core II (96×3 = 288 conditions). After 15 days during crystallization, about 10 crystals had formed in the condition of 0.1 M Tris-HCl (pH 8.5) and 25% (v/v) tert-butanol (*see* **Figure 7.4**). Prior to X-ray diffraction and analysis, the crystals were unstable and disappeared as suddenly.

Figure 7.4 Crystal form in condition of 0.1 M Tris-HCl (pH 8.5) and 25% (v/v) tert-butanol

Plate-shaped crystals (0.05×0.05×0.1 mm) can be seen in the crystallization drop.

7.2 Structure prediction of CyaC-acyltransferase *via* homology-based modeling

7.2.1 Multiple sequence alignment with homologous protein structure

Sequence comparison of CyaC with the known 3D structures in protein data bank database (PDB) was identified *L*-2,4-diaminobutyric acid acetyltransferase (DABA) structure as the best-fit template available so far (**Figure 7.5**). DABA is classified in the group of acetytransferase, which catalyzes the transfer of an acetyl group to a nitrogen atom on the acceptor molecule. The sequences of the RTX-C proteins, groups of closely related protein in the RTX family, were also aligned with ClustalX. Visual inspection and manual correction were used to give higher percent amino acid sequence identity or lessen gap distances in some aligned regions. The final multiple sequence alignment and the percentage amino acid sequence similarity determined are shown in **Figure 7.6**.

As revealed from **Figure 7.6**, although pair-wise alignment between DABA and CyaC displays only ~30% sequence similarity, multiple alignments show relatively high similarity (~50%) among all the nine related RTX-acyltransferases with the same template, implying a common 3D-folded structure for these enzymes. Furthermore, the secondary structure comparing between DABA known structure and CyaC could be detected in the neighboring of corresponding position.

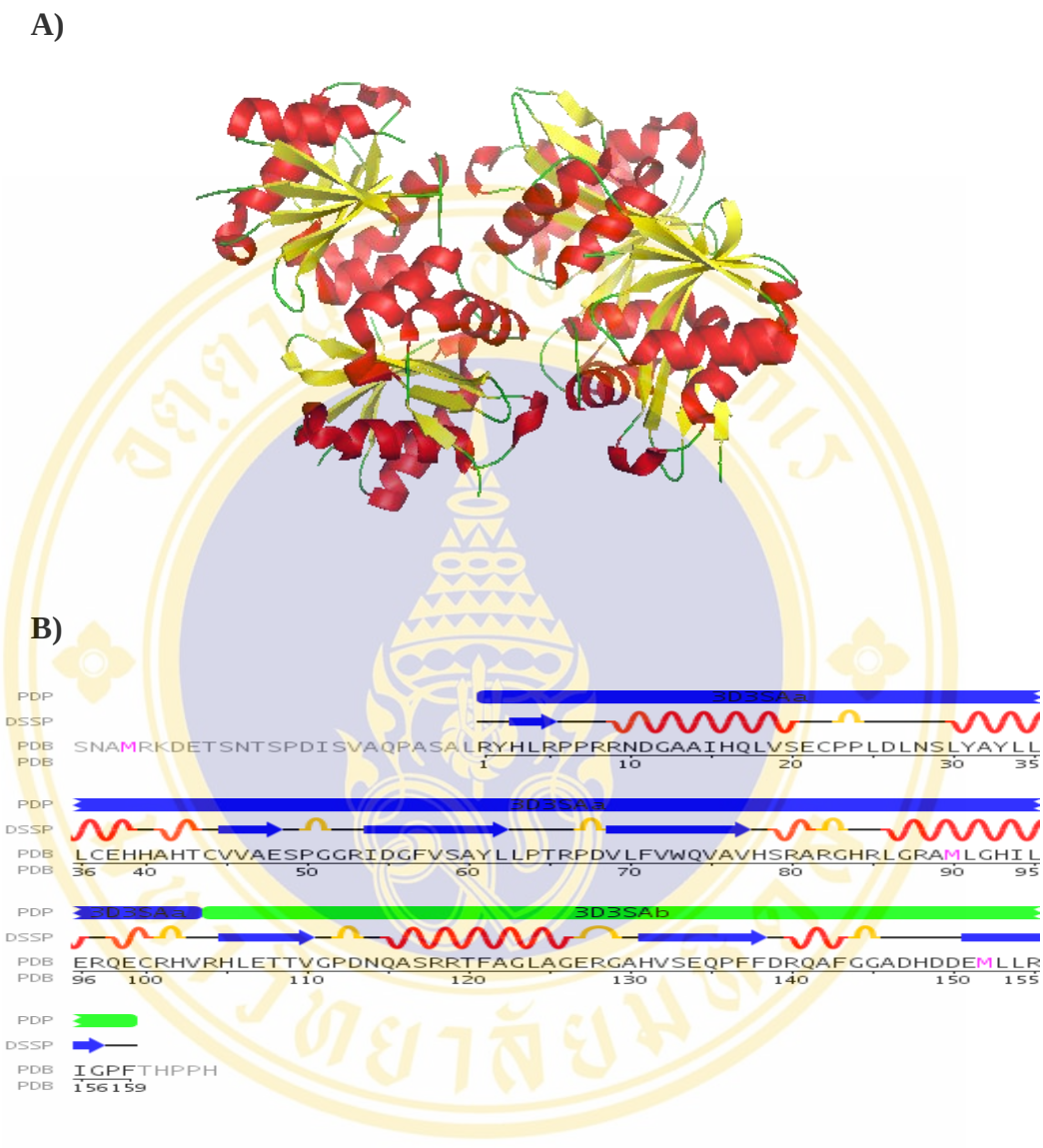

Figure 7.5 Ribbon representations of the DABA template structure

A) Crystal structure of *L*-2,4-diaminobutyric acid acetyltransferase from *Bordetella parapertussis* (DABA, PDB no. 3D3S). Ribbon representations of DABA display the alpha-beta-alpha sandwich monomers in the tetramer.

B) Dictionary of protein (DSSP) secondary structure of DABA acetyltransferase. DSSP secondary structure of DABA reveals pattern recognition of hydrogen-bonded and geometrical features containing 30% helical (9 helices; 58 residues) and 24% beta sheet (7 strands; 46 residues).

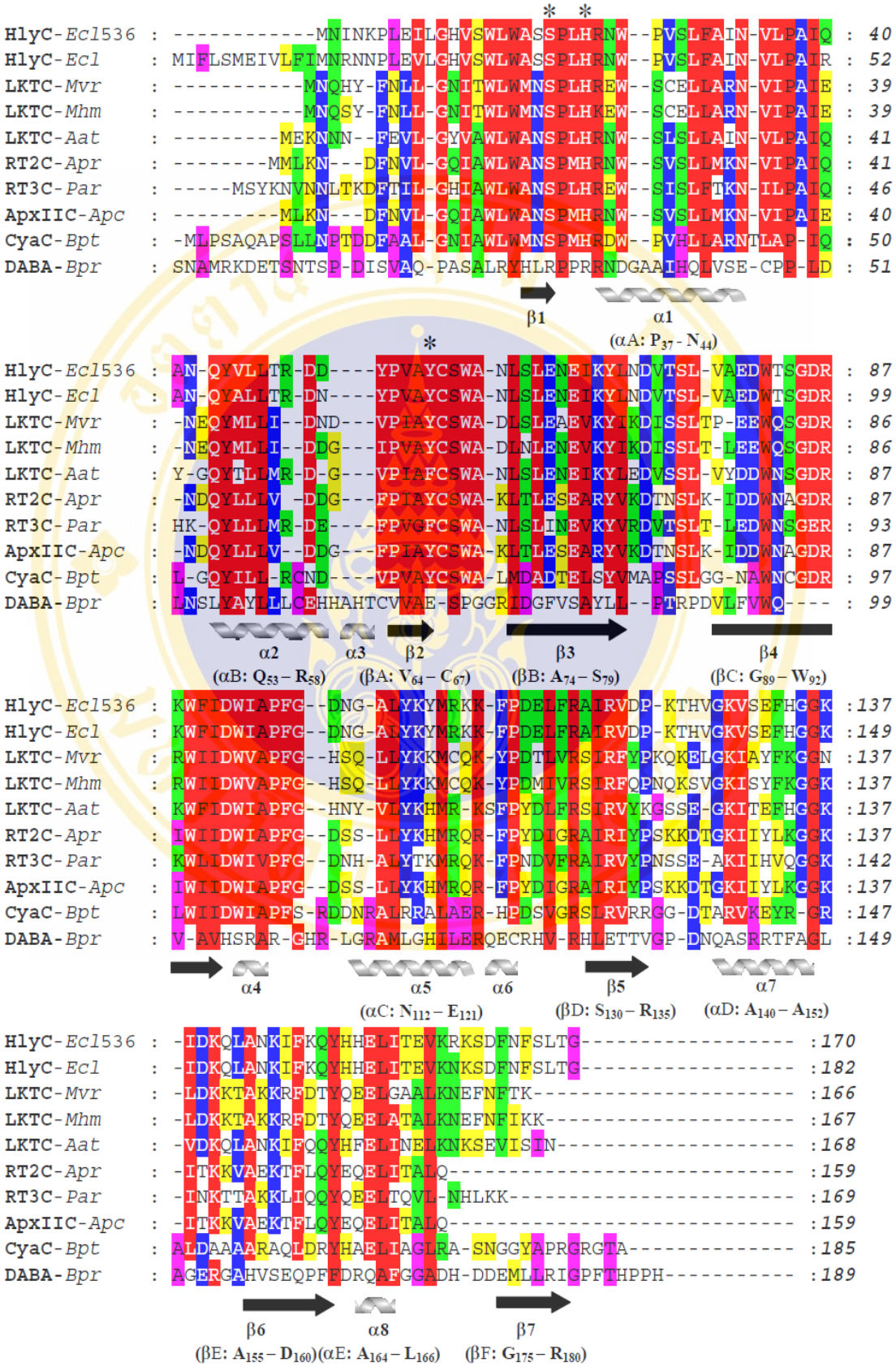

Figure 7.6 Multiple sequence alignments of nine RTX-C acyltransferases with DABA acetyltransferase

HlyC-*Ecl536*, *E.coli*-536 hemolysin-acyltransferase (NC008253.1); HlyC-*Ecl*, *E.coli* hemolysin-acyltransferase (AJ488511.1); LKTC-*Mvr*, *Mannheimia varigena* leukotoxin-acyltransferase (Q6TB08); LKTC-*Mhm*, *M. haemolytica* leukotoxin-acyltransferase (P55121); LKTC-*Aat*, *Actinobacillus actinomycetemcomitans* leukotoxin-acyltransferase (X16829.1); RT2C-*Apr*, *A.pleuropneumoniae* RTX-II toxin-acyltransferase (P0A3I3); RT3C-*Par*, *Pasteurella aerogenes* PaxC-acyltransferase (U66588.1); ApxIIC-*Apr*, *A. pleuropneumoniae* ApxIIC-acyltransferase (Q5DI85); ApxIIC-*Apc*, *A. porcitonsillarum* ApxIIC-acyltransferase (Q5DI90); CyaC-*Bpt*, *B.pertussis* CyaC-acyltransferase (EF 592556); DABA-*Bpr*, *B. parapertussis* DABA-domain A (PDB code 3D3S). Degree of conservation among the sequences is highlighted by shading residues with red (white-black characters), blue, green and yellow for 90%-100%, 70-80%, 50-60% and 30-40% homology, respectively. More regions of homology between CyaC and DABA are highlighted with pink. Catalytic triad residues (Ser^{30}, His^{33}, Tyr^{66}) are indicated by ∗. Positions of secondary structure elements of DABA and CyaC (in blanket) are illustrated under the alignments.

7.2.2 Homology modeling by WHATIF program (57)

The protein backbone (Cα) and side chains of CyaC were generated from the aligned sequences placed on DABA template model (PDB code 3D3S). The final structure is optimized by energy minimization to reduce steric hindrance. As described in previous section, a CyaC model begins with Leu^{26} and terminates at Ala^{185}. There are some gaps in the alignment because there is no template structure for building a model in these regions. Consequently, the CyaC structure in the following regions of DABA was built from amino acids at residues 26-185 (*see* **Figure 7.6**).

CyaC structure (Leu^{26}-Ala^{185}) comprises of a single domain with a β-sheet core of six strands (βA, βB, βC, βD, βE and βF) connected by five α-helices (αA, αB, αC, αD and αE) to form a two-layer α/β sandwich which is a typical fold of α/β hydrolase family (69) as shown in **Figure 7.7A**. By molecular surface analysis, a hydrophobic groove was clearly visible in the CyaC structure as shown in **Figure 7.7B**. This putative substrate-binding groove could likely serve as an acyl-binding pocket. This thus might explain highly efficient catalysis of pNPP hydrolysis or acyl transfer by this enzyme as the hydrophobic interactions would contribute more significantly to the palmitate-binding affinity in this apolar cavity.

By analogy to the feature of α/β hydrolase-fold enzymes, including acetyltransferases, chymotrypsin-like serine proteases and esterases (68), the CyaC model also reveals a putative catalytic triad (Ser^{30}, His^{33}, Tyr^{66}**)** with good geometric relationships corresponding to that of chymotrypsin (Ser^{195}, His^{57}, Asp^{102}) (**Figures 7.7 C and D**).

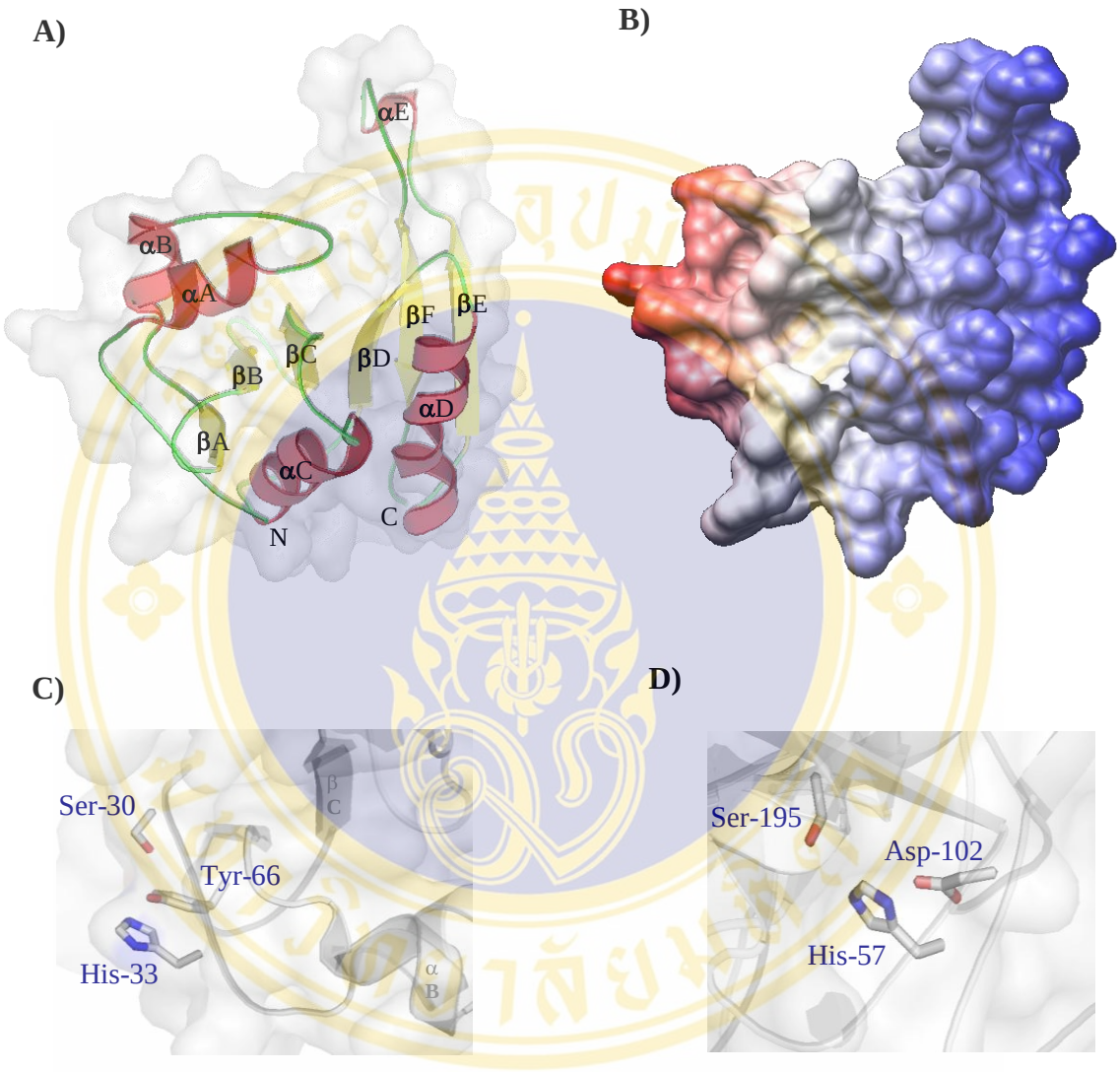

Figure 7.7 Homology-based modeling of CyaC structure

(A) Ribbon diagram of the homology-based CyaC structure. Helices, strands and coils are colored in red, yellow and green, respectively.
(B) Molecular surface electrostatic potential of CyaC model as analyzed by Chimera program as surface is colored according to electrostatic potential contoured from -10 (red) to 10 (blue) kT/e.
(C) Proposed catalytic triad of CyaC consisting of Ser^{30}, His^{33} and Tyr^{66} in comparison with that of (D) chymotrypsin (PDB-1ACB) (Ser^{195}, His^{57}, Asp^{102}). Figures A, C and D were generated by using PyMOL program.

7.2.3 Model evaluation by WHATCHECK and PROCHECK programs

For validating the model, the packing environment of the modeled structure as measured by the Check options of the program WHATIF, which gave Z-score of -1.2. This value is within the acceptable range (minimum value of –2.0) of a correctly folded structure. Stereochemistry evaluated by the program PROCHECK showed an overall G-factor value of −0.15, which is in the range of good quality (the best model displaying a value close to zero) (59). These values are equivalent to the expected value of a crystal structure resolved at 2.0 Å. Another important criterion for the stereochemical quality of the models is the distribution of Phi and Psi torsion angles (59). The resulting Ramachandran plots of the CyaC model revealed that over 91.3% of non-glycine and non-proline residues possess ϕ/ψ backbone-dihedral angles in energetically favorable and allowed regions, and 5.1% of non-glycine and non-proline residues in the generously allowed region (**Figure 7.8**). This indicates that the modeled structure has most of sterically favorable main-chain conformations.

7.2.4 Model evaluation by circular dichroism spectroscopy analysis

Analysis of CD spectra of the purified soluble CyaC protein against that of 50 reference proteins using CDsstr Program (variable selection method) reveals its secondary structure contents to be 25% helices, 27% β-strands and 48% turns and coils to a total secondary structure content of 100% with RMS difference between CALC. and EXPT. CD = 0.058 (**Figure 7.9**).

The secondary structure contents assigned from program Swiss PDB viewer shows that derived CyaC model contains 26% helices and 22% β-strands. Therefore, the secondary structural contents of CyaC assessed by CD spectroscopy were found to be comparable to those estimated from the derived model, supporting the validity of this model.

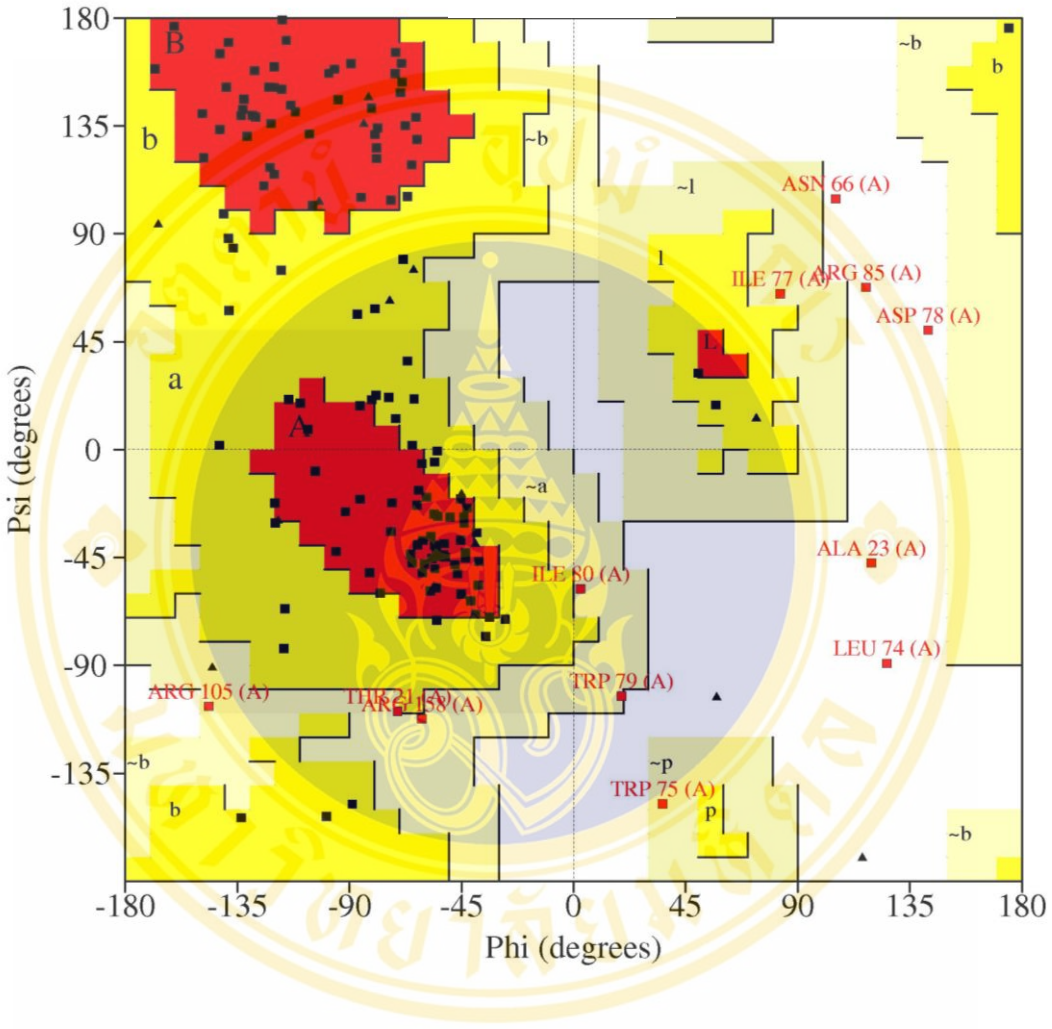

Figure 7.8 Ramachandran plot of CyaC model generated from PROCHECK program

Residues in the most favor regions (red area) and allowed regions (yellow area) are about 91.3 % of 137 amino acid residues. Residues in disallowed regions (white area) are labeled.

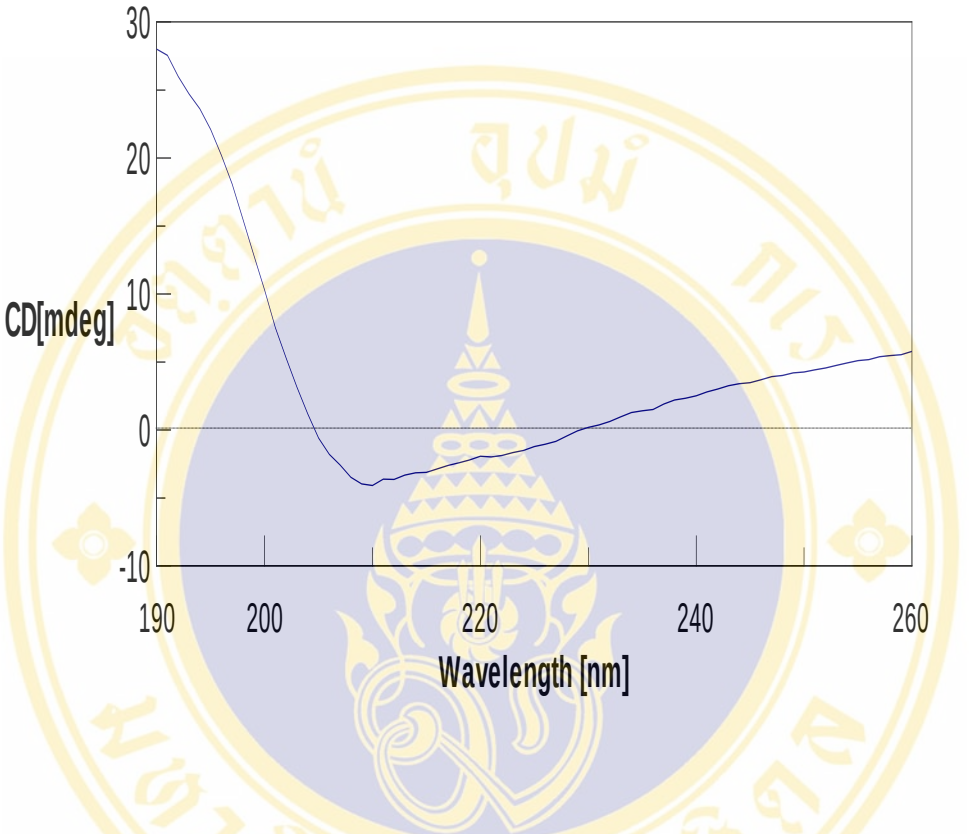

Figure 7.9 CD spectra of the purified CyaC protein in 20 mM Tris-HCl, pH 8.0

CD measurements of the 21-kDa FPLC-purified CyaC protein (0.4 mg/ml) were performed on a Jasco J-715 CD spectropolarimeter in the far UV region (190-280 nm) at 25°C. CD signals (mdeg) averaged from five measurements were converted into mean residue ellipticity ($deg \cdot cm^{2} \cdot dmole^{-1}$). Secondary structure contents were estimated from the spectra using CDPro software (55).

CHAPTER VIII
RESULT IV:
STRUCTURE-FUNCTION RELATIONSHIP STUDIES OF CyaC

Based on 3D model of CyaC, it was observed that the structural feature of CyaC is similar to that of α/β hydrolase-fold enzymes. CyaC model also revealed a putative catalytic triad (Ser^{30}, His^{33}, Tyr^{66}**)** with good geometric relationships corresponding to that of chymotrypsin (Ser^{195}, His^{57}, Asp^{102}). Interestingly, the catalytic triad Ser^{30}–His^{33}–Tyr^{66} proposed for CyaC-acyltransferase is highly conserved among the RTX-acyltransferase family. It was therefore performed single-alanine substitutions at these individual residues in order to validate their structural and functional relationships of CyaC mechanism.

PCR-based mutagenesis was performed to generate a single alanine substitution at each proposed residues (Ser^{30}, His^{33} and Tyr^{66}**)**. The wild-type recombinant plasmids, pCyaC encoding the 21-kDa CyaC acyltransferase and pCyaAC-PF encoding both the 126-kDa CyaA-PF fragment and the 21-kDa CyaC acyltransferase, were used as templates for site-directed mutagenesis. Each refolded monomeric CyaC mutant, which was expressed from pCyaC plasmid, was tested for esterolytic activity toward pNPP and *in vitro* proCyaA-PF activation. Activity of CyaC mutant in palmitoylating CyaA *in vivo* was evaluated from the hemolytic activity of CyaA-PF coexpressed with the CyaC mutant of interest.

8.1 Constructions of the alanine-substituted mutant plasmids

The pCyaC plasmid and pCyaAC-PF were used as templates for PCR-based mutagenesis. The mutagenic oligonucleotide primers (**Table 4.1**) were used to mutate nucleotides of interest and introduce restriction enzyme recognition site for screening the mutant plasmids. Following the thermal cycle (**Tables 4.2 and 4.3**), the amplified products were digested with *Dpn*I endonuclease and analysed on agarose gel electrophoresis. All PCR products showed 3.8-kb and 7.6-kb major DNA bands, corresponding to the size of pCyaC (**Figure 8.1**) and pCyaAC-PF (**Figure 8.5**), respectively.

The *Dpn*I-treated PCR products (**Figures 8.1 and 8.5**) were transformed into *E. coli* JM109 competent cells. The transformants from each mutation were screened for the desired mutation by restriction endonuclease analysis. After the appropriate restriction endonuclease digestion, the mutant plasmids could be distinguished from the wild-type plasmid as shown in **Figures 8.2A-8.4A and 8.6A-8.8A.** The nucleotide sequences of the mutated position of all desired mutants were verified by DNA sequencing (**Figures 8.2B-8.4B and 8.6B-8.8B**).

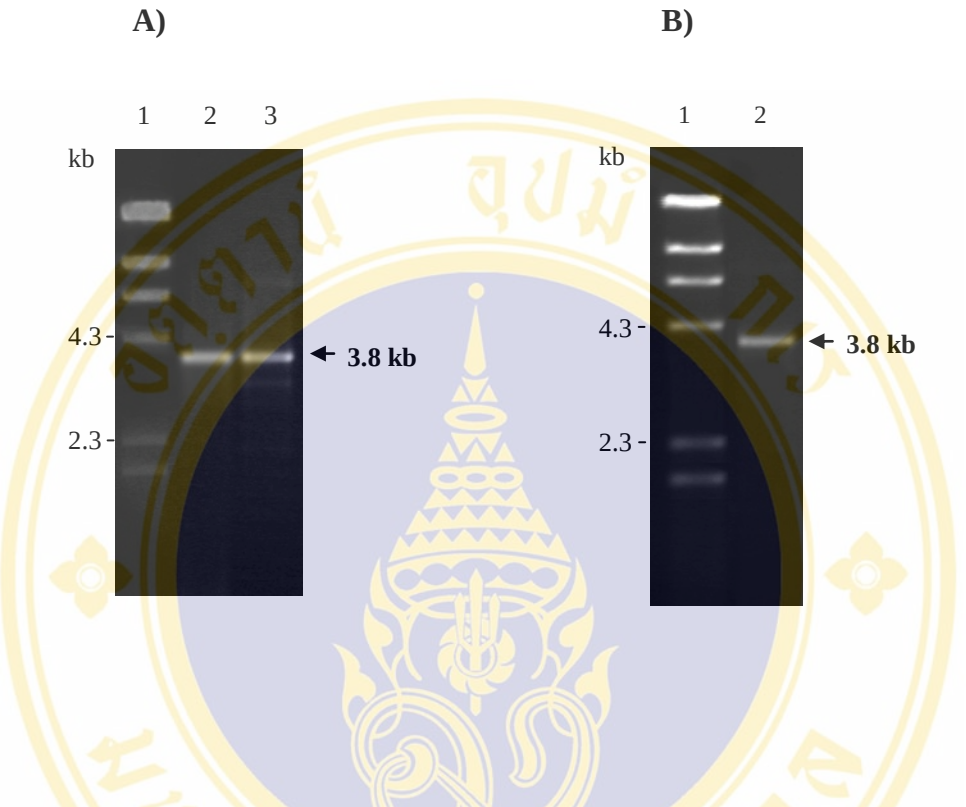

Figure 8.1 PCR amplification of pCyaC mutant plasmids digested with *Dpn*I

The figures show 1% agarose gel electrophoresis (ethidium bromide-stained) of PCR products of CyaC mutant plasmids, A) PCR products of pS30A and pY66A amplification using Ta = 60°C. B) PCR products of pH33A amplification using Ta = 50°C. The expected 3.8-kb DNA band is indicated by the arrow.

A) Lane 1: λ/*Hin*dIII digested DNA marker
Lane 2: The PCR product of the pS30A plasmid digested with *Dpn*I
Lane 3: The PCR product of the pY66A plasmid digested with *Dpn*I

B) Lane 1: λ/*Hin*dIII digested DNA marker
Lane 2: The PCR product of the pH33A plasmid digested with *Dpn*I

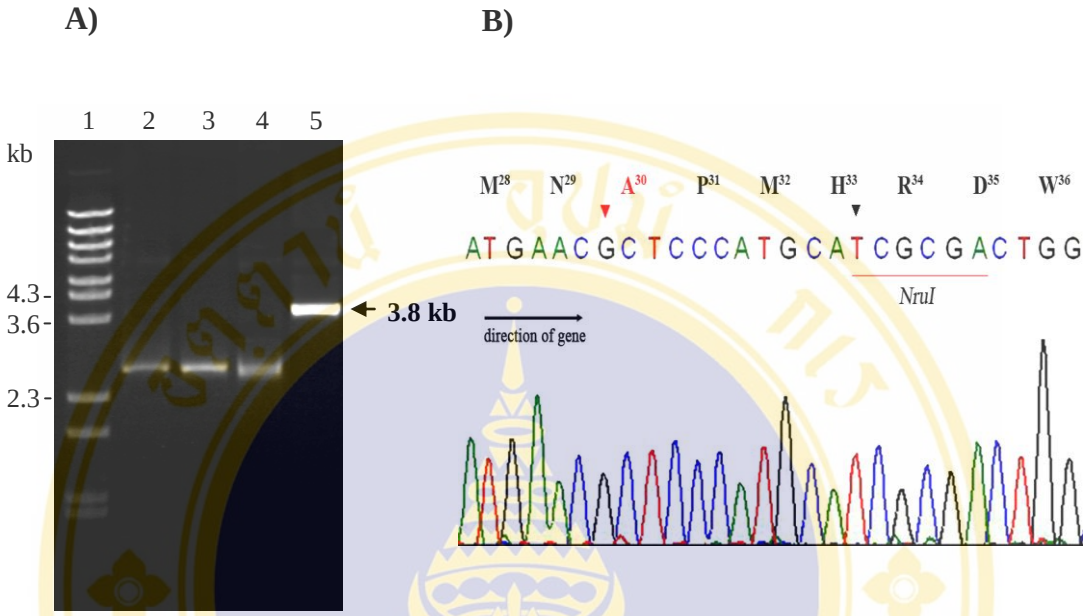

Figure 8.2 Restriction digestion and DNA sequencing analysis of pCyaC_S30A

A) 1% agarose gel electrophoresis of *Nru*I digestion patterns of the wild-type and mutant plasmids. The 3,810-bp mutant DNA band is indicated with the arrow. The presence of linear band in pS30A mutant plasmid (lane 5) is also shown in comparison to the wild-type band (lane 3) as indicated by the arrow.

Lane 1: λ/*Bst*EII digested DNA marker
Lane 2: The uncut pCyaC wild-type plasmid
Lane 3: The *Nru*I digested pCyaC wild-type plasmid
Lane 4: The uncut pS30A mutant plasmid
Lane 5: The *Nru*I digested pS30A mutant plasmid

B) The DNA sequencing chromatogram of pS30A using T7 promoter primer (5′– TAATACGACTCACTATA– 3′) as a sequencing primer. Part of the sense strand sequence is shown. The red-arrow head represents the mutated nucleotide (from T to G) resulting in substitution of serine with alanine. The black-arrowhead represents the substituted nucleotide (from C to T) generating a silent mutation and a *Nru*I restriction site. The letters above the chromatogram represent the corresponding deduced amino acid residues.

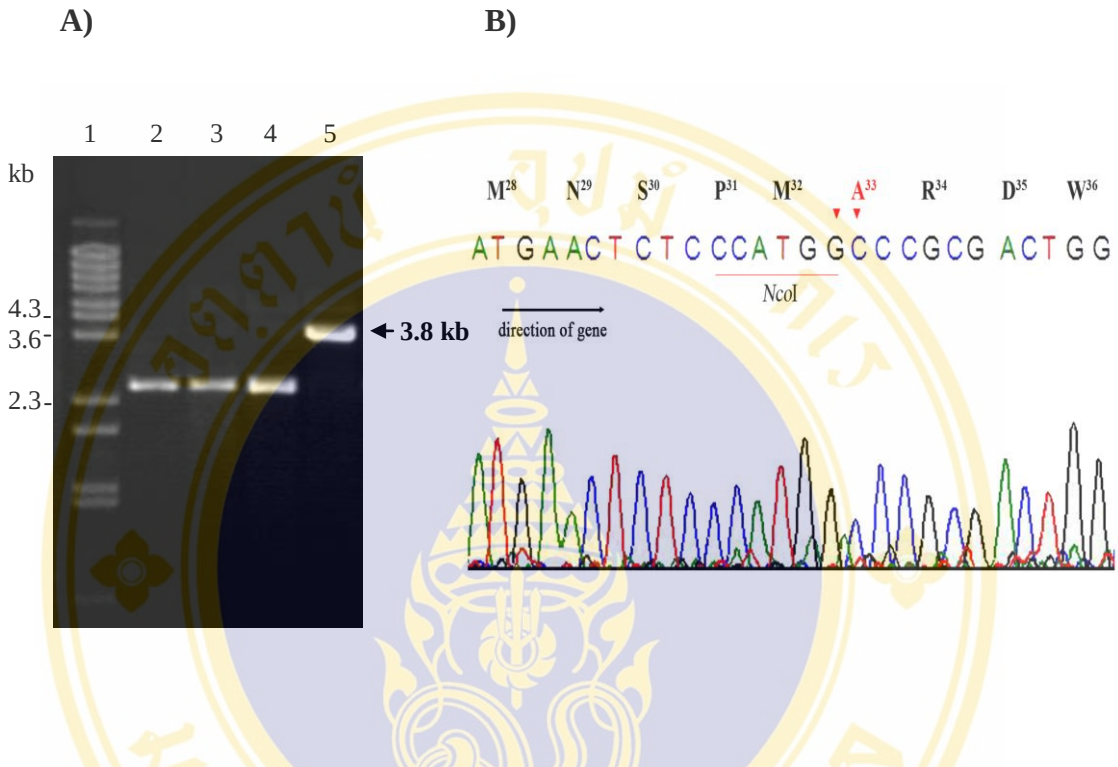

Figure 8.3 Restriction digestion and DNA sequencing analysis of pCyaC_H33A

A) 1% agarose gel electrophoresis of *Nco*I digestion patterns of the wild-type and mutant plasmids. The 3,810-bp mutant DNA band is indicated with the arrow. The presence of linear band in pH33A mutant plasmid (lane 5) is also shown compared to the wild-type band (lane 3) as indicated by the arrow.

Lane 1: λ/*Bst*EII digested DNA marker
Lane 2: The uncut pCyaC wild-type plasmid
Lane 3: The *Nco*I digested pCyaC wild-type plasmid
Lane 4: The uncut pH33A mutant plasmid
Lane 5: The *Nco*I digested pH33A mutant plasmid

B) The DNA sequencing chromatogram of pH33A using T7 promoter primer as a sequencing primer. Part of the sense strand sequence is shown. The red-arrow head represents the mutated nucleotide (from CA to GC) resulting in substitution of histidine with alanine. The substituted nucleotide (from C to G) generating a *Nco*I restriction site. The letters above the chromatogram represent the corresponding deduced amino acid residues.

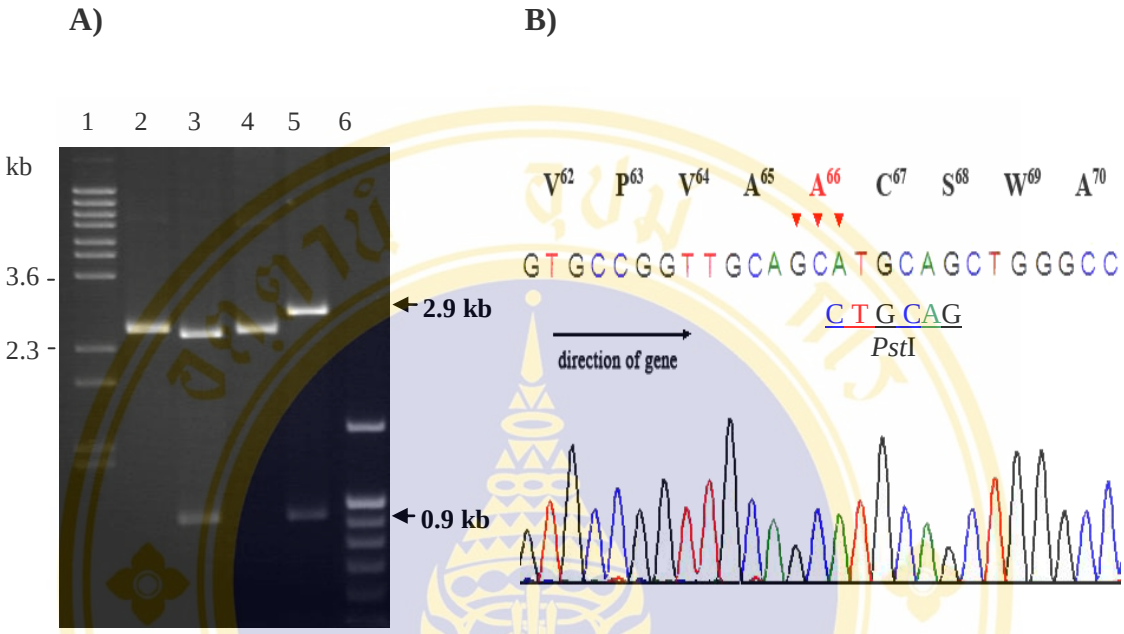

Figure 8.4 Restriction digestion and DNA sequencing analysis of pCyaC_Y66A

A) 1% agarose gel electrophoresis of *Pst*I digestion patterns of the wild-type and mutant plasmids. The 2887 and 923-bp mutant DNA bands (lane 5) are indicated by the arrow.

Lane 1: λ/*Bst*EII digested DNA marker
Lane 2: The uncut pCyaC wild-type plasmid
Lane 3: The *Pst*I digested pCyaC wild-type plasmid
Lane 4: The uncut pY66A mutant plasmid
Lane 5: The *Pst*I digested pY66A mutant plasmid
Lane 6: 100 bp DNA marker

B) The DNA sequencing chromatogram of pY66A using T7 promoter primer as a sequencing primer. Part of the sense strand sequence is shown. The red-arrow head represents the mutated nucleotide (from TAC to GCA) resulting in substitution of tyrosine with alanine. The substituted nucleotide (from C to A) for deleting a *Pst*I restriction site. The letters above the chromatogram represent the corresponding deduced amino acid residues.

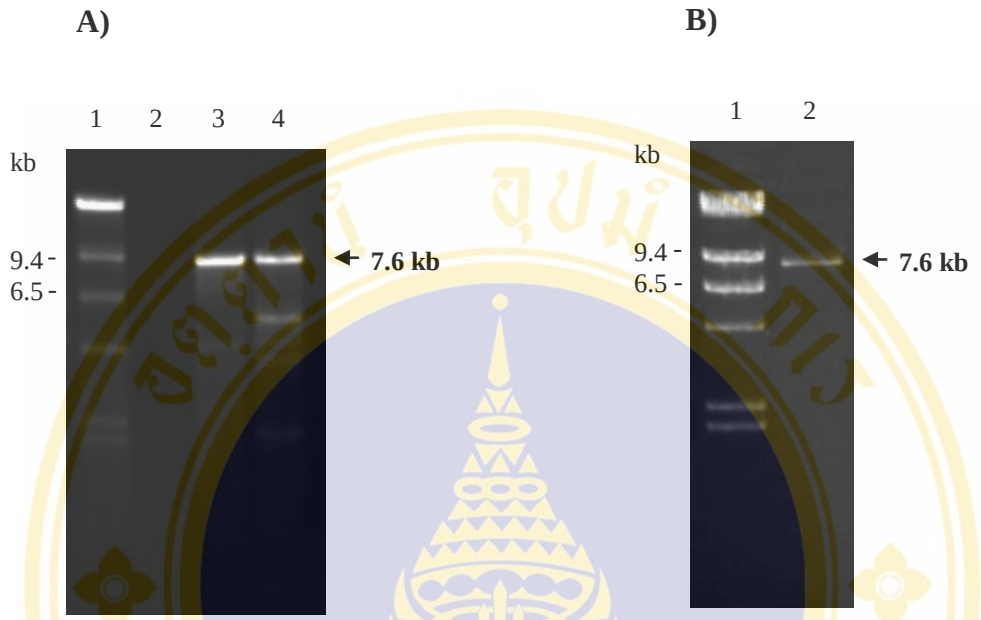

Figure 8.5 PCR amplification of pCyaAC-PF mutant plasmids digested with *Dpn*I

The figures show 0.8% agarose gel electrophoresis (ethidium bromide-stained) of PCR products of CyaA-PF mutant plasmids, A) PCR products of pH33A and pY66A amplification using Ta = 53°C and 60°C, respectively. B) PCR products of pS30A amplification using Ta = 62°C. The expected 7.6-kb DNA band is indicated by the arrow.

A) Lane 1: λ/*Hind*III digested DNA marker
Lane 2: A negative control
Lane 3: The PCR product of the pH33A plasmid digested with *Dpn*I
Lane 4: The PCR product of the pY66A plasmid digested with *Dpn*I

B) Lane 1: λ/*Hind*III digested DNA marker
Lane 2: The PCR product of the pS30A plasmid digested with *Dpn*I

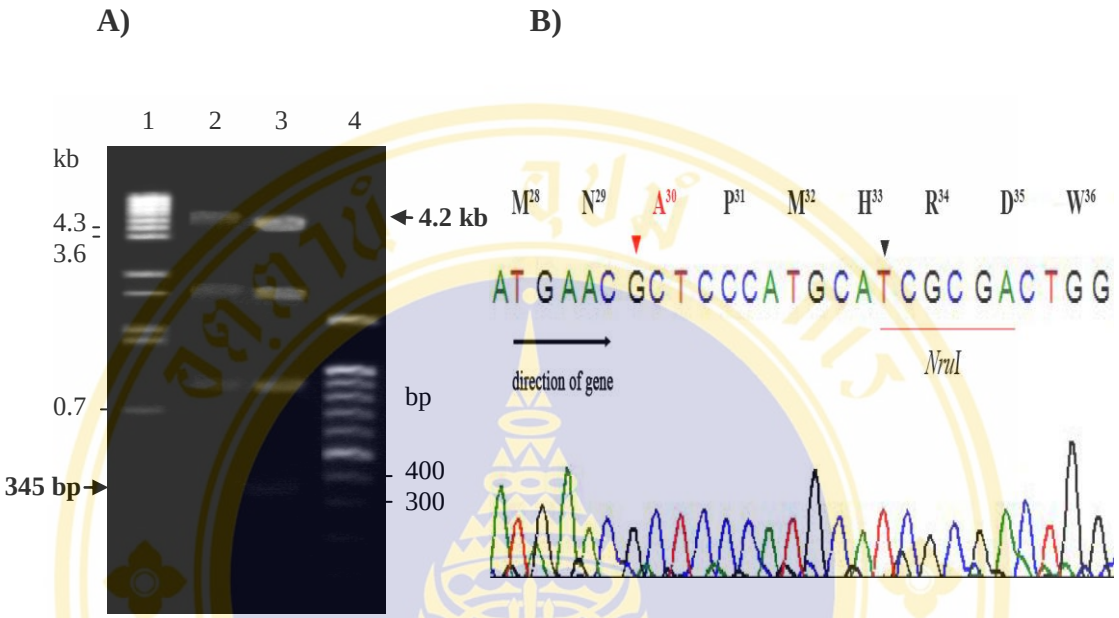

Figure 8.6 Restriction digestion and DNA sequencing analysis of pCyaAC-PF_S30A

A) 1.2% agarose gel electrophoresis of *Nru*I digestion patterns of the wild-type and mutant plasmids. The 4242 and 345-bp mutant DNA bands (lane 3) are indicated by the arrow.

Lane 1: λ/*Bst*EII digested DNA marker
Lane 2: The *Nru*I digested pCyaAC-PF wild-type plasmid
Lane 3: The *Nru*I digested pY66A mutant plasmid
Lane 4: 100 bp DNA marker

B) The DNA sequencing chromatogram of pS30A using *cyaC*_rbs-f primer (5′–CCCAAGCTTCCACAACGGTTTCCCTC– 3′) as a sequencing primer. Part of the sense strand sequence is shown. The red-arrow head represents the mutated nucleotide (from T to G) resulting in substitution of serine with alanine. The black-arrowhead represents the substituted nucleotide (from C to T) generating a silent mutation and a *Nru*I restriction site. The letters above the chromatogram represent the corresponding deduced amino acid residues.

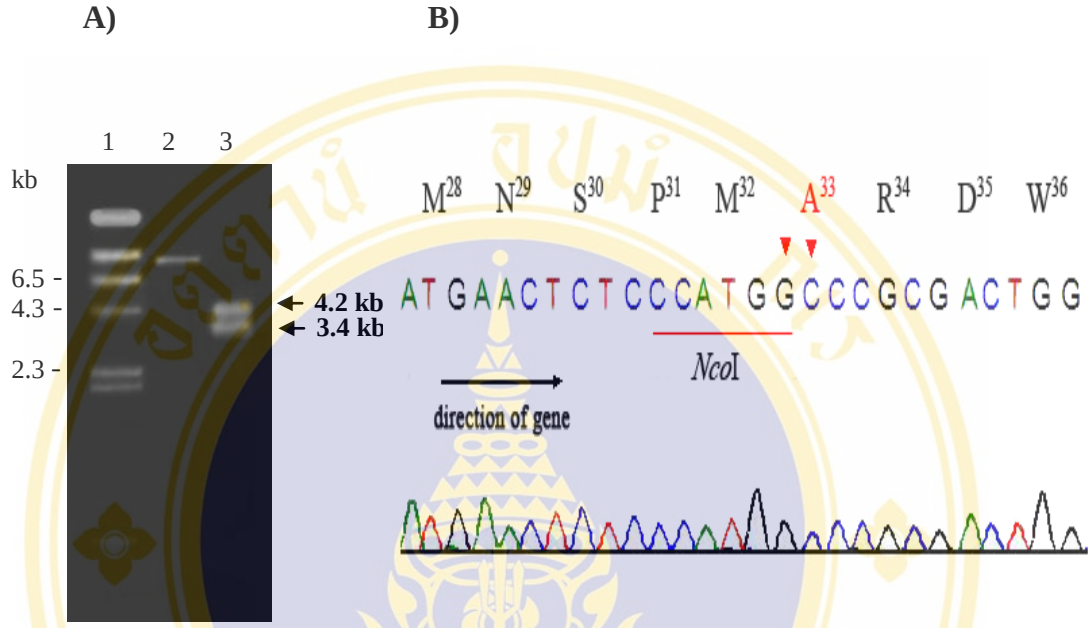

Figure 8.7 Restriction digestion and DNA sequencing analysis of pCyaAC-PF_H33A

A) 1.2% agarose gel electrophoresis of *Nco*I digestion patterns of the wild-type and mutant plasmids. The 4134 and 3417-bp mutant DNA band are indicated by the arrow.

Lane 1: λ/*Hin*dIII digested DNA marker
Lane 2: The *Nco*I digested pCyaAC wild-type plasmid
Lane 3: The *Nco*I digested pH33A mutant plasmid

B) The DNA sequencing chromatogram of pH33A using *cyaC*_rbs-f primer as a sequencing primer. Part of the sense strand sequence is shown. The red-arrow head represents the mutated nucleotide (from CA to GC) resulting in substitution of histidine with alanine. The substituted nucleotide (from C to G) generating a *Nco*I restriction site. The letters above the chromatogram represent the corresponding deduced amino acid residues.

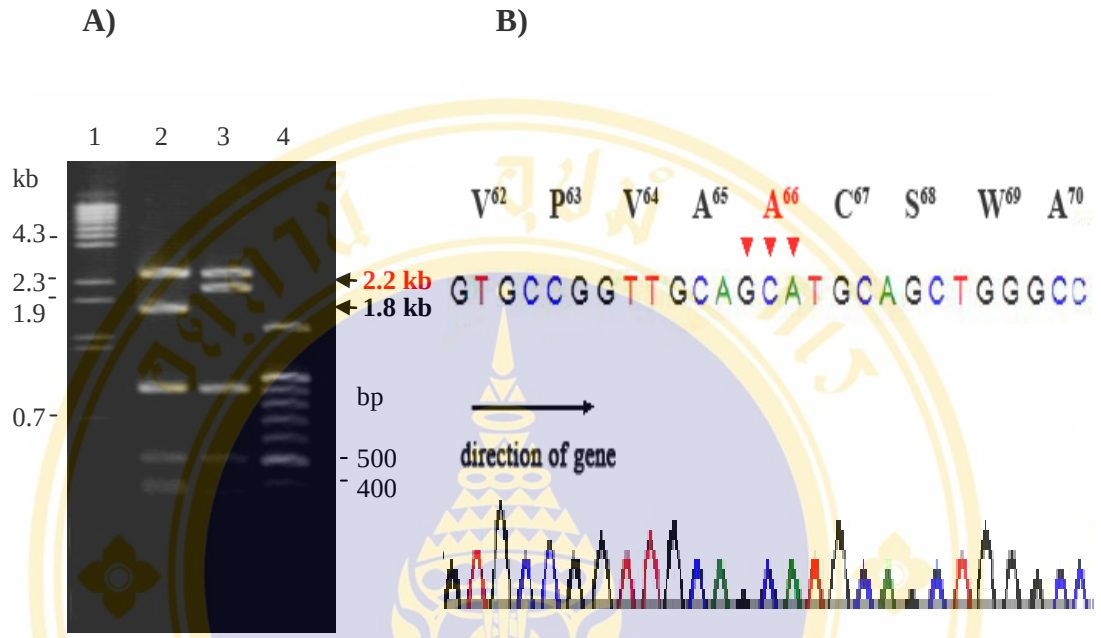

Figure 8.8 Restriction digestion and DNA sequencing analysis of pCyaAC-PF_Y66A

A) 1.2% agarose gel electrophoresis of *Pst*I digestion patterns of the wild-type and mutant plasmids. The 2,213-bp mutant DNA band is indicated with the arrow. The absence of the 1,815-bp band in pY66A mutant plasmid (lane 3) is also shown compared to the wild-type band (lane 2) as indicated by the arrow.

Lane 1: λ/*Bst*EII digested DNA marker
Lane 2: The *Pst*I digested pCyaAC-PF wild-type plasmid
Lane 3: The *Pst*I digested pY66A mutant plasmid
Lane 4: 100 bp DNA marker

B) The DNA sequencing chromatogram of pY66A using *cyaC*_rbs-f primer as a sequencing primer. Part of the sense strand sequence is shown. The red-arrow head represents the mutated nucleotide (from TAC to GCA) resulting in substitution of tyrosine with alanine. The substituted nucleotide (from C to A) for deleting a *Pst*I restriction site. The letters above the chromatogram represent the corresponding deduced amino acid residues.

8.2 Expression of the CyaC-acyltransferase mutants

Each verified pCyaC plasmid mutant was transformed into *E. coli* BL21(DE3)pLysS for expression. Upon IPTG induction at 30°C for 6 h, the mutant enzymes were almost produced as inclusion bodies. The expression levels of all 21-kDa mutant enzymes were approximately equal to that of the wild-type enzyme as shown in **Figures 8.9**.

For pCyaAC-PF mutant plasmids, all mutant CyaC were produced as a 21-kDa soluble protein upon IPTG induction at 30°C for 6 h, with comparable yields to the wild-type enzyme (**Figure 8.10**).

8.3 Purification of mutant CyaC enzymes

The 21-kDa CyaC inclusions of three selected mutants were subjected to unfolding-refolding according to the method previously described for the wild type protein. The refolded CyaC mutants were subjected to size-exclusion FPLC (Superdex 75), which was equilibrated with 20 mM Tris-HCl (pH 8.0). Similar to the CyaC wild-type enzyme, the purified mutants (S30A, H33A and Y66A) were eluted from the column in a distinct single peak corresponding to the eluted fractions of monomeric CyaC. These collected fractions were then analyzed on SDS-PAGE (*see* **Figure 8.11**).

8.4 Hemolytic activity of CyaA-PF activated by CyaC mutants *in vivo* and *in vitro*

The hemolytic activities of CyaA-PF activated by various CyaC mutants with pNPP *in vitro* are shown in **Table 8.1**. Crude soluble extracts from *E. coli* cells coexpressing CyaA-PF protein with each CyaC mutant were examined for their relative hemolytic activity against sheep red blood cells, considering as *in vivo* CyaA-PF activation (**Table 8.1**). The hemolysis data recorded in comparison with that of the CyaA-PF revealed that all S30A, H33A and Y66A CyaC mutants exhibited a dramatic ~80-90% decrease in hemolytic activity.

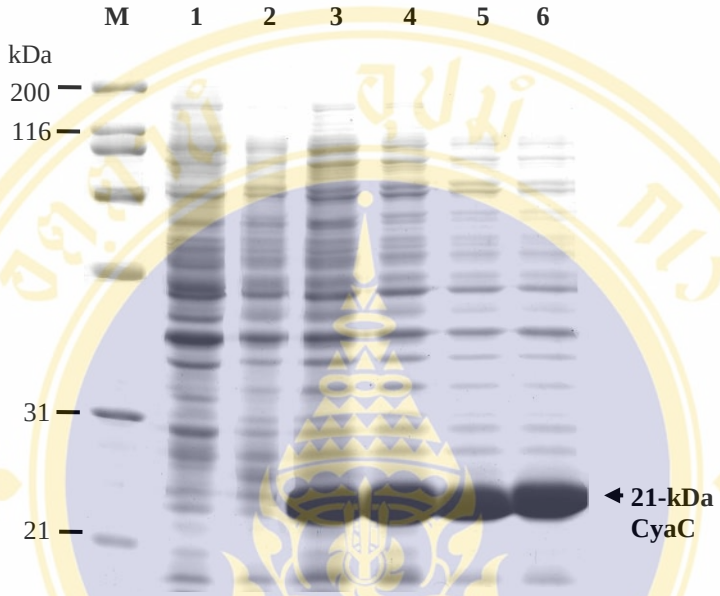

Figure 8.9 Expression of the CyaC wild-type and its mutant enzymes

SDS-PAGE (Coomassie brilliant blue-stained 12% gel) analysis of lysates of *E. coli* cells expressing 21-kDa wild-type CyaC (lane 3) and S30A, H33A and Y66A mutants (corresponding to lanes 4-6, respectively). M represents molecular mass standards. *E. coli* cells harboring pET-17b and pCyaC without IPTG induction were used as negative controls (lanes 1 and 2, respectively).

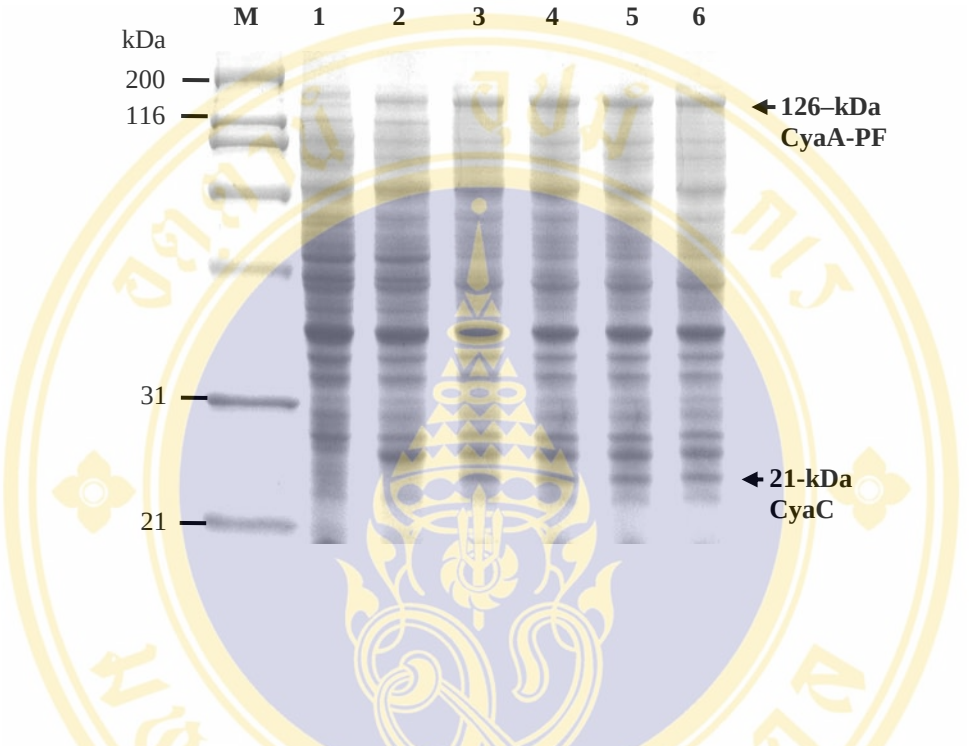

Figure 8.10 Coexpression of the CyaA-PF wild-type with CyaC and its mutants

SDS-PAGE (Coomassie brilliant blue-stained 12% gel) analysis of lysates extracted from *E. coli* cells coexpressing CyaA-PF with CyaC and its mutants (S30A, H33A and Y66A) lanes 3-6, respectively). M represents molecular mass standards. *E. coli* cells harboring pET-17b and pCyaAC-PF without IPTG induction were used as negative controls (lanes 1 and 2, respectively).

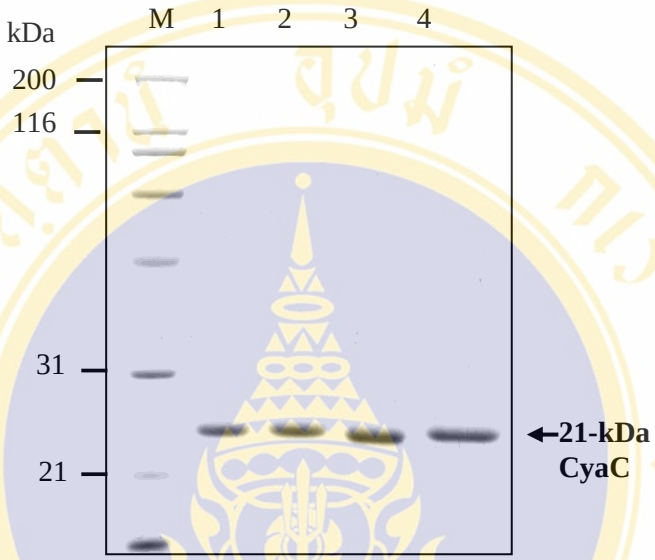

Figure 8.11 Purification of the refolded CyaC wild-type and its mutants

SDS-PAGE (Coomassie brilliant blue-stained 12% gel) analysis of the 21-kDa purified CyaC wild-type (lane 1) and its mutants (S30A, H33A and Y66A corresponding to lanes 2-4, respectively). M represents molecular mass standards.

Table 8.1 Hemolytic activities of CyaA-PF toxin activated *in vitro* and *in vivo* by CyaC mutants (S30A, H33A and Y66A) against sheep erythrocytes

CyaC proteins	**Hemolytic activity of activated CyaA-PF**[a] (% Hemolysis ± SEM)	
	In vivo	***In vitro***[b]
Wild-type	83.2 ± 3.4	88.3 ± 2.7
S30A_mutant	1.5 ± 0.6	5.3 ± 1.6
H33A_mutant	3.2 ± 0.6	4.6 ± 1.4
Y66A_mutant	2.1 ± 1.2	5.5 ± 1.3

[a] Hemolytic activity is presented as averaged from three independent experiments performed in duplicates. SEM represents standard errors of the mean.

[b] *In vitro* activation using pNPP as an acyl donor.

8.5 Esterase activity of CyaC mutants

Kinetic constant of pNPP hydrolysis by CyaC was measured for the wild-type and the mutants. If these residues were involved in the positioning of the active site, the rate of deacylation of the acyl-enzyme intermediate should be affected. The results revealed that all three mutations (S30A, H33A, Y66A) caused a severe loss in esterolytic activity of the mutant enzymes toward pNPP (*see* **Figure 8.12**), signifying a vital role in the catalytic behavior for these three conserved residues.

Steady-state kinetics were performed with various concentrations of pNPP as a substrate. The reactions followed Michaelis–Menten kinetics, and the kinetic parameters k_{cat} and K_m were determined by non-linear regression analysis (**Figure 8.13**). The S30A and H33A mutants decreased K_m values for pNPP, except for Y66A, which had values similar to the wild-type, demonstrating a changed affinity toward substrate. Both general kinetic constants (K_m and k_{cat}) of S30A and H33A mutants were affected to the binding of the substrate and the rate of catalysis. The Y66A mutant was found to have a similar K_m as the wild-type, only the V_{max} was significantly different from the wild-type (4-fold decrease). The largest change of catalytic efficiency (k_{cat}/K_m) observed for all mutants (**Table 8.2**).

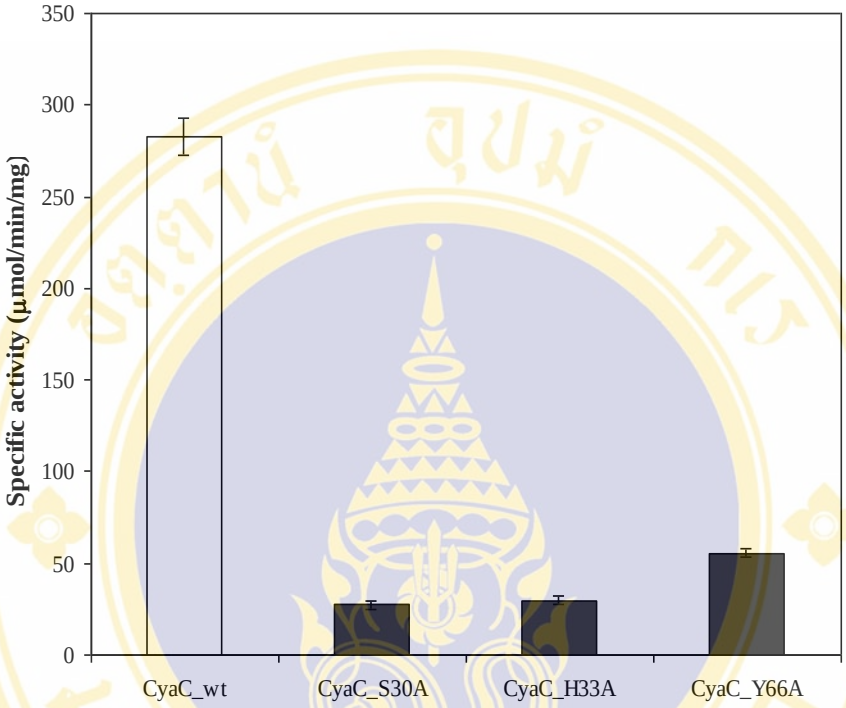

Figure 8.12 Specific activities of wild-type and mutant CyaC enzymes toward pNPP substrate

Specific activity of each enzyme was obtained using 100 µM pNPP as the substrate concentration. Shaded boxes represent the specific activity of the mutants that are significantly different (*p* values < 0.001) from that of the wild-type enzyme. Error bars indicated standard errors of the mean from three independent experiments.

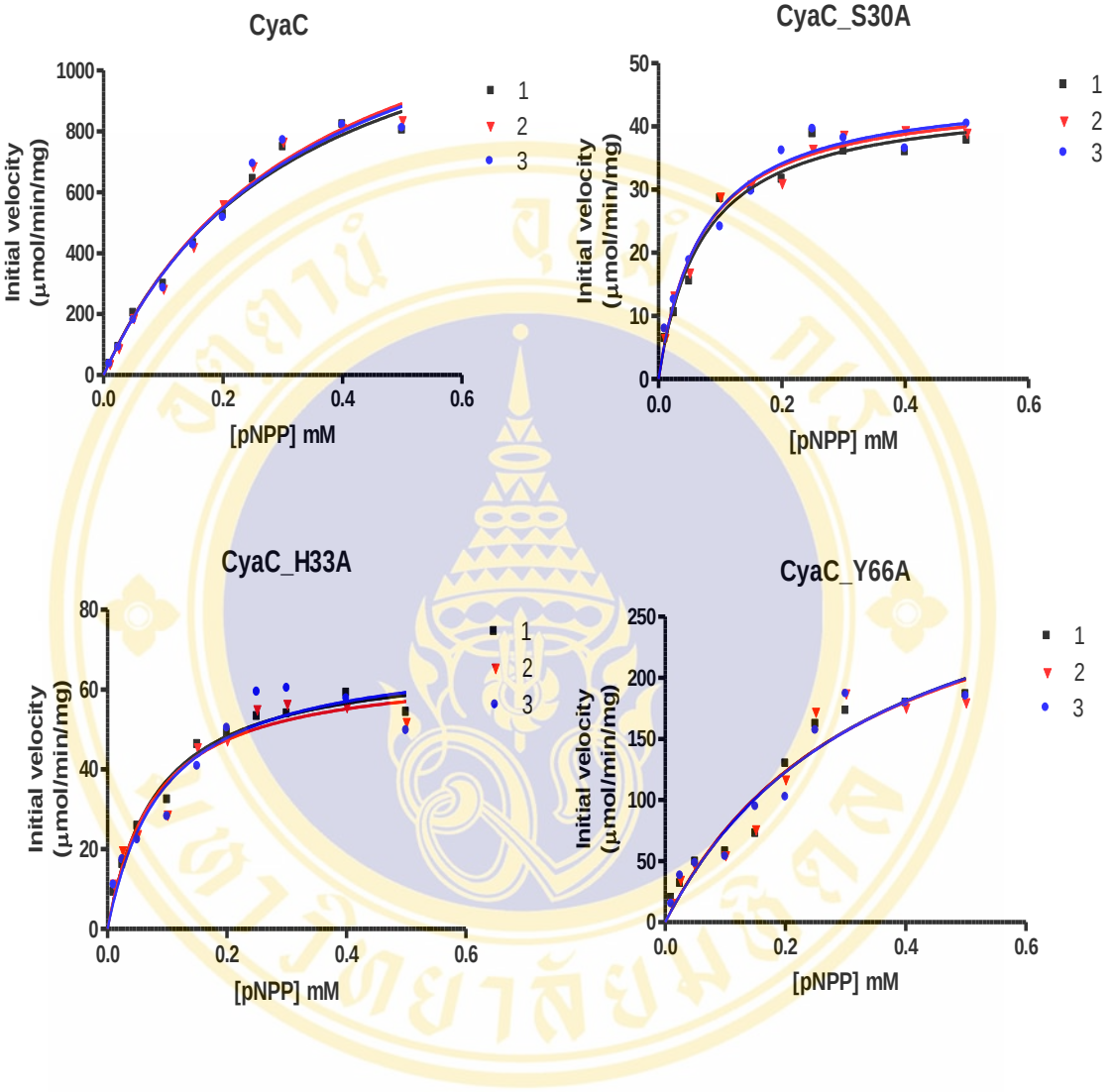

Figure 8.13 Comparison of CyaC wild-type and mutant hydrolysis rates at different substrate concentrations

The graph shows the reaction velocities of CyaC for hydrolysis of pNPA and pNPP at concentrations in the range of 10-500 µM. Assay was performed at 25ºC in 50 mM Tris-HCl, pH 7.4. Kinetic parameters were determined from nonlinear fitting of untransformed data to the Michaelis-Menten equation. Data are reported as the means of duplicate in three independents (lines 1, 2 and 3).

Table 8.2 Steady-state kinetic parameters for CyaC of wild-type and mutants for hydrolysis of pNPP reaction at pH 7.4 and 25°C

Enzyme	K_m (mM)	V_{max} ($\mu mol.min^{-1}.mg^{-1}$)	k_{cat} (s^{-1})	k_{cat} / K_m ($s^{-1}mM^{-1}$)
CyaC_WT	0.3370 ± 0.0139	1266 ± 38.94	443 ± 13.68	1315
CyaC_S30A	0.0709 ± 0.0005	45 ± 0.33	15 ± 0.12	225
CyaC_H33A	0.0849 ± 0.0033	68 ± 0.91	23 ± 0.32	282
CyaC_Y66A	0.3493 ± 0.0029	338 ± 1.54	118 ± 0.53	339

The enzyme activities were measured at various concentrations of pNPP in 50 mM Tris-HCl buffer, pH 7.4. The reaction was monitored at 400 nm, ε =11.6 $mM^{-1}cm^{-1}$.

8.7 LC-MS-MS analysis of CyaA-PF activated by CyaC mutants

As mentioned earlier, CyaA-PF fragment activated with CyaC was able to be *in vivo* or *in vitro* palmitoylated at Lys^{983} to become hemolytically active. Experiments *via* MALDI-TOF-MS and LC-MS-MS analyses were therefore performed to verify such *in vivo* or *in vitro* palmitoylation of the CyaA-PF toxins that can be activated by CyaC mutants. In the case of MALDI-TOF-MS analysis, the presence of the trypsin-generated peptide mass encompassing E^{972}GV ATQTTAYGK^{983} at *m/z* 613 reveals the non-palmitoylated Lys^{983} of CyaA-PF toxin. On this basis, the corresponding non-palmitoylated peptide mass was found for all the three mutants (**Figure 8.14**, above). Moreover, the peptide sequence encompassing Lys^{983} subsequently identified by LC-MS-MS could confirm the absence of palmitoylation for all mutants (**Figure 8.14**, below).

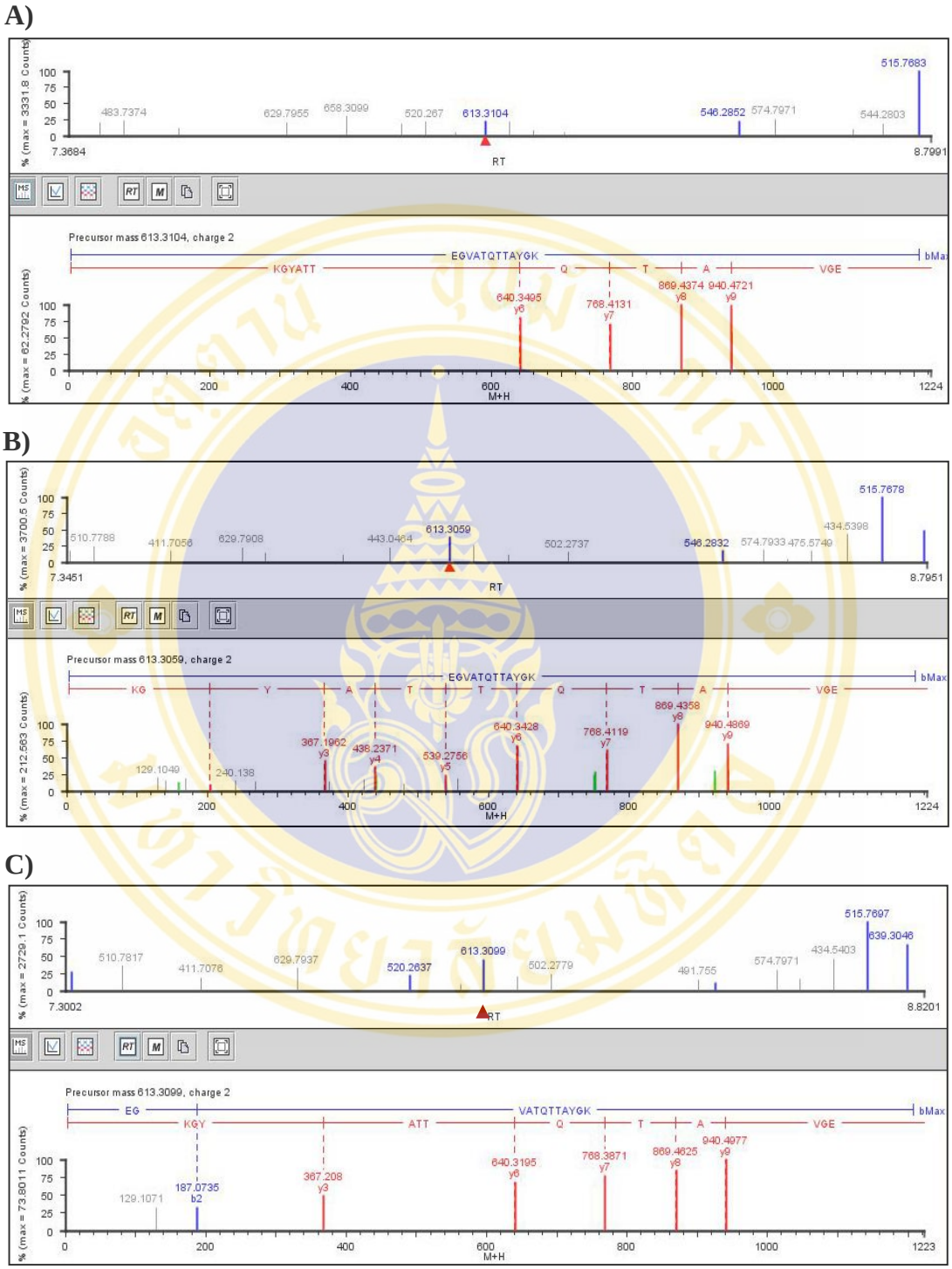

Figure 8.14 Representative MALDI-TOF-MS and LC-MS-MS spectra of CyaA-PF coexpressed with CyaC mutant

The figure shows the MALDI-TOF-MS mass spectra of the tryptic peptide fragments (Above) and the sequence of the non-acylated peptide confirmed with LC-MS-MS analysis (Below). The peptide fragment with *m/z* 613.31 (indicated by arrow) was found matched the non-acylated peptide, Glu^{972} to Lys^{983}. The *m/z* values of fragment ions (b_i and y_i) of the non-acylated peptide are shown. Panel A, B and C represent the spectra of CyaA-PF activated by CyaC mutants, S30A, H33A and Y66A, respectively.

CHAPTER IX
DISCUSSION

9.1 Expression and purification of CyaC and proCyaA-PF proteins

Upon IPTG induction at 30°C, the 21-kDa CyaC protein was highly expressed mostly as insoluble inclusions fraction (**Figure 5.1A**). The best strategy to recover the active CyaC from inclusions (solubilized in 8 M urea) was achieved using buffer-exchange with 2 M urea and 150 mM NaCl *via* gel filtration (**Figure 5.8**). NaCl was added into the refolding solution and successfully suppressed the aggregation as it was reported to facilitate the folding of denatured proteins into globular shapes favoring a native conformation (70). The elution profile from size exclusion FPLC analysis revealed that the 21-kDa CyaC protein was eluted at a single peak corresponding to the elution volume of the 43-kDa ovalbumin protein marker (*see* **Appendix 1**), suggesting that it exists as a monomer in the native condition.

On the other hand, the 126-kDa proCyaA-PF and CyaA-PF proteins were expressed almost exclusively as the soluble fraction (**Figure 5.1B**). The soluble proCyaA-PF protein was successfully purified by anion-exchange and size-exclusion chromatographic techniques. In western blot analysis, the proCyaA-PF toxin was recognized by anti-RTX specific monoclonal antibody-9D4, confirming its identity to be an RTX related toxin (**Figure 5.11A**). However, several smaller immuno-reactive bands were also detected even in the presence of PMSF-protease inhibitor, indicating that the protein was highly sensitive to proteolytic degradation by non-serine proteases from *E. coli* host.

9.2 Functional characterization of CyaC-acyltransferase

The purified CyaC monomeric form was found to significantly activate the proCyaA-PF as well as to hydrolyze pNPA and pNPP. As mentioned earlier, the

CyaA-PF fragment can be acylated *in vivo* by co-expressed CyaC to exhibit hemolytic activity (15). When the cell lysate containing proCyaA-PF mixed with the purified CyaC protein, it showed high hemolytic activity against sheep erythrocytes. This indicated that CyaC can activate the proCyaA-PF fragment *in vitro*. The ability of CyaC to activate the hemolytic activity of proCyaA-PF implied the acyl group was transferred onto proCyaA-PF. It was also observed that both soluble and refolded CyaC were able to *in vitro* activate the proCyaA-PF fragment to show comparable hemolysis, suggesting that the refolded CyaC is likely to exist as active monomer corresponding to the native-folded protein in the soluble fraction.

Noticeably, the hemolytic activity given rise from *in vitro* activation was rather lower than that from the *in vivo* acylation, implying the lack of cellular environment for the *in vitro* condition simulated here. It has been also observed for such inefficient *in vitro* activation in other studies of RTX toxins, including *E. coli* HlyA with HlyC (67), *P. haemolytica* LktA with LktC (71) and the full-length CyaA with refolded CyaC (5). Notwithstanding the lower efficiency of *in vitro* activation, the CyaA-PF hemolytic activity could be inferred as the CyaC capability in transferring an acyl group to the target acceptor.

From the results shown in **Table 5.2**, specific activities of the purified CyaC enzyme in catalyzing hydrolysis of pNPA and pNPP are ~48 U/mg and ~289 U/mg, respectively, indicating that CyaC exerted a much higher esterase activity towards a palmitoyl group, which has been shown to be a preferred physiological substrate (6, 72). Conversely, pNPA was preferred over pNPP the esterolytic activity of chymotrypsin under conditions used. It can be noted that both soluble and refolded CyaC showed relatively the same specific activity in catalyzing pNPA that was consistent with the CyaA-PF hemolytic activities upon *in vitro* activation by either form of CyaC. Despite the fact that CyaC-acyltransferase and chymotrypsin exhibit different substrate preferences, their reactions toward these analogs may share a common feature regarding the hydrolysis of oxygen-ester bond. Therefore, structural insights into the mechanistic basis for the esterolytic reaction of CyaC in comparison with this serine esterase are of very much interest.

9.3 *p*-Nitrophenyl palmitate mimics acyl-ACP for activating proCyaA-PF by CyaC *in vitro*

As previously shown, CyaC was able to hydrolyze the pNPP substrate, followed by the release of palmitoyl-free group and *p*-nitrophenol products. Here, the specific pNPP (palmitoyl group) substrate was used for *in vitro* activation system and interpreted in the term of CyaC acylated CyaA-PF reaction. From the results shown in **Table 5.1 and Figure 5.2**, CyaC was able to transfer the acyl group from pNPP onto proCyaA-PF to become active toxin. The result of hemolytic activities of acylated CyaA-PF by CyaC *in vitro* revealed that CyaA-PF activated by CyaC in the presence of pNPP exerts comparable hemolytic activity, to that of when using *E. coli* lysate containing acyl-ACP. It indicated that pNPP analogue effectively mimicked the acyl-ACP as an acyl donor for CyaA acylation process, signifying various catalytic behaviors for CyaC in transferring the functional groups (SH or OH). The result of LC-MS-MS analysis also confirmed that the CyaA-PF was palmitoylated at Lys^{983} upon *in vitro* activation by CyaC with utilizing pNPP as the substrate. This is in agreement with the previous study that N-acetylcysteamine (NAC) thioester derivative effectively mimics acylated ACP intermediate in biosynthetic pathways and can serve as a substrate for polyketide synthase and nonribosomal peptide synthetase (73, 74).

9.4 Substrate specificity of CyaC

From the result shown in **Table 6.2**, the rank order of substrate specificity (from the highest to the lowest) for CyaC hydrolysis was as follows: pNPP equal to pNPM > pNPD > pNPC > pNPS > pNPA. These results reveal that CyaC enzyme can hydrolyze the longer chain of fatty acids, and is highly selective and specific for the palmitoyl group and myristoyl group. By "C14-16 preferring" are meant that the CyaC enzyme prefers to cleave myristate and palmitate substrates of different acyl carbon lengths. Among the acyl chain length, the K_m value for palmitoyl group (pNPP) was the best fit binding site to CyaC protein. However, whether one or both of the proCyaA acylation sites was acylated by each of the different acyl-donors is still not known.

The hemolysis results shown in **Figure 6.2** also indicated that the different acyl-chain lengths of *p*-nitrophenyl derivatives would result in a different potency of lytic agents. A marked increase in lytic capability was seen in palmitoyl-CyaA-PF and the hemolytic efficacies declined with increasing chain length. However, without knowing the degree of acylation of CyaA-PF toxin with each acyl group, it is difficult to draw a conclusion concerning the relative toxic efficiencies of each acylated protein in the *in vitro* activation reactions reported here. Nevertheless, whatever acyl groups were used to activate CyaA-PF, the activated toxin retained hemolytic activity. Notably that the toxins acylated with all chain-length fatty acids were present in different quantities but produced amounts of lysis which were close at ≥ 300 μM pNP-substrate concentration. Perhaps distinct acyl groups favor different efficiencies of membrane insertion which contribute to the overall lytic efficiency of a particular toxin.

9.5 Binding affinity of CyaC to palmitate

Using the method of extrinsic fluorescence emission and fluorescence quenching show the maximal binding ratios (n) of palmitate with CyaC to be 10:1 (**Figure 6.3A**). This result tends to support a notion that CyaC posses ten independent palmitate binding sites. When CyaC added with substrate experiments showed a palmitate data, suggesting that a surface low-affinity binding site would appear to satisfy most of the reported experimental observations, especially co-crystallization.

Analysis of the binding shows that the dissociation constant (K_d^{app}) between CyaC and palmitate is relatively high, within the nM range (**Figure 6.3B**). The possibilities may be due to the different concentrations of CyaC used, pH, fluorescence of Trp in protein affected by ionization of neighboring prototropic groups or by conformational changes (43) and ultimately the nature of the substrate or ligand, such as their size, structure, and hydrophobicity.

9.6 Homology-based CyaC structure with implications for its catalysis

Although crystallization attempts have been made over long-time periods, it is still unsuccessful to obtain a good crystal for the purified CyaC protein. A plausible 3D structure of this enzyme was built instead by modeling based on the known DABA structure (PDB code 3D3S), which is the best-fit template available so far in the group of acetyltransferases. As shown in **Figure 7.7**, the CyaC structure (Leu^{26}-Ala^{185}) comprises of a single domain with an α/β hydrolase fold. Interestingly, CyaC model also reveals a putative catalytic triad Ser^{30}–His^{33}–Tyr^{66}, which is highly conserved among the RTX-acyltransferase family (**Figure 7.6**). For HlyC-acyltransferase, the homologous RTX toxin, the residues of Ser^{20}, His^{23}, Tyr^{70} and Tyr^{150} have been identified to be potentially involved in acyl transfer catalysis (75-77). As can be also inferred from the model, Tyr^{66} is likely to help orient the imidazole ring of His^{33} and make a better proton acceptor through hydrogen bonding, similar to Asp^{102} in the catalytic triad of chymotrypsin. It is thus proposed that CyaC-acyltransferase is conceivably a serine esterase in which Ser^{30} is part of a catalytic triad that also includes His^{33} and Tyr^{66} forming hydrogen bonding network. Acylation-deacylation steps of CyaC are perhaps similar to that was found for chymotrypsin-like esterase. However, the CyaC mechanism proposed for the catalytic triad still needs to be tested for the contribution of individual residues (Ser^{30}, His^{33} and Tyr^{66}**)** to the catalytic power of this enzyme.

9.7 Mutagenic definition of CyaC-like catalytic triad

Single-alanine substitutions at catalytic triad residues (Ser^{30}- His^{33}-Tyr^{66}) were performed in order to validate their contribution to the CyaC esterolytic mechanism and capability of activating proCyaA-PF *in vitro*. The results of specific activities of wild-type and mutant CyaC enzymes toward pNPP substrate revealed that all three mutations (S30A, H33A and Y66A) caused a severe loss in esterolytic activity of the mutant enzymes toward pNPP (*see* **Figure 8.12**), signifying a vital role in the catalytic behavior for these three conserved residues.

The weak activity in esterase catalysis of S30A and H33A variants (**Table 8.2**) suggests that a water molecule may act as a poor substitute and possibly be endowed with the nucleophilic-attacking character by the rest residue hydrogen-bonding, although through a much slower catalytic mechanism (78). The catalytic efficiency (k_{cat}/K_m) values of S30A and H33A were also shown to be reduced to 17.11% and 21.44% of the wild-type, indicating that without the hydrogen-bonding between the side chains of His^{33} and Ser^{30}, the ester substrate would retain approximate accessibility to the active cleft, and thus the barely detectable catalytic efficiency would be resulted from the extremely low k_{cat} values of the mutants.

Y66A showed a similar K_m value (0.349 ± 0.003 mM) compared with the wild-type (0.337 ± 0.014) but it showed a dramatically reduced k_{cat}/K_m value (25.78% of the wild-type). This indicates that Tyr^{66} is not essential for substrate binding when compared to the two other residues in the triad. However, Tyr^{66} could significantly affect enzymatic activity as it probably provides hydrogen-bonding contribution to stabilize oxyanion of the acyl–enzyme intermediate during the catalytic process (79).

The capability of activating proCyaA-PF of all CyaC mutants *via* the assessment of hemolysis clearly showed that the toxins had lost their hemolytic activity (**Table 8.1**) consistent with the results of the kinetic studies. The mass spectroscopy also confirmed that mutations of these proposed three critical residues in CyaC abate the acylation on CyaA-PF toxin.

On the basis of esterase, hemolysis and mass spectroscopy studies, all three mutations (S30A, H33A and Y66A) caused a severe loss in acyltransferase activity, signifying a vital role in the catalytic behavior for these three conserved residues. This is in agreement with the previous study that a nearly complete loss in acyltransferase activity of CyaC was observed for S30R, S30W, H33S and H33D mutants (6). Also for HlyC-acyltransferase, Ser^{20}, His^{23}, Tyr^{70} and Tyr^{150} have been identified to be involved in acyl-transfer catalysis (75-77). Altogether, it is thus proposed that CyaC-acyltransferase is conceivably a serine esterase in which Ser^{30} is part of a catalytic triad that also includes His^{33} and Tyr^{66} forming a hydrogen-bonding network.

9.8 Proposed mechanism of CyaC-catalyzed acyltransferase reaction

Trypsin and chymotrypsin are structurally very similar, although they recognize different substrates (80). Trypsin acts on lysine and arginine residues, while chymotrypsin acts on large hydrophobic residues such as tryptophan, tyrosine and phenylalanine, both with extraordinary catalytic efficiency. Therefore, amidase activity of trypsin was usually evaluated by a colorimetric assay using *L*-lysine ρ-nitroanilide as a substrate (81) while [alpha]-chymotrypsin has been used pNPA as a substrate in kinetic studies (82, 83). However, both enzymes have a catalytic triad of serine, histidine and aspartate within the S1 binding pocket.

In experiments of substrate analogues hydrolysis in comparison with chymotrypsin activity, CyaC-acyltransferase may share a similar mechanism of acyltransferase with a serine esterase, such as catalytic triad catalysis and catalysis *via* acyl-enzyme intermediate. Acylation of CyaC and then deacylation of the acyl-enzyme intermediate would be considered to apply for the hydrolysis of specific substrates. It was found that CyaC was able to catalyze the hydrolysis of pNPP substrate without an encounter of the second target substrate CyaA-PF. This suggests that acyltransferase reaction would employ a simple ping-pong (double displacement) rather than random sequential mechanism as was also proposed for chymotrypsin (82) and HlyC-acyltransferase (67). This observation, hence, supports the ping-pong mechanism in which one or more products are released before all substrate have been added rather than random sequential mechanism.

By analogy to the pNPA hydrolysis system (**Figure 9.1A**), the mechanism of CyaC-catalyzed group transfer reaction is likely to proceed into two steps linked by a covalent bond intermediate as the enzyme becoming acylated during the catalytic reaction (**Figure 9.1B**). In the first stage, an acyl group of the first substrate A (acyl-ACP) is displaced from the substrate by the enzyme E (CyaC) to yield the first product P (ACPSH) and a stable enzyme form F (acyl-ACP) in which acyl group is covalently bound to the enzyme (ping). In the second stage of the reaction, the acyl group is displaced from the enzyme by the second substrate B (proCyaA) to yield the second product Q (CyaA), thereby regenerating the original form of CyaC enzyme, E (pong).

A)

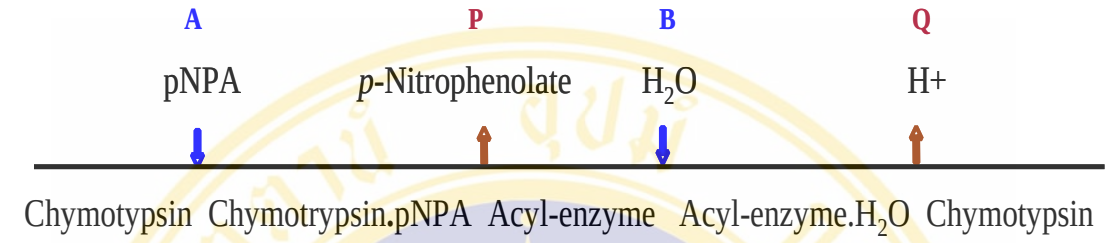

B)

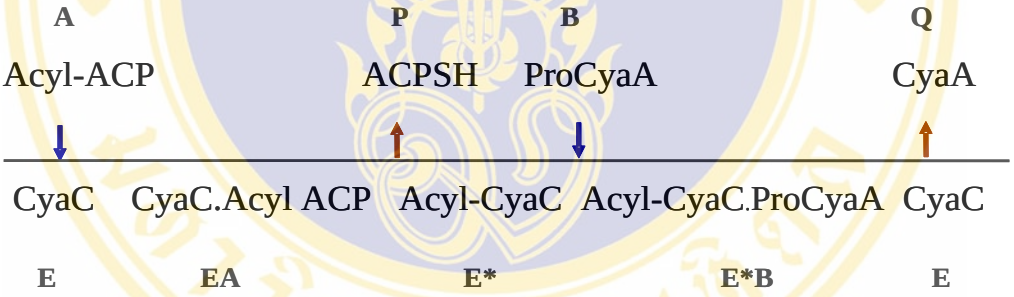

Figure 9.1 The proposed mechanism of CyaC-catalyzed acyltransferase reaction

(A) Chymotrypsin catalyzes the hydrolysis of pNPA and that during the course of this reaction there occur the formation of an acetyl-enzyme complex (65, 82).

(B) Simulated reaction of CyaC catalyzing group-transfer reaction represented by ping pong bi bi reaction. CyaC transfer the acyl group from acyl-ACP which reacts with the substrate to form a covalent acyl-enzyme intermediate.

CHAPTER X
CONCLUSION

1. This study has provided pivotal evidence for the first time that the *Bordetella pertussis* CyaC-acyltransferase, which was purified from *E. coli* recombinant clone exists as an active monomer and exhibits an esterase activity *via* the hydrolysis of ester bond of *p*-nitrophenyl derivatives determined by spectrophotometry.
2. CyaC can cleave both oxygen-ester and thio-ester linkages of its hydrolysable substrates, *p*-nitrophenyl derivatives and acyl-ACP, respectively.
3. The *p*-nitrophenyl palmitate (pNPP) can mimic the acyl-ACP, as acyl donor, for proCyaA-PF activation *in vitro* by CyaC. The activation of proCyaA-PF was determined by its hemolytic activity with palmitoylation of Lys^{983}.
4. CyaC can hydrolyze *p*-nitrophenyl derivatives of 8-18 carbon chain length with the most preference for acyl chains of 14-16 carbons.
5. The palmitoylation (C16) of CyaA-PF toxin was found to give the highest toxin activity, conferring the nature of acyl-modification of CyaA toward toxicity.
6. Based on structure, the modeled CyaC structure built *via* the known DABA structure together with mutagenesis studies, three highly conserved residues, Ser^{30}, His^{33} and Tyr^{66}, were proposed to be a catalytic triad essentially required for its esterase activity.
7. CyaC-acyltransferase enzyme was proposed to catalyze the transfer of acyl group from acyl-ACP and conjugate to CyaA-PF toxin *via* acyl-CyaC intermediate forming transient bond between acyl group and Ser^{30} of CyaC.

REFERENCES

1. Carbonetti, N. H., Artamonova, G. V., Andreasen, C. & Bushar, N. (2005). Pertussis toxin and adenylate cyclase toxin provide a one-two punch for establishment of *Bordetella pertussis* infection of the respiratory tract. *Infect Immun 73*, 2698-2703.
2. Sebo, P. & Ladant, D. (1993). Repeat sequences in the *Bordetella pertussis* adenylate cyclase toxin can be recognized as alternative carboxy-proximal secretion signals by the *Escherichia coli* alpha-haemolysin translocator. *Mol Microbiol 9*, 999-1009.
3. Lally, E. T., Hill, R. B., Kieba, I. R. & Korostoff, J. (1999). The interaction between RTX toxins and target cells. *Trends Microbiol 7*, 356-361.
4. Hackett, M., Guo, L., Shabanowitz, J., Hunt, D. F. & Hewlett, E. L. (1994). Internal lysine palmitoylation in adenylate cyclase toxin from *Bordetella pertussis*. *Science 266*, 433-435.
5. Westrop, G. D., Hormozi, E. K., Da Costa, N. A., Parton, R. & Coote, J. G. (1996). *Bordetella pertussis* adenylate cyclase toxin: proCyaA and CyaC proteins synthesised separately in *Escherichia coli* produce active toxin in vitro. *Gene 180*, 91-99.
6. Basar, T., Havlicek, V., Bezouskova, S., Hackett, M. & Sebo, P. (2001). Acylation of lysine 983 is sufficient for toxin activity of *Bordetella pertussis* adenylate cyclase. Substitutions of alanine 140 modulate acylation site selectivity of the toxin acyltransferase CyaC. *J Biol Chem 276*, 348-354.
7. Simsova, M., Sebo, P. & Leclerc, C. (2004). The adenylate cyclase toxin from *Bordetella pertussis* - a novel promising vehicle for antigen delivery to dendritic cells. *Int J Med Microbiol 293*, 571-576.
8. Guermonprez, P., Khelef, N., Blouin, E., Rieu, P., Ricciardi-Castagnoli, P., *et al*. (2001). The adenylate cyclase toxin of *Bordetella pertussis* binds to target

cells *via* the alpha(M)beta(2) integrin (CD11b/CD18). *J Exp Med 193*, 1035-1044.

9. Glaser, P., Elmaoglou-Lazaridou, A., Krin, E., Ladant, D., Barzu, O., *et al*. (1989). Identification of residues essential for catalysis and binding of calmodulin in *Bordetella pertussis* adenylate cyclase by site-directed mutagenesis. *Embo J 8*, 967-972.
10. Khelef, N., Zychlinsky, A. & Guiso, N. (1993). *Bordetella pertussis* induces apoptosis in macrophages: role of adenylate cyclase-hemolysin. *Infect Immun 61*, 4064-4071.
11. Vojtova, J., Kofronova, O., Sebo, P. & Benada, O. (2006). *Bordetella* adenylate cyclase toxin induces a cascade of morphological changes of sheep erythrocytes and localizes into clusters in erythrocyte membranes. *Microsc Res Tech 69*, 119-129.
12. Bellalou, J., Sakamoto, H., Ladant, D., Geoffroy, C. & Ullmann, A. (1990). Deletions affecting hemolytic and toxin activities of *Bordetella pertussis* adenylate cyclase. *Infect Immun 58*, 3242-3247.
13. Masin, J., Basler, M., Knapp, O., El-Azami-El-Idrissi, M., Maier, E., *et al*. (2005). Acylation of lysine 860 allows tight binding and cytotoxicity of *Bordetella* adenylate cyclase on CD11b-expressing cells. *Biochemistry 44*, 12759-12766.
14. Stanley, P., Koronakis, V. & Hughes, C. (1998) Acylation of *Escherichia coli* hemolysin: a unique protein lipidation mechanism underlying toxin function. *Microbiol Mol Biol Rev 62*, 309-333.
15. Powthongchin, B. & Angsuthanasombat, C. (2008). High level of soluble expression in *Escherichia col*i and characterisation of the CyaA pore-forming fragment from a *Bordetella pertussis* Thai clinical isolate. *Arch Microbiol 189*, 169-174.
16. Mattoo, S. & Cherry, J. D. (2005). Molecular pathogenesis, epidemiology, and clinical manifestations of respiratory infections due to *Bordetella pertussis* and other *Bordetella* subspecies. *Clin Microbiol Rev 18*, 326-382.

17. Smith, A. M., Guzman, C. A. & Walker, M. J. (2001). The virulence factors of *Bordetella pertussis*: a matter of control. *FEMS Microbiol Rev 25*, 309-333.

18. van den Berg, B. M., Beekhuizen, H., Willems, R. J., Mooi, F. R. & van Furth, R. (1999). Role of *Bordetella pertussis* virulence factors in adherence to epithelial cell lines derived from the human respiratory tract. *Infect Immun 67*, 1056-1062.

19. Guiso, N. (1997). Isolation, identification and characterization of *Bordetella pertussis*. *Dev Biol Stand 89*, 233-238.

20. Ahmad, F. & Calder, M. A. (1984). Isolation of *Bordetella pertussis*: benefits of using both Bordet-Gengou and charcoal agar media. *J Clin Pathol 37*, 1071-1072.

21. Powthongchin, B. (2007). Molecular characterisation of the pore-forming domain of the *Bordetella pertussis* adenylate cyclase-haemolysin toxin**.** [Ph.D. thesis], Bangkok, Faculty of Graduated Studies, Mahidol University.

22. Crowcroft, N. S. & Pebody, R. G. (2006). Recent developments in pertussis. *Lancet 367*, 1926-1936.

23. Wood, N. & McIntyre, P. (2008). Pertussis: review of epidemiology, diagnosis, management and prevention. *Paediatr Respir Rev 9*, 201-211.

24. Locht, C. (1999) Molecular aspects of *Bordetella pertussis* pathogenesis. *Int Microbiol 2*, 137-144.

25. Ladant, D. & Ullmann, A. (1999). *Bordetella pertussis* adenylate cyclase: a toxin with multiple talents. *Trends Microbiol 7*, 172-176.

26. Welch, R. A. (2001). RTX toxin structure and function: a story of numerous anomalies and few analogies in toxin biology. *Curr Top Microbiol Immunol 257*, 85-111.

27. Goodwin, M. S. & Weiss, A. A. (1990). Adenylate cyclase toxin is critical for colonization and pertussis toxin is critical for lethal infection by *Bordetella pertussis* in infant mice. *Infect Immun 58*, 3445-3447.

28. Harvill, E. T., Cotter, P. A., Yuk, M. H. & Miller, J. F. (1999). Probing the function of *Bordetella bronchiseptica* adenylate cyclase toxin by manipulating host immunity. *Infect Immun 67*, 1493-1500.

29. Guiso, N., Szatanik, M. & Rocancourt, M. (1991). Protective activity of *Bordetella pertussis* adenylate cyclase-hemolysin against bacterial-colonization. *Microbiol Pathog 11*, 423-431.

30. Binet, R., Letoffe, S., Ghigo, J. M., Delepelaire, P. & Wandersman, C. (1997). Protein secretion by Gram-negative bacterial ABC exporters - a review. *Gene 192*, 7-11.

31. Barry, E. M., Weiss, A. A., Ehrmann, I. E., Gray, M. C., Hewlett, E. L. & Goodwin, M. S. (1991). *Bordetella pertussis* adenylate cyclase toxin and hemolytic activities require a second gene, cyaC, for activation. *J Bacteriol 173*, 720-726.

32. Bauche C, Chenal A, Knapp O, Bodenreider C, Benz R, Chaffotte A, Ladant D. Structural and functional characterization of an essential RTX sub-domain of *Bordetella pertussis* adenylate cyclase toxin. *J Biol Chem* 2006; 281:16914-16926.

33. Rose, T., Sebo, P., Bellalou, J. & Ladant, D. (1995). Interaction of calcium with *Bordetella pertussis* adenylate cyclase toxin. Characterization of multiple calcium-binding sites and calcium-induced conformational changes. *J Biol Chem 270*, 26370-26376.

34. El-Azami-El-Idrissi, M., Bauche, C., Loucka, J., Osicka, R., Sebo, P., *et al*. (2003). Interaction of *Bordetella pertussis* adenylate cyclase with CD11b/CD18: Role of toxin acylation and identification of the main integrin interaction domain. *J Biol Chem 278*, 38514-38521.

35. Forestier, C. & Welch, R. A. (1991). Identification of RTX toxin target cell specificity domains by use of hybrid genes. *Infect Immun 59*, 4212-4220.

36. Osickova, A., Osicka, R., Maier, E., Benz, R. & Sebo, P. (1999). An amphipathic alpha-helix including glutamates 509 and 516 is crucial for membrane translocation of adenylate cyclase toxin and modulates formation and cation selectivity of its membrane channels. *J Biol Chem 274*, 37644-37650.

37. Gueirard, P., Druilhe, A., Pretolani, M. & Guiso, N. (1998). Role of adenylate cyclase-hemolysin in alveolar macrophage apoptosis during *Bordetella pertussis* infection *in vivo*. *Infect Immun 66*, 1718-1725.

38. Gray, M., Szabo, G., Otero, A. S., Gray, L. & Hewlett, E. (1998). Distinct mechanisms for K+ efflux, intoxication, and hemolysis by *Bordetella pertussis* AC toxin. *J Biol Chem 273*, 18260-18267.

39. Ehrmann, I. E., Gray, M. C., Gordon, V. M., Gray, L. S. & Hewlett, E. L. (1991). Hemolytic activity of adenylate cyclase toxin from *Bordetella pertussis*. *FEBS Lett 278*, 79-83.

40. Szabo, G., Gray, M. C. & Hewlett, E. L. (1994). Adenylate cyclase toxin from *Bordetella pertussis* produces ion conductance across artificial lipid bilayers in a calcium- and polarity-dependent manner. *J Biol Chem 269*, 22496-22499.

41. Lee, S. J., Gray, M. C., Zu, K. & Hewlett, E. L. (2005). Oligomeric behavior of *Bordetella pertussis* adenylate cyclase toxin in solution. *Arch Biochem Biophys 438*, 80-87.

42. Carr, P. D. & Ollis, D. L. (2009). Alpha/beta Hydrolase Fold; an Update. *Protein Pept Lett 16* (10), 1137-1148.

43. Wang, Q., Allen, J. C. & Swaisgood, H. E. (1997). Binding of vitamin D and cholesterol to beta-lactoglobulin. *J Dairy Sci 80*, 1054-1059.

44. Bratschi, M. W., Burrowes, D. P., Kulaga, A., Cheung, J. F., Alvarez, A. L., *et al.* (2009). The glycerol 3-phosphate acyltransferases Gat1p and Gat2p are microsomal phosphoproteins with differential contributions to polarized cell growth. *Eukaryot Cell 8*, 1184-1196.

45. Raju, R. V., Datla, R. S. & Sharma, R. K. (1996). Expression of human N-myristoyltransferase in *Escherichia coli*. Comparison with N-myristoyltransferases expressed in different tissues. *Mol Cell Biochem 155*, 69-76.

46. Magee, A. I., Gutierrez, L., Marshall, C. J. & Hancock, J. F. (1989). Targeting of oncoproteins to membranes by fatty acylation. *J Cell Sci Suppl 11*, 149-160.

47. Smotrys, J. E. & Linder, M. E. (2004). Palmitoylation of intracellular signaling proteins: regulation and function. *Annu Rev Biochem 73*, 559-587.

48. Bizzozero, O. A., Bixler, H. A. & Pastuszyn, A. (2001). Structural determinants influencing the reaction of cysteine-containing peptides with palmitoyl-coenzyme A and other thioesters. *Biochim Biophys Acta 1545*, 278-288.

49. Bharadwaj, M. & Bizzozero, O. A. (1995). Myelin P0 glycoprotein and a synthetic peptide containing the palmitoylation site are both autoacylated. *J Neurochem 65*, 1805-1815.

50. Dietrich, L. E. & Ungermann, C. (2004). On the mechanism of protein palmitoylation. *EMBO Rep 5*, 1053-1057.

51. Sambrook, J. & Russell, D. W. Molecular cloning a laboratory manual. 3rd edition. New York: Cold Spring Harbor Laboratory Press; 2001.

52. Bradford, M. M. (1976). A rapid and sensitive method for the quantitation of microgram quantities of protein utilizing the principle of protein-dye binding. *Anal Biochem 72*, 248-254.

53. Iwaki, M., Ullmann, A. & Sebo, P. (1995) Identification by in vitro complementation of regions required for cell-invasive activity of *Bordetella pertussis* adenylate cyclase toxin. *Mol Microbiol 17*, 1015-1024.

54. Elbaum, D. & Nagel, R. L. (1981). Esterase activity of hemoglobin. Differences between HB A and HB S. *J Biol Chem 256*, 2280-2283.

55. Manavalan, P. & Johnson, W. C., Jr. (1987). Variable selection method improves the prediction of protein secondary structure from circular dichroism spectra. *Anal Biochem 167*, 76-85.

56. Thompson, J. D., Gibson, T. J., Plewniak, F., Jeanmougin, F. & Higgins, D. G. (1997). The CLUSTAL_X windows interface: flexible strategies for multiple sequence alignment aided by quality analysis tools. *Nucleic Acids Res 25*, 4876-4882.

57. Vriend, G. (1990). WHAT IF: a molecular modeling and drug design program. *J Mol Graph 8*, 52-56, 29.

58. Christen, M., Hunenberger, P. H., Bakowies, D., Baron, R., Burgi, R., *et al*. (2005). The GROMOS software for biomolecular simulation: GROMOS05. *J Comput Chem 26*, 1719-1751.

59. Laskowski, R. A., Rullmannn, J. A., MacArthur, M. W., Kaptein, R. & Thornton, J. M. (1996). AQUA and PROCHECK-NMR: programs for checking the quality of protein structures solved by NMR. *J Biomol NMR 8*, 477-486.

60. Otwinowski, Z. & Minor, W. (1997). Processing of X-ray diffraction data collected in oscillation mode. *Methods Enzymol 276*, 307–326.

61. Brunger, A. T., Adams, P. D., Clore, G. M., DeLano, W. L., Gros, P., *et al.* (1998). Crystallography & NMR system: A new software suite for macromolecular structure determination. *Acta Crystallogr D Biol Crystallogr 54*, 905-921.

62. Mattanovich, D., Weik, R., Thim, S., Kramer, W., Bayer, K., *et al.* (1996). Optimization of recombinant gene expression in *Escherichia coli*. *Ann NY Acad Sci 782*, 182-190.

63. Ziegler, K., Yusupov, M., Bishop, B. & Born, T. L. (2007). Substrate analysis of homoserine acyltransferase from *Bacillus cereus. Biochem Biophys Res Commun 361*, 510-515.

64. Pluvinage, B., Dairou, J., Possot, O. M., Martins, M., Fouet, A., *et al*. (2007). Cloning and molecular characterization of three arylamine N-acetyltransferase genes from *Bacillus anthracis*: identification of unusual enzymatic properties and their contribution to sulfamethoxazole resistance. *Biochemistry 46*, 7069-7078.

65. Hardman, M. J., Valenzuela, P. & Bender, M. L. (1971). Acylation of α- and β-chymotrypsins by *p*-nitrophenyl acetate. Enzyme-substrate complex formation and pH dependence. *J Biol Chem 246*, 5907-5913.

66. Hardie, K. R., Issartel, J. P., Koronakis, E., Hughes, C. & Koronakis, V. (1991). *In vitro* activation of *Escherichia coli* prohaemolysin to the mature membrane-targeted toxin requires HlyC and a low molecular-weight cytosolic polypeptide. *Mol Microbiol 5*, 1669-1679.

67. Worsham, L. M., Trent, M. S., Earls, L., Jolly, C. & Ernst-Fonberg, M. L. (2001). Insights into the catalytic mechanism of HlyC, the internal protein acyltransferase that activates *Escherichia coli* hemolysin toxin. *Biochemistry 40*, 13607-13616.

68. Bergfors, T. (2007) Screening and optimization methods for nonautomated crystallization laboratories. *Methods Mol Biol 363*, 131-151.

69. Holmquist, M. (2000). Alpha/beta-hydrolase fold enzymes: structures, functions and mechanisms. *Curr Protein Pept Sci 1*, 209-235.

70. Lairez, D., Pauthe, E. & Pelta, J. (2003). Refolding of a high molecular weight protein: salt effect on collapse. *Biophys J 84*, 3904-3916.

71. Hormozi, K., Parton, R. & Coote, J. (1998). Target cell specificity of the Pasteurella haemolytica leukotoxin is unaffected by the nature of the fatty-acyl group used to activate the toxin in vitro. *FEMS Microbiol Lett 169*, 139-145.

72. Havlicek, V., Higgins, L., Chen, W., Halada, P., Sebo, P., *et al.* (2001). Mass spectrometric analysis of recombinant adenylate cyclase toxin from *Bordetella pertussis* strain 18323/pHSP9. *J Mass Spectrom 36*, 384-391.

73. Lai, J. R., Fischbach, M. A., Liu, D. R. & Walsh, C. T. (2006). A protein interaction surface in nonribosomal peptide synthesis mapped by combinatorial mutagenesis and selection. *Proc Natl Acad Sci U S A 103*, 5314-5319.

74. Holzbaur, I. E., Harris, R. C., Bycroft, M., Cortes, J., Bisang, C., *et al.* (1999). Molecular basis of Celmer's rules: the role of two ketoreductase domains in the control of chirality by the erythromycin modular polyketide synthase. *Chem Biol 6*, 189-195.

75. Trent, M. S., Worsham, L. M. & Ernst-Fonberg, M. L. (1999). HlyC, the internal protein acyltransferase that activates hemolysin toxin: role of conserved histidine, serine, and cysteine residues in enzymatic activity as probed by chemical modification and site-directed mutagenesis. *Biochemistry 38*, 3433-3439.

76. Trent, M. S., Worsham, L. M. & Ernst-Fonberg, M. L. (1999). HlyC, the internal protein acyltransferase that activates hemolysin toxin: the role of conserved tyrosine and arginine residues in enzymatic activity as probed by chemical modification and site-directed mutagenesis. *Biochemistry 38*, 8831-8838.

77. Trent, M. S., Worsham, L. M. & Ernst-Fonberg, M. L. (1999). HlyC, the internal protein acyltransferase that activates hemolysin toxin: roles of various

conserved residues in enzymatic activity as probed by site-directed mutagenesis. *Biochemistry 38*, 9541-9548.

78. Benning, M. M., Wesenberg, G., Liu, R., Taylor, K. L., Dunaway-Mariano, D., *et al.* (1998). The three-dimensional structure of 4-hydroxybenzoyl-CoA thioesterase from *Pseudomonas* sp. strain CBS-3. *J Biol Chem 273*, 33572-33579.
79. Kato-Toma, Y. & Ishiguro, M. (2001). Reaction of Lys-Tyr-Lys triad mimics with benzylpenicillin: insight into the role of Tyr150 in class C beta-lactamase. *Bioorg Med Chem Lett 11*, 1161-1164.
80. Ma, W., Tang, C. & Lai, L. (2005). Specificity of trypsin and chymotrypsin: loop-motion-controlled dynamic correlation as a determinant. *Biophys J 89*, 1183-1193.
81. Kawamura, A., Yoshioka, Y., Harada, A. & Kono, K. (2005). Acceleration of enzymatic reaction of trypsin through the formation of water-soluble complexes with poly(ethylene glycol)-block-poly (alpha, beta-aspartic acid). *Biomacromolecules 6*, 627-631.
82. Gutfreund, H. & Sturtevant, J. M. (1956). The mechanism of chymotrypsin-catalyzed reactions. *Proc Natl Acad Sci USA 42*, 719-728.
83. Hartley, B. S. & Kilby, B. A. (1954). The reaction of *p*-nitrophenyl esters with chymotrypsin and insulin. *Biochem J 56*, 288-297.

APPENDICES

APPENDIX A
MOLECULAR WEIGHT MARKER FOR GEL FILTRATION CHROMATOGRAPHY

Gel filtration chromatography is a well-accepted method for determining the size and molecular weight of proteins. The molecular weight of 21-kDa of CyaC protein was determined by comparing its elution volume with those of known protein standards as shown in this figure.

Superdex™75 10/300 GL Columns (Tricorn)

Exclusion limit (M_r)	1×10^5 globular protein
Separation range (M_r)	3,000-70, 000 globular protein
Matrix	Spherical composite of cross-linked agarose and dextran
Bed dimensions	10 × 300 mm
Recommended sample volume	25-250 µl
Bed volume	24 ml
Max. pressure	18 bar (261 psi, 1.8 MPa)
Max. flow rate (H_2O at 25°C)	1.5 ml/min

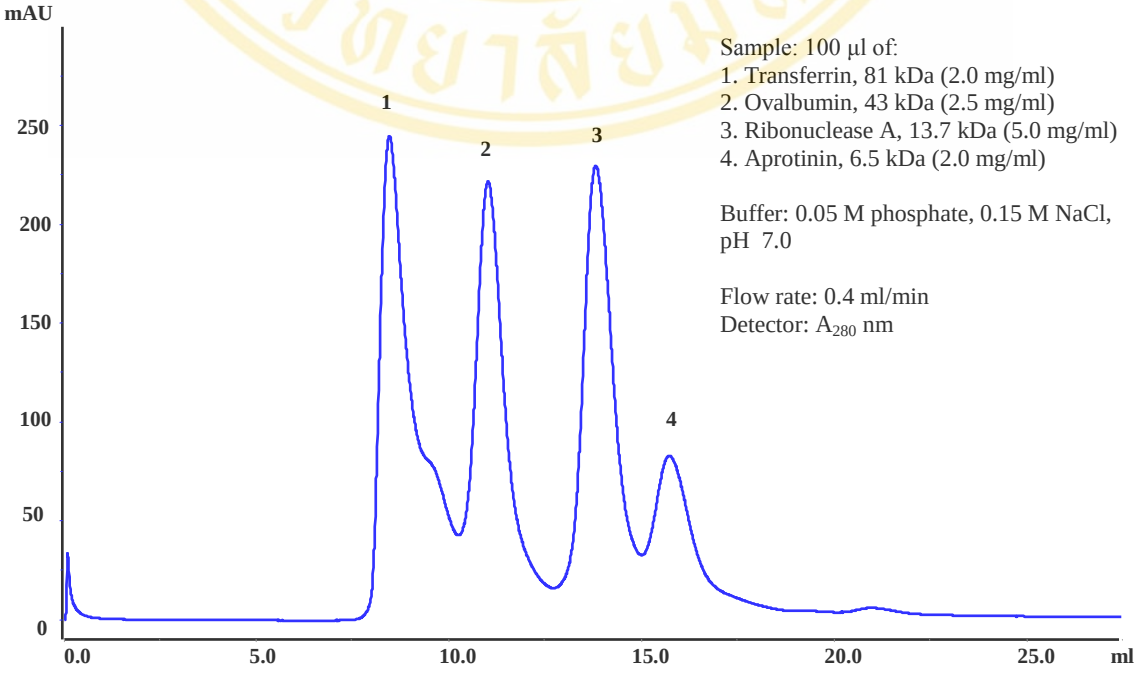

Separation of standard proteins on Superdex™75

APPENDIX B
DETERMINATION OF SUBSTRATE AND ENZYME CONCENTRATION

Effect of enzyme concentration on enzyme activity

In order to study the effect of increasing the enzyme concentration upon the reaction rate, the hydrolysis assay was determined by various enzyme concentrations at excess amount of pNPA substrate concentration (1 mM) in 50 mM Tris-HCl buffer, pH 7.4 at 25°C.

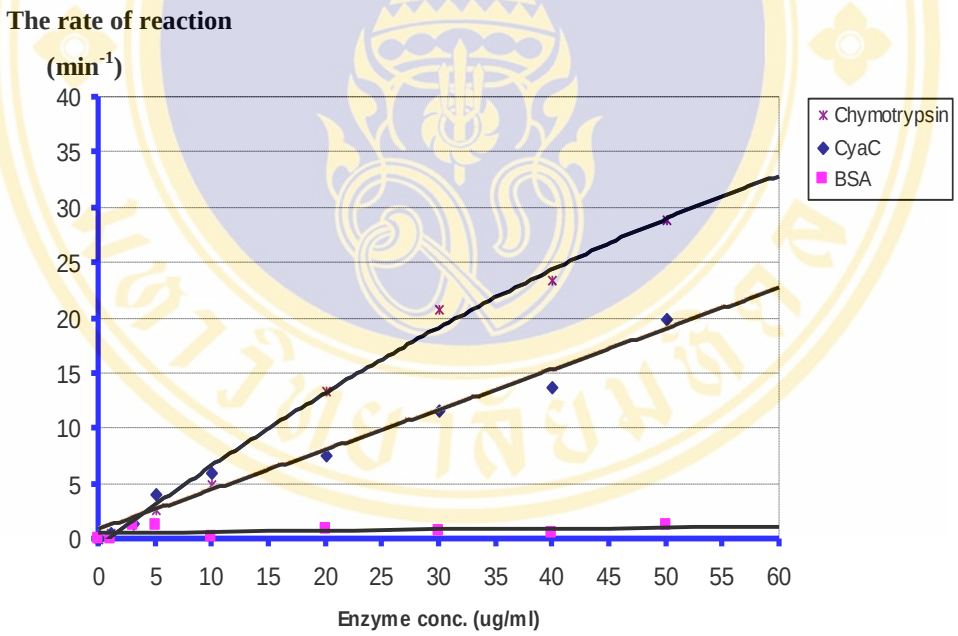

The slope of each sample toward pNPA (1 mM) substrate at indicated enzyme concentrations

This figure shows that at enzyme concentration ≤ 20 μg/ml, the rate of reaction is increase in proportional to the enzyme concentration but at higher enzyme concentrations, increasing enzyme has not much effect on the reaction rate. The velocity is likely to be plateau curve since 40 μg/ml. This enzyme assay is designed so that the observed activity is proportional to the amount of enzyme present in order that the enzyme concentration is the only limiting factor.

Progress curve for an enzyme reaction

To measure the initial (and maximal) rate, enzyme assays are typically carried out while the reaction has progressed only a few percent towards total completion. The enzyme produces product at an initial rate that is approximately linear for a short period after the start of the reaction. The hydrolysis assay was performed by fixed enzyme concentrations (15 μg/ml) with 500 μM pNPA substrate concentration in 50 mM Tris-HCl buffer, pH 7.4 at 25°C.

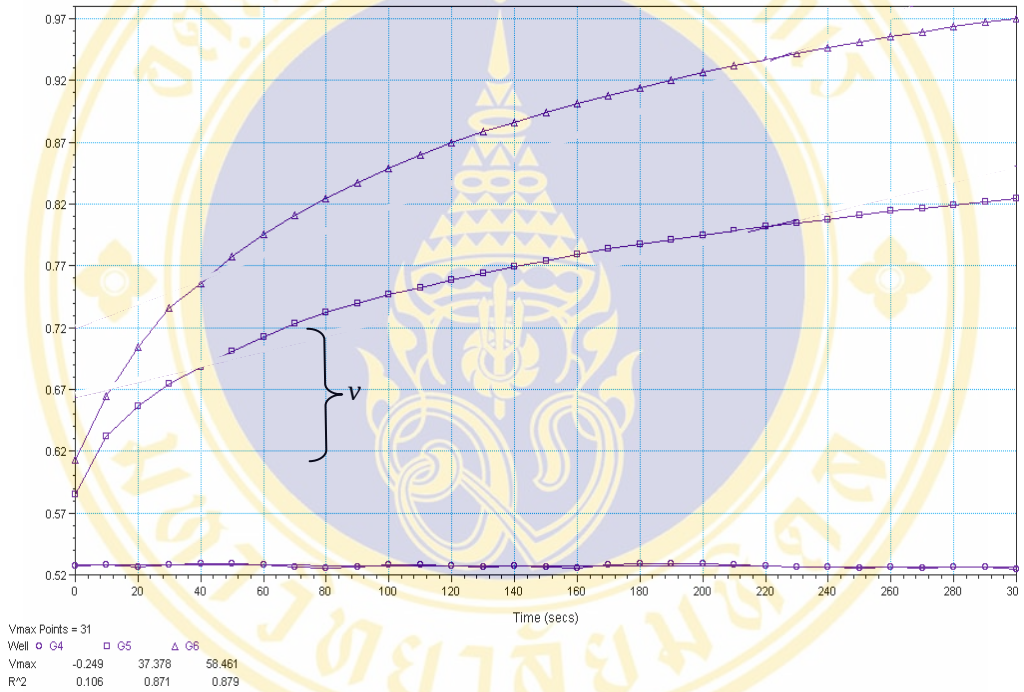

G4 represents the autohydrolysis in the blank. G5 and G6 represent the rate of reaction (min^{-1}) of CyaC in duplicates.

The slope in the initial rate period is the initial rate of reaction v.

When the concentration of the product of an enzymatic reaction is plotted against time, a progress curve results were shown in this figure. The figure shows the length of the initial rate period (10-60 sec) during the time range from 0 seconds to 5 minutes of CyaC reaction (15 μg/ml) toward pNPP (500 μM) substrate. For a given enzyme concentration and for relatively low substrate concentrations, the reaction rate increases linearly with substrate concentration; the enzyme molecules are largely free to catalyze the reaction, and increasing substrate concentration means an increasing rate at which the enzyme and substrate molecules encounter one another.

OD_{400} recorded at indicated enzyme concentration and time

The enzymatic reactions of each sample (50 μg/ml) catalyzed pNPA (1 mM substrate concentration) are shown in the graph. The product of reaction, pNP (*p*-nitrophenol), was quantified by spectrophotometry at 400 nm. After adding enzyme into the reaction, light absorbance was recorded at 10, 20, 30, 40, 50, 60, 70, 80 and 90 second. Relationships between product (represented by OD_{400}) and time were calculated from the slope of each graph (min^{-1}).

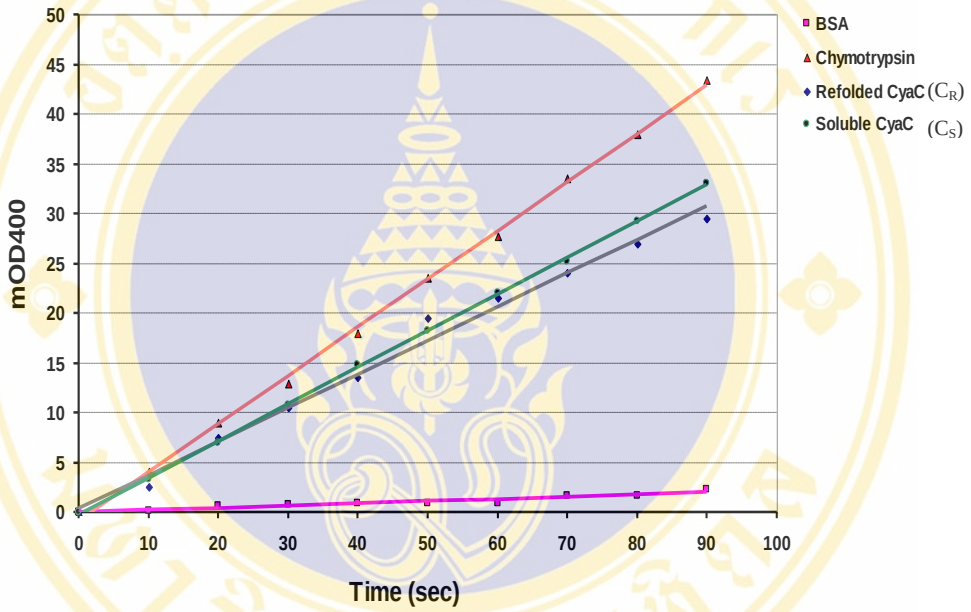

Relationships between product (represent by mOD_{400}) and time (sec).

To measure enzyme activity, the slope (dA/dt) of each graph (min^{-1}) was calculated from the graph in linear part and converted this term to velocity (μM/min) by using Beer's law: $A = \varepsilon cl$

ε = molar absorptivity or extinction coefficient (11.6 $mM^{-1}cm^{-1}$ in this case)

c = molar concentration of the absorbing species (pNP in this case)

l = path length (0.7 cm)

$dA/dt = \varepsilon(dc)l/dt$

$dc/dt = dA/\varepsilon ldt = slope/\varepsilon l$ = velocity (μM/min)

Calculation of the initial rate (dA/dt) of each graph in linear part is shown that rate of BSA = 1.31, rate of C_R = 19.94, rate of C_S = 22.0 and rate of chymotrypsin = 28.92 mOD/min.

APPENDIX C

OD_{400} RECORD AT DIFFERENT SUBSTRATE CONCENTRATIONS

CyaC activity for hydrolysis of pNPA substrate

The assay was conducted in a 96-well plate with a final reaction volume of 300 µl containing purified CyaC (4.5 µg) in 50 mM Tris-HCl (pH 7.4) and 1% (v/v) final acetonitrile concentration at 25ºC (method 4.2.16). Esterolytic reaction was determined from the formation of *p*-nitrophenol (pNP) product by measuring OD_{400} with a SoftMax Pro spectrophotometer. The reaction was performed simultaneously with a CyaC-free blank as a control. The rate of reactions (ΔA_{400nm}/min) at the maximum linear rate for both the test and blank were converted to velocity expressed in units of product formed per time ($\mu mol.min^{-1}.mg^{-1}$) (method 4.2.15). Data were recorded as the means of duplicate in three independents experiments.

1st experiment

pNPA (µM)	**OD_{400}** (mAU)					**Velocity** ($\mu mol.min^{-1}.mg^{-1}$)
	BLK	#1	#2	AVG	AVG-BLK	
0	0	0	0	0	0	0
1	0.107	0.129	0.214	0.150	0.043	0.3530
2.5	0.120	0.240	0.300	0.270	0.150	1.2315
5	0.015	0.229	0.393	0.311	0.296	2.4302
10	0.257	0.621	0.799	0.710	0.453	3.7192
25	0.021	1.107	1.100	1.104	1.083	8.8875
50	0.582	2.855	2.721	2.788	2.206	18.1117
100	0.000	2.820	3.000	2.910	2.910	23.8916
250	1.471	6.286	5.691	5.989	4.518	37.0895
500	2.116	7.422	7.023	7.223	5.107	41.9253
1000	2.979	7.756	8.679	8.218	5.239	43.0090

2nd experiment

pNPA (μM)	**OD_{400}** (mAU)					**Velocity** ($\mu mol.min^{-1}.mg^{-1}$)
	BLK	#1	#2	AVG	AVG-BLK	
0	0	0	0	0	0	0
1	0.060	0.107	0.103	0.107	0.047	0.3859
2.5	0.155	0.250	0.300	0.275	0.120	0.9852
5	0.155	0.618	0.38	0.499	0.344	2.8243
10	0.121	0.840	0.363	0.602	0.481	3.9449
25	0.021	1.173	1.013	1.093	1.072	8.80131
50	1.650	4.586	2.721	3.654	2.004	16.4490
100	3.874	7.154	5.406	6.28	2.406	19.7536
250	2.024	6.286	6.120	6.203	4.179	34.3103
500	5.400	7.500	14.00	10.75	5.350	43.9244
1000	3.000	8.679	8.200	8.440	5.440	44.6593

3rd experiment

pNPA (μM)	**OD_{400}** (mAU)					**Velocity** ($\mu mol.min^{-1}.mg^{-1}$)
	BLK	#1	#2	AVG	AVG-BLK	
0	0	0	0	0	0	0
1	0.086	0.150	0.107	0.129	0.043	0.3489
2.5	0.120	0.270	0.275	0.273	0.153	1.2520
5	0.015	0.311	0.499	0.405	0.390	3.2019
10	0.257	0.710	0.602	0.656	0.399	3.2738
25	0.021	1.104	1.093	1.098	1.077	8.8444
50	3.835	4.586	6.771	5.679	1.844	15.1355
100	0.420	2.910	4.020	3.465	3.045	25.0000
250	1.471	5.989	6.203	6.096	4.625	37.9700
500	5.460	12.00	9.750	10.875	5.415	44.4581
1000	2.979	8.2175	8.2175	8.2175	5.239	43.0090

Sum

pNPA (μM)	**Velocity** (μmol.min^{-1}.mg^{-1})				
	1	**2**	**3**	**AVG**	**SEM**
0	0	0	0	0	0
1	0.353	0.386	0.3489	0.3626	0.0082
2.5	1.232	0.985	1.2520	1.1563	0.0606
5	2.430	2.824	3.2019	2.8188	0.1575
10	3.719	3.945	3.2738	3.6460	0.1394
25	8.888	8.801	8.8444	8.8444	0.0176
50	18.112	16.449	15.1355	16.5654	0.6089
100	23.892	19.754	25.0000	22.8818	1.1288
250	37.090	34.310	37.9700	36.4566	0.7798
500	41.925	43.924	44.4581	43.4360	0.5451
1000	43.009	44.659	43.0090	43.5591	0.3889

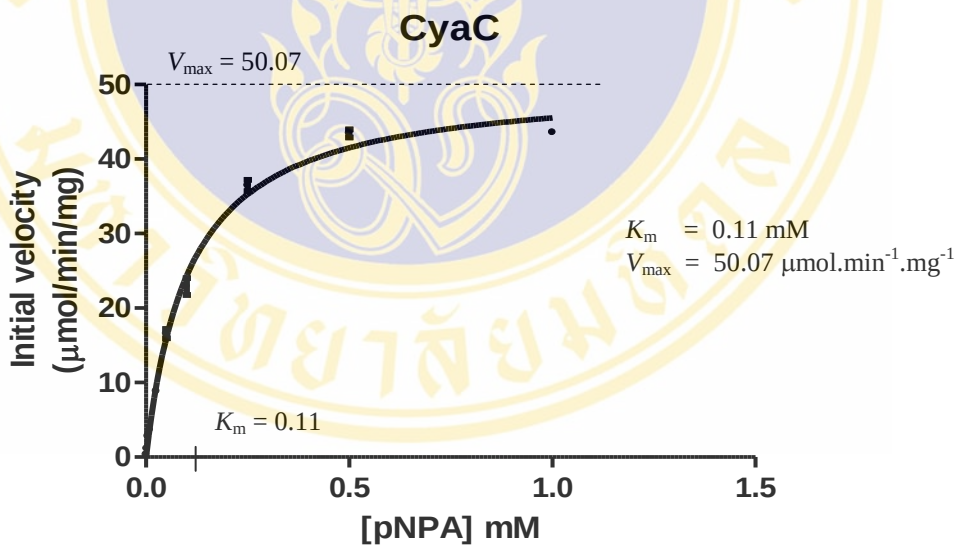

Enzyme velocity as a function of pNPA substrate concentration follows the Michaelis-Menten equation

The graph shows the reaction velocities of CyaC for hydrolysis of pNPA at concentrations in the range of 1-1000 μM. Kinetic parameters were determined from nonlinear fitting of untransformed data to the Michaelis-Menten equation. V_{max} is the limiting velocity as substrate concentrations get very large. K_M is the concentration of substrate that leads to half-maximal velocity. Data are reported as the means of three experiments ± standard error of the mean (SEM).

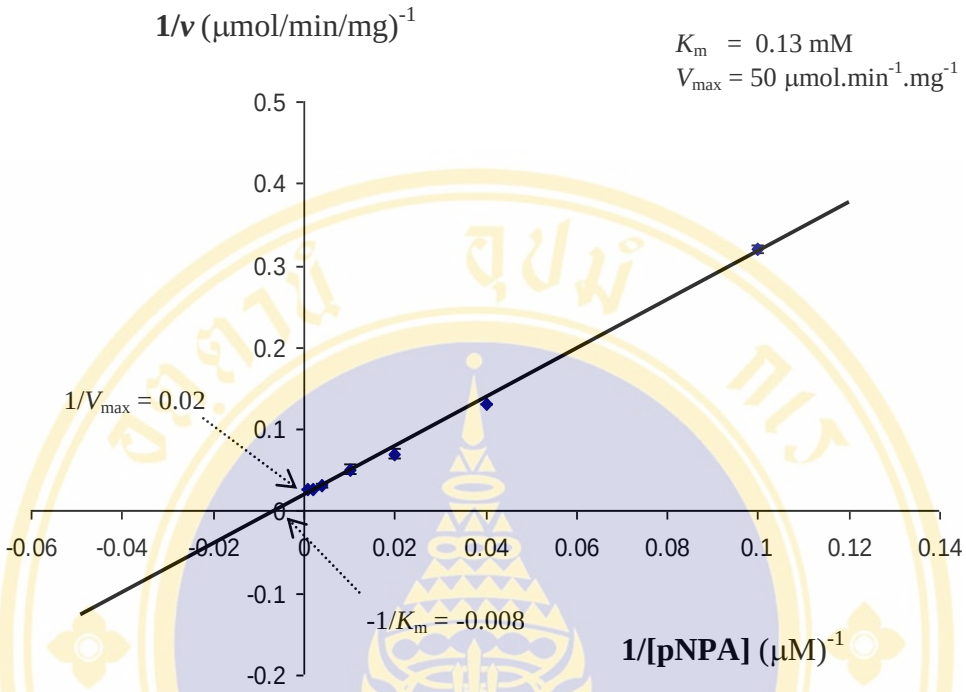

Displaying enzyme kinetic data on a Lineweaver- Burk plot

The data was display to a Lineweaver-Burk plot. Take the inverse of the Michaelis-Menten equation and simplify: Ignoring experimental error, a plot of 1/*V* vs. 1/S will be linear, with a Y-intercept of $1/V_{max}$ and a slope equal to K_m/V_{max}. The X-intercept equals $-1/K_m$. The slope and intercept of a linear regression line don't be used to determine values for V_{max} and K_m because the transformations (reciprocals) distort the experimental error, so the double-reciprocal plot does not obey the assumptions of linear regression. In my experiment, nonlinear regression was used to obtain the most accurate values of K_m and V_{max} throughout the results.

CyaC activity for hydrolysis of pNPP substrate

The assay was conducted in a 96-well plate with a final reaction volume of 300 µl containing purified CyaC (4.5 µg) in 50 mM Tris-HCl (pH 7.4) and 5% (v/v) final isopropanal concentration at 25ºC (method 4.2.16). Velocity in units of product formed per time (µmol.min^{-1}.mg^{-1}) was determined according to the method 4.2.15. Data were recorded as the means of duplicate in three independents experiments.

1st experiment

pNPP (µM)	**OD_{400}** (mAU)					**Velocity** (µmol.min^{-1}.mg^{-1})
	BLK	#1	#2	AVG	AVG-BLK	
0	0	0	0	0	0	0
10	0.991	5.550	5.507	5.5285	4.538	37.2537
25	0.840	13.526	10.860	12.193	11.353	93.2107
50	1.007	26.507	25.093	25.800	24.793	203.5550
100	0.364	35.520	38.220	36.870	36.506	299.7208
150	2.425	56.000	54.279	55.140	52.715	432.7956
200	0.000	63.900	64.800	64.350	64.350	528.3251
250	0.120	81.720	75.360	78.540	78.420	643.8423
300	0.446	99.540	83.910	91.725	91.279	749.4170
400	0.249	96.000	105.15	100.580	100.326	823.6945
500	0.005	99.000	97.020	98.010	98.005	804.6388

2nd experiment

pNPP (µM)	**OD_{400}** (mAU)					**Velocity** (µmol.min^{-1}.mg^{-1})
	BLK	#1	#2	AVG	AVG-BLK	
0	0	0	0	0	0	0
10	0.000	4.680	4.221	4.451	4.451	36.5394
25	0.360	10.860	11.340	11.100	10.740	88.1773
50	0.120	23.340	22.440	22.890	22.770	186.9458
100	0.060	33.300	35.700	34.500	34.440	282.7586
150	0.840	51.300	52.800	52.050	51.210	420.4433
200	0.240	72.120	64.800	68.460	68.220	560.0985
250	0.120	87.240	80.000	83.620	83.500	685.5500
300	0.943	93.171	95.400	94.286	93.343	766.3587
400	2.340	97.020	105.15	101.09	98.745	810.7142
500	1.457	99.540	107.18	103.36	101.90	836.6420

3rd experiment

pNPP (μM)	**OD_{400}** (mAU)					**Velocity** ($\mu mol.min^{-1}.mg^{-1}$)
	BLK	#1	#2	AVG	AVG-BLK	
0	0	0	0	0	0	0
10	0.100	4.157	5.040	4.599	4.499	36.9335
25	0.900	12.120	11.820	11.970	11.070	90.8867
50	0.810	24.600	21.060	22.830	22.020	180.7880
100	0.300	33.000	37.200	35.100	34.800	285.7143
150	0.840	51.300	54.279	52.790	51.950	426.5148
200	1.800	52.886	76.620	64.753	62.953	516.8555
250	1.080	83.914	87.240	85.577	84.497	693.7356
300	1.440	93.914	96.780	95.347	93.907	770.9934
400	0.916	97.020	105.15	101.09	100.17	822.4056
500	0.137	79.354	118.50	98.927	98.790	811.0837

Sum

pNPP (μM)	**Velocity** ($\mu mol.min^{-1}.mg^{-1}$)				
	1	**2**	**3**	**AVG**	**SEM**
0	0	0	0	0	0
10	37.254	36.539	36.934	36.909	0.1460
25	93.211	88.177	90.887	90.758	1.0283
50	203.555	186.946	180.788	190.430	4.8077
100	299.721	282.759	285.714	289.398	3.6992
150	432.796	420.443	426.515	426.585	2.5215
200	528.325	560.099	516.856	535.093	9.1455
250	643.842	685.550	693.736	674.376	10.924
300	749.417	766.359	770.993	762.256	4.6369
400	823.695	810.714	822.406	818.938	2.9194
500	804.639	836.642	811.084	817.455	6.9100

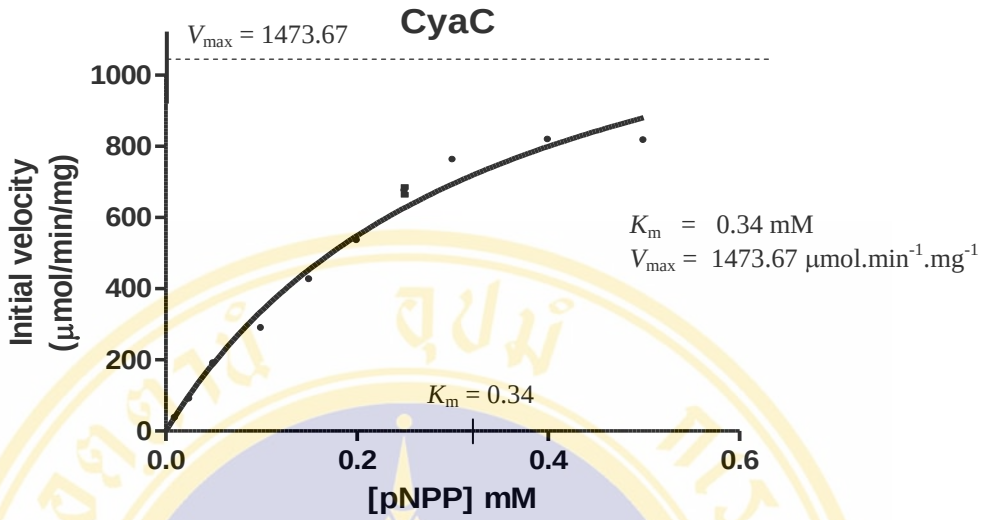

Enzyme velocity as a function of pNPP substrate concentration follows the Michaelis-Menten equation

The graph shows the reaction velocities of CyaC for hydrolysis of pNPP at concentrations in the range of 10-500 μM. Kinetic parameters were determined from nonlinear fitting of untransformed data to the Michaelis-Menten equation. V_{max} is the limiting velocity as substrate concentrations get very large. K_M is the concentration of substrate that leads to half-maximal velocity.

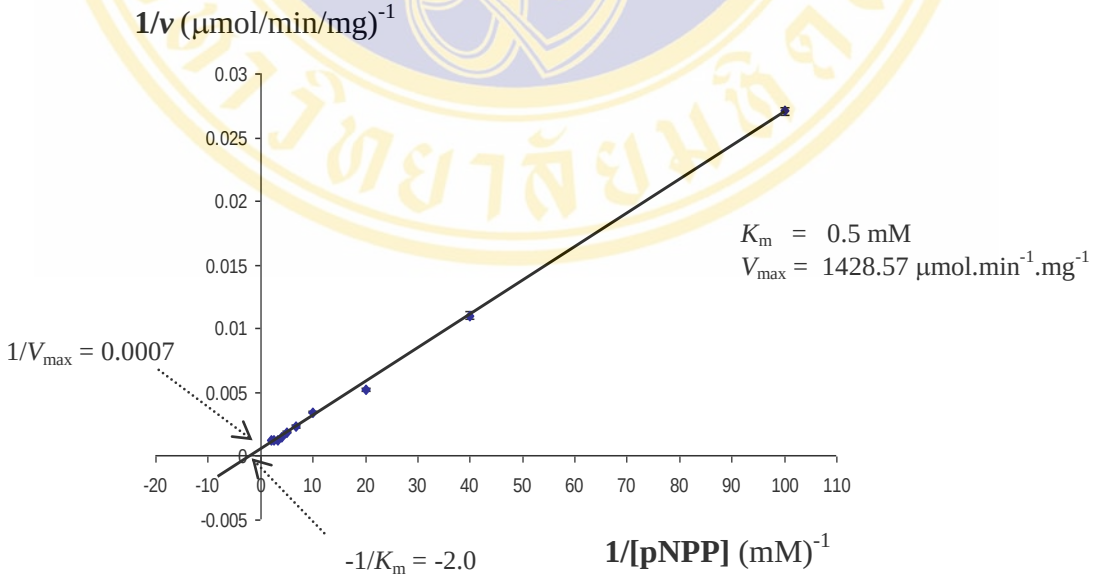

Displaying enzyme kinetic data on a Lineweaver- Burk plot

The data was display to a Lineweaver-Burk plot. Take the inverse of the Michaelis-Menten equation and simplify: a plot of 1/*V* vs. 1/S will be linear, with a Y-intercept of $1/V_{max}$ and a slope equal to K_m/V_{max}. The X-intercept equals $-1/K_m$.

APPENDIX D
MOLAR RATIO OF proCyaA-PF TO CyaC ACTIVATION AND ASSESSMENT OF HEMOLYSIS

Toxin activation *in vitro* mediated by CyaC was performed by varying the molar ratio between CyaC and proCyaA-PF protein. The molar ratios of proCyaA-PF to CyaC were 10:1, 2:5, 2:1, 1:1, 1:2, 1:3, 1:4, 1:5 and 1:10. The mixture was adjusted to 1-ml reaction with TBS buffer at 37°C for 5 min and tested for hemolytic activity of the activated CyaA-PF toxin.

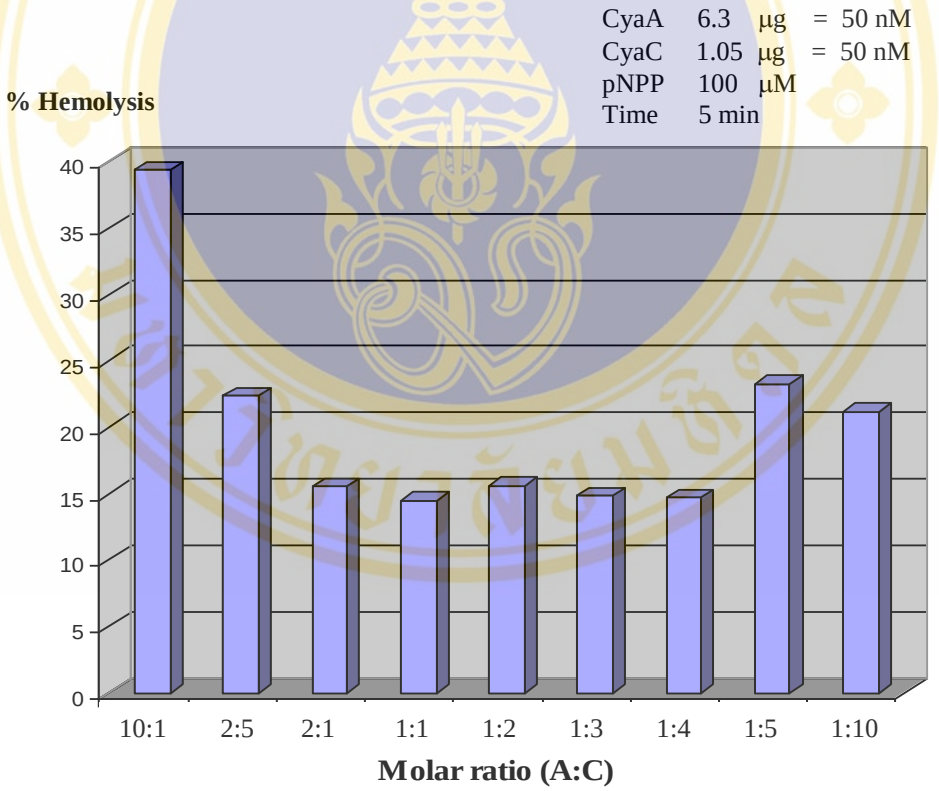

The dose response for the in vitro activated CyaA-PF

It was observed that there were some fixed ranges of A:C molar ratio that affect the hemolytic activity of CyaA-PF toxin. The optimal ranges of molar ratio (A:C) activation were 1:5-1:10. These results are useful for controlling activated proCyaA-PF by CyaC *in vitro*.

APPENDIX E
INHIBITION OF CyaC ACTIVITY

Effect of PMSF on inhibition of CyaC activity

To characterize the active serine residue of CyaC, PMSF (0.1, 1 and 5 mM) were added into the esterolytic reaction. As shown in this table, CyaC enzyme was inhibited with PMSF, suggesting that CyaC may share a similar mechanism of serine protease in which the serine residue served as the active site.

Reaction	**Specific activity**[a] (U/mg)
CyaC (15 μg/ml)	804.7
CyaC (15 μg/ml) + 0.1 mM PMSF	665.2
CyaC (15 μg/ml) + 1 mM PMSF	395.7
CyaC (15 μg/ml) + 5 mM PMSF	13.4

[a] Specific activity was calculated by using purified CyaC (4.5 μg) added to 300 μl of 50 mM Tris-HCl (pH 7.4) containing 500 μM pNPP with various PMSF concentrations. The results were the mean of single experiment performed in duplicates.

Effect of proCyaA-PF on inhibition of CyaC activity

The reaction was performed using the different proCyaA-PF concentrations and fixed concentration of CyaC (4.5 μg) for measuring hydrolysis of the various pNPP substrate concentrations (10-500 μM). Kinetic parameters, K_m and V_{max}, were determined from Lineweaver–Burk plots and non-linear least squares regression analysis of initial reaction velocities obtained with proCyaA-PF concentrations of 3 μg and 4.5 μg per 300 μl. The reactions were assayed in duplicates (single experiment).

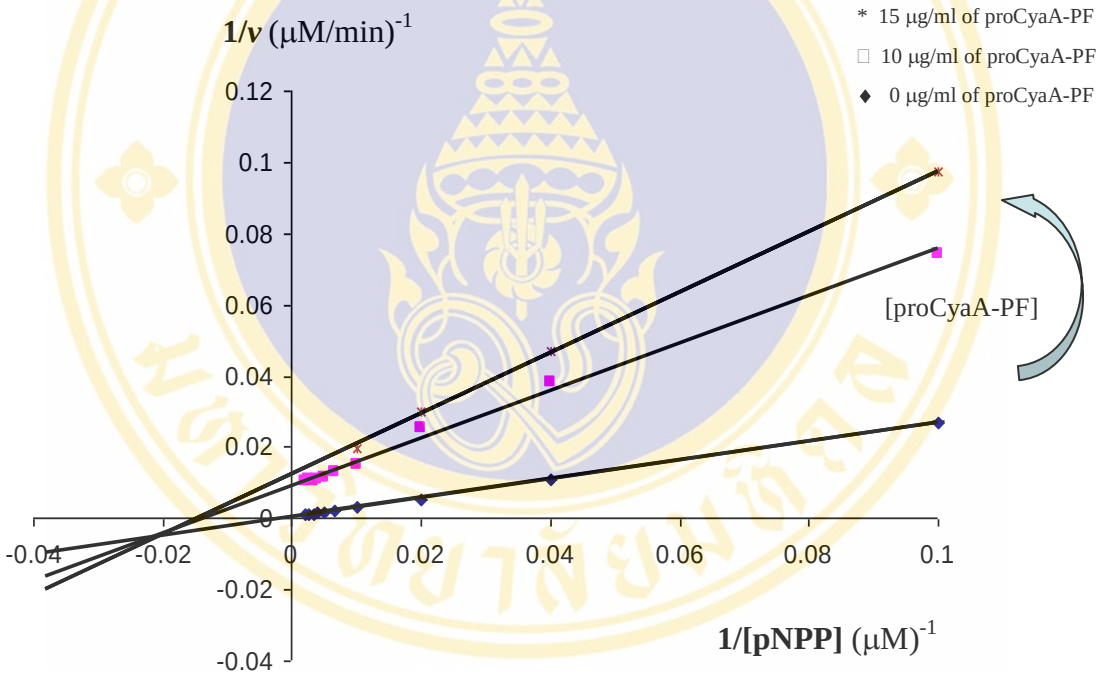

Lineweaver–Burk plots show the intercept of ploted lines

It was found that CyaA-PF as a mixed-type inhibitor of CyaC enzyme which can bind to either the free enzyme (E) or the enzyme-substrate complexes (ES). In mixed inhibition, the inhibitor binds to a site different from the active site where the substrate binds. Thus, CyaA-PF interferes with substrate binding (decrease K_m) and hampers catalysis in the ES complex (decrease V_{max}).

APPENDIX F

IN VITRO ACTIVATION OF CyaA-PF TOXIN VIA MEMBRANE PERTUBING ACTIVITY

To test the effect of CyaA-PF toxin activated by CyaC on the integrity of membrane vesicles, the degree of large unilamellar vesicles (LUVs) perturbation was determined as an increase in the fluorescence intensity of the released calcein. Upon adding the purified activated CyaA-PF toxin (0.5-1 μg), the activated toxin was able to fast induce the release of entrapped calcein from LUVs with ~40% release.

A)

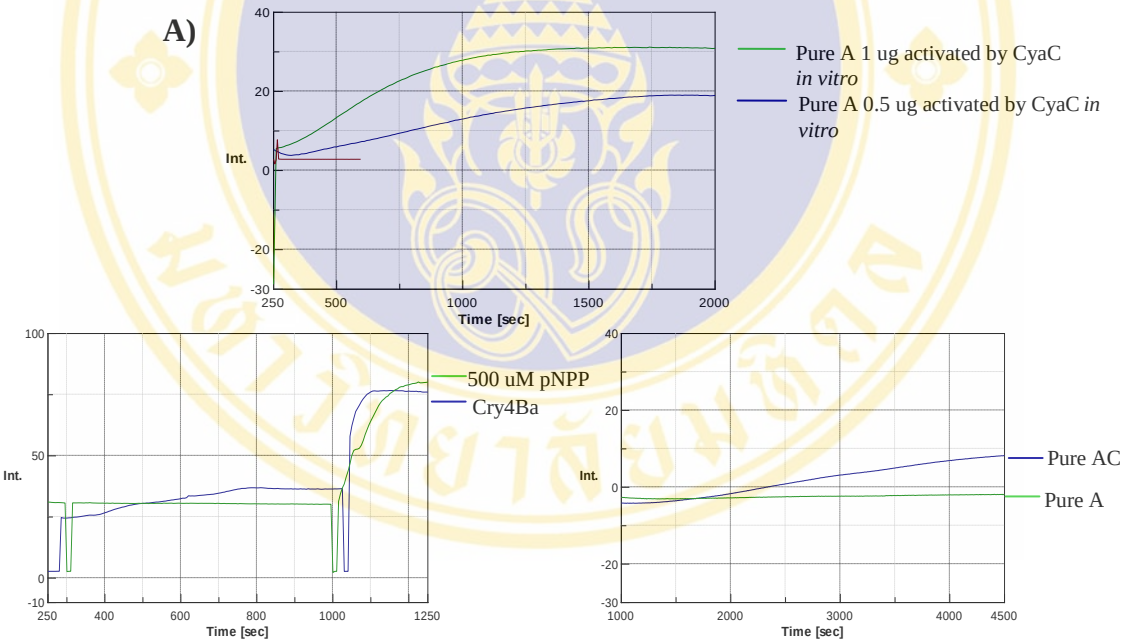

B)

Protein conc. (μg)	% Calcein release activity		
	CyaA activated by CyaC *in vivo*	CyaA activated by CyaC *in vitro*	Cry4Ba
1.0	20	40	17
0.5	ND	23	ND

The figure shows (A) fluorescence intensity traces after adding the activated toxins into calcein entrapped LUVs. The curves were obtained at each toxin. (B) The relative release activity of each protein sample with different concentrations. Fluorescence was monitored at 25°C on a Perkin-Elmer LS50 spectro fluorimeter with excitation and emission wavelengths set at of 485 and 520 nm, respectively.

BIOGRAPHY

NAME Miss Niramon Thamwiriyasati

DATE OF BIRTH 3 August 1982

PLACE OF BIRTH Chachoengsao, Thailand

HOME ADDRESS 7 Chumpon Road, Tambon Namueang , Amphoe Mueang, Chachoengsao, 24000, Thailand
Tel: 0-3851-3705
E-mail: niramon25@yahoo.com

INSTITUTION ATTENDED Thammasat University, 2000-2004
Bachelor degree of Science (Medical Technology)
Mahidol University, 2004-2010
Doctor of Philosophy (Molecular Genetics and Genetic Engineering)

AWARD & SCHOLARSHIP Royal Golden Jubilee Ph.D. Scholarship (2006-2010) from Thailand Research Fund

King Bhumibol's Scholarship (2003) for top performance student

Honorable mention award for poster presentation (2006): Molecular Medicine from Research to Clinical Practice, Institute of Science and Technology for Research and Development, Mahidol University, Thailand

First Class Honor upon Graduation with Golden Medal (2003), Thammasat University

PUBLICATION & INTERNATIONAL MEETING ABSTRACTS

1. **Thamwiriyasati N**, Sakdee S, Chuankhayan P, Katzenmeier G, Chen C.J, Angsuthanasombat C. Crystallization and preliminary X-ray crystallographic analysis of a full-length active form of Cry4Ba toxin from *Bacillus thuringiensis*. ***Acta Crystallogr F*** 2010 (manuscript with minor revision).

2. **Thamwiriyasati N**, Powthongchin B, Kittiworakarn J, Katzenmeier G, Angsuthanasombat C. Esterase activity of *Bordetella pertussis* CyaC-acyltransferase against synthetic substrates: Implications for catalytic mechanism *in vivo*. ***FEMS Microbiol Letters*** 2010; 304 (2): 183-190.

3. Ruchiwit K, **Thamwiriyasati N**, Sukavest P, Na-Ubol M. The isolation of *Vibrio cholerae* in the lower Chao Phraya River: virulence genes and DNA patterns. ***J Med Technol Assoc Thailand*** 2003; 31: 450-62.

4. **Thamwiriyasati N**, Powthongchin B, Kittiworakarn J, Katzenmeier G, Angsuthanasombat C. 'Hydrolysis of synthetic substrate *in vitro* by purified CyaC-acyltransferase cloned from *Bordetella pertussis*: Implication for catalytic mechanism'. In Abstract of **Biophysical Society**: 54th Annual Meeting. February 20-24, 2010, San Francisco, California, the United States of America.

5. **Thamwiriyasati N**, Powthongchin B, Angsuthanasombat C. 'Purified CyaC-acyltransferase cloned from *Bordetella pertussis* catalyzes the hydrolysis of synthetic substrates *in vitro*'. In Abstract of **The American Society for Cell Biology**: 48th Annual Meeting. December 13-17, 2008, San Francisco, California, the United States of America.

6. **Thamwiriyasati N**, Powthongchin B, Ketterman A, Angsuthanasombat C. 'Purified CyaC-acyltransferase cloned from *Bordetella pertussis* catalyzes the hydrolysis of synthetic substrates *in vitro'*. In Abstract **of Biochemistry and Molecular Biology (BMB) 2008**. November 7-11, 2008, Kobe, Japan.

7. **Thamwiriyasati N**, Powthongchin B, Katzenmeier G, Angsuthanasombat C. 'Purification and Characterization of the *Bordetella pertussis* Acyltransferase, CyaC'. In Abstract of **The 11th Biological Sciences Graduate Congress**: Explorations Towards the Improved Quality of Life, Sustainable Development, and Secured Future. December 15-17, 2006, Chulalongkorn University, Bangkok, Thailand.

8. **Thamwiriyasati N**, Rungpragayphan S, Powthongchin B, Katzenmeier G, Angsuthanasombat C. 'Expresssion, Purification and Characterization of the *Bordetella pertussis* Acytransferase (CyaC)'. In Abstract of **Molecular Medicine 2006**. November 28-30, 2006, Institute of Science and Technology for Research and Development, Mahidol University, Nakornpathom, Thailand.

9. **Thamwiriyasati N**, Rungpragayphan S, Powthongchin B, Angsuthanasombat C. 'Expression and Purification of the *Bordetella pertussis* acyltransferase (CyaC)'. In Abstract of **First Annual Symposium of Protein Society of Thailand**. October 24-25, 2006, Chulabhorn Research Institute Conference Center, Bangkok, Thailand.